Lire
la première partie
de la thèse

Chapter 4

VALIDATING THE VALUE OF MICROWAVES IN CONCRETE RECYCLING

The value of microwave treatment to concrete recycling is confirmed by the large increase in aggregate and cement liberation observed after concrete samples are exposed to microwaves. Increasing the duration of microwave exposure led to increased aggregate liberation which was matched by a decrease in strength and stiffness of the concrete sample. The change in strength, stiffness and liberation was large between short microwave treated and untreated concrete, small between short and medium treated and large again between medium and long microwave treated concrete.

The capacity of microwaves to severely damage concrete, while also leaving aggregate particles intact and therefore useful for recycling purposes is clearly demonstrated but the actual mechanisms that lead to this level of damage are left unclear. The desire to uncover these mechanisms later inspired local investigation of textural changes.

The following chapter validates the value of microwave heating in a concrete recycling process, by investigating the effect of microwave heating on concrete recycling at a macro scale. These effects will then be revisited in the following chapter at the micro scale, seeking to establish the link between macroscopic observations and changes which occur inside the texture of concrete.

TABLE OF CONTENTS FOR CHAPTER 4

4. VALIDATION OF THE VALUE OF MICROWAVES FOR CONCRETE RECYCLING

The complexity of concrete makes it necessary to use a combination of techniques to characterise its changes under heat treatment. On the other hand demonstrating that a change has occurred in the material as a result of microwave heating is a much simpler endeavour. Single-impact fracture on the Hopkinson bar can demonstrate how microwave heating reduces concrete strength and thermogravimetric analysis can show that heating has changed the chemical composition of concrete.

Since most of this information was published in 2012 in the international journal Minerals Engineering [4.1], this chapter starts with the complete published article in section 4.1, followed by section 4.2. which contains a number of unpublished supplementary comments. Where references are made to tables and figures in this section, they refer to the paper published in full in section 4.1 unless the number is prefixed by a "4."

The international journal of Minerals Engineering paper sets the foundation for the project. It identifies the applicability of microwave heating to concrete processing and shows how the designed series of microwave treatments followed by breakage and analysis is a logical sequence given the nature of comminution processes (Fig. 1).

The first key results presented are those that demonstrate the effect of microwave heating on concrete stiffness (Fig. 7 and Fig. 8). These figures show the force experienced by samples under impact and the gradient of those is directly related to the particle stiffness which can be seen to decrease substantially, even to the point that concrete sample no longer seems to behave like a true solid. The strength of samples saw a similar decrease (Fig. 9). Interestingly the decrease in strength due to microwave treatment observed in the concrete samples showed a similar pattern to the change in fragmentation (Fig. 10) and liberation (Fig. 13), that is to say short and medium treated concrete saw similar results but long treated and untreated saw significantly different results from both the other two treatment sets and each other. This might suggest that the most efficient microwave communition techniques lie at both ends of the microwave treatment spectrum; either a very short exposure or an extreme treatment. This idea is reiterated by comparing the comminution energy to the liberation fraction (Fig. 14).

This investigation was macroscopic in nature and while it demonstrated microwave's efficacy the embrittlement mechanisms remained unclear which led to the use of localised techniques (see Chapter 5).

4.1 Investigation of microwave-assisted concrete recycling using single-particle testing

The following 11 pages are devoted to the article Investigation of microwave-assisted concrete recycling using single-particle testing publishing in the journal Minerals Engineering volume 31 in 2012.

Minerals Engineering 31 (2012) 71–81

Contents lists available at SciVerse ScienceDirect

Minerals Engineering

journal homepage: www.elsevier.com/locate/mineng

Investigation of microwave-assisted concrete recycling using single-particle testing

Nicholas Lippiatt *, Florent Bourgeois

Université de Toulouse, INPT, UPS, LGC (Laboratoire de Génie Chimique), 4 allée Emile Monso, BP 44362, 31432 Toulouse Cedex 4, France

ARTICLE INFO

Article history:
Available online 24 October 2011

Keywords:
Concrete
Recycling
Comminution
Liberation

ABSTRACT

Microwave heating stands as a strong candidate for selective liberation of multiphase materials like concrete. It takes advantage of the differences in thermal, dielectric and mechanical properties of each of the components to create stress gradients that can lead to grain boundary fracture and embrittlement.

The work and results reported are concerned with selective liberation of concrete's raw constituents for recycling by combination of microwave heating and comminution. A single particle testing approach is presented for detailed analysis of the process. Concrete particles 10 mm in size are treated individually in a single mode cavity microwave (2.45 GHz, 2 kW) test apparatus. The microwave induced effects are quantified by single particle impact testing on a fast Hopkinson bar. Analysis of impact traces reveals a thorough embrittlement of concrete particles from microwave treatment and fragment analysis confirms the potential of microwaves for selective liberation of the raw constituents of concrete. These results validate that microwaves and comminution can be combined to liberate concrete's raw constituents.

1. Introduction

More natural resources are consumed for the production of concrete than for any other product (Nawy, 2008). For new concrete structures requiring standard performance levels, the use of recycled concrete aggregate (RCA) is generally accepted to be limited to 20–30% of total aggregate volume (Tam and Tam, 2006) however for Europe this number is much lower. Of 21 countries listed by the European Aggregates Association, 18 source less than 10% of total aggregate from recycled material (Klee, 2009). Promising results have been obtained with 60% recycled concrete aggregate volume fraction in some applications (Soutsos et al., 2010) though going beyond these limits produces a significant decrease in concrete strength (Malesev et al., 2010; Tam et al., 2007). Recycling of construction waste, of which concrete is a major component, is over 50% for many European countries (Fischer and Davidsen, 2010) but this is largely backfill operations for which many other materials with much less added value are also suitable, so could be considered a waste. It also means a significant proportion of material is ending in landfill that could easily be recycled. One key reason is that RCA particles produced by conventional means contain too high a cement to aggregate ratio, the presence of cement being the cause of the adverse effect of RCA on concrete properties. Reducing the amount of cement in RCA is an important area of research and development (Tam et al., 2007).

The mechanical performance of concrete with 30% of coarse aggregate replaced with RCA is almost identical to concrete with 100% of coarse aggregate replaced with treated RCA, when the RCA has been treated so as reduce mortar content by 30% (Akbarnezhad et al., 2011). However, the mortar content bears no direct relationship with the degree of liberation of aggregates, which is likely to be the most important factor determining the recycling potential of RCA. Indeed, it appears to be the interaction of surfaces during cement curing that determines the disparity in mechanical performance of concrete made with RCA or natural aggregate (NA). In the extreme, the reduction of mortar content could be near 100% but if the remaining mortar was spread evenly over the surface of aggregate, the liberation value would be zero and the mechanical performance of concrete made with such RCA would be poor. The fragmentation method, which should promote fracturing along the aggregate-cement interface, is therefore pivotal to the issue of concrete and RCA recycling, and justifies the focus on microwave induced fracture as an alternative to current mechanical methods used for producing RCA.

To the best of the authors' knowledge, the level of aggregate liberation required so that RCA can replace NA in concrete is unknown. The values above were achieved using similar processes and materials to those of this work and therefore are assumed to rely on the same fracture pattern, therefore 30% is likely a good target until more information is available. What this means in terms of liberation though is dependant on the original ratio of concrete to cement. This problem of finding a necessary liberation fraction is related to the more generic question of selective liberation with multiphase materials.

* Corresponding author. Tel.: +33 05 34 32 36 33; fax: +33 05 34 32 37 00.
E-mail addresses: nicholasrichard.lippiatt@inp-toulouse.fr (N. Lippiatt), florent.bourgeois@inp-toulouse.fr (F. Bourgeois).

0892-6875/$ - see front matter © 2011 Elsevier Ltd. All rights reserved.
doi:10.1016/j.mineng.2011.09.017

Another important factor to consider is that if cement and aggregate are separated then both can be reused in their original manner, as concrete components. Cement can be made from as much as 100% recycled material and still have acceptable mechanical performance (Galbenis and Tsimas, 2006; Costes et al., 2010). The production of cement uses more energy and releases more carbon dioxide than any other part of the concrete production process, thus cement recycling is likely to have a large environmental impact, possibly even larger than recycling aggregate.

Microwave technology has long been recognised as one possible solution for achieving selective liberation of multiphase materials, with beneficiation of mineral ores receiving significant attention. Microwave treatment has been shown to increase the metal recovery from copper (Vorster et al., 2001) and gold (Amankwah and Ofori-Sarpong, 2011) ores. Similarly, significant reduction in strength and improvement in grindability have also been obtained with coal (Marland et al., 1998) and iron ores (Kumar et al., 2010).

Even more so than mineral ores, concrete is a multiphase material, hence microwaves are expected to be effective for fracturing concrete. Indeed, it contains particulate phases (aggregate and sand particles) embedded in a continuous phase (cement paste), which includes water containing pores. The cement matrix creates additional complications to a theoretical understanding of the interaction between microwaves and concrete because of its multiphase and multiscale nature (Lee et al., 2009; Constantinides and Ulm, 2004). It bears many distinct mineral phases in itself (Lee et al., 2009) whose concentrations vary throughout the bulk of the cement phase, particularly at the interface of aggregate and cement. Pores are also not homogeneously distributed throughout cured cement, and porosity is highest near the interface of aggregate and cement interface (Roy et al., 1993). A valuable understanding of the interaction between microwaves and cement would be gained by measuring and comparing relevant properties for all the phases present. When dealing with microwave heating, which affects concrete from multiple sources from within the material itself, the presence of heterogeneities at small scales inside the cement matrix likely plays a pivotal role on the interactions between microwaves and concrete. It seems that these interactions would require a multiscale analysis of the dielectric and thermal properties of concrete, in very much a similar way to that done by Constantinides and Ulm (2004) who investigated local mechanical properties of concrete by micro-indentation and micro-mechanical modelling. One area of particular interest is the 10–20 μm thick interfacial transition zone (ITZ) around aggregate particles, with higher porosity and lower mechanical strength than the bulk of the cement paste (Scrivener et al., 2004) that must play a major role in the fracture and liberation behaviour of concrete.

The complex, multiscale and multiphase nature of cement and the effect that this has on the interaction between concrete and microwaves is difficult to describe in general terms as the spatial distribution of different phases and water through cement is likely to be the most important factor in the distribution of power density and fracture growth given the highly localised nature of microwave-material interaction. In particular, the behaviour of water during microwave heating of concrete, which gives rise to both heat and stress sources, is without doubt the most important and complex issue in the process investigated. Recognition that the localised nature of the microwave-concrete interaction is of paramount importance because of the textural complexity of cured cement raises issues about the relevance of using average properties, such as mean power density or loss constant for cured cement, for describing and analysing microwave-concrete interactions. In depth analysis of cement at very fine levels would add valuable understanding to the interaction between microwaves and concrete but at this early stage it is probably enough to recognise that water is the controlling phase and focus on a simpler macroscopic approach.

Average properties of concrete phases are listed in Table 1. It is the differences in these properties that make it possible to separate these phases with rapid microwave heating. The values are average for the bulk at 20 °C and exposed to 2.45 GHz microwaves making them applicable only to the initial stages of heating. This discontinuity of properties is what leads to stress and fracture formation in concrete during rapid microwave heating.

From Table 1, aggregate and cement phases exhibit differences in thermal properties, which are favourable for phase boundary fracture and separation during rapid heating (Vorster et al., 2001). Indeed, extensive simulations of microwave heating of mineral ores have highlighted the importance of specific heat and coefficient of thermal expansion (Ali, 2010). Density is also important as the heating is volumetric. Heating rate is proportional to the applied power density W/m^3 and a change in temperature leads to a change in volume, which in turn generates internal stresses. This is good for the separation of aggregate and cement as the difference in thermal expansion can be 50–300%. The importance of thermal conductivity decreases the shorter that microwave exposure times become. So, ignoring conduction, assuming equal heat flux, including density and specific heat for volumetric heating, the difference in heating rates between aggregate and cement could be as much as 20%. From these numbers water will heat 4–60 times faster than the other concrete phases. Ignoring conduction this means initial expansion of water will be 150–2000 times the other concrete phases.

Already, a convincing body of evidence indicates the high potential of microwaves for selective fracture and liberation of concrete, from the early work by Figg (1974) who observed a reduction in concrete strength and increase in the ease of separation of cement and aggregate phases when concrete is exposed to lower power microwaves, to the more recent work on improved beneficiation of recycled concrete aggregates using microwaves by Akbarnezhad et al. (2011). It is worth emphasising that microwaves induce stresses from multiple sources located within the particle. This is in contrast with standard comminution techniques that apply stresses through few external contact loads and the reason microwave based comminution techniques are deemed to have such potential. Using purely physical means, namely through a series of high velocity impacts, Tomas et al. (2000) achieved an aggregate liberation grade of approximately 50% with specific energy consumption of 5.5–9.5 kWh/t, depending on the fragment size under consideration. Fracture behaviour favours the liberation of aggregate from cement due to the higher strength and stiffness of aggregate compared to cement (see Table 1).

This work presents a single-particle testing approach for studying the possibility of combining microwaves and physical comminution for recycling concrete, the goal being to produce material that can be reused as the raw constituents of concrete. This is clearly a technical challenge, but if selective liberation of aggregate and cement could be harnessed efficiently then the recycling of concrete would not be restricted to downcycling operations like backfilling or as RCA with the aforementioned limitations, arguably neither of which is an efficient recycling option for such a high impact and added value product. The single-particle test work combines a single-mode cavity microwave test rig and a fast Hopkinson bar.

Fig. 1 presents the concrete recycling process rationale, which uses a combination of microwave-induced embrittlement followed by physical comminution and/or separation, and the translation to single-particle experimental testing and characterisation.

The justification for applying a single-particle approach to microwave-assisted embrittlement and recycling of concrete is that it permits breaking the process into its most elementary steps.

Table 1
Typical properties of aggregates and cement found in the literature.

Concrete phases	Relative dielectric constant	Loss factor	Expansion coefficient (μm/°C)	Specific heat (J/kg °C)	Modulus of elasticity (GPa)	Compressive strength (MPa)	Density (kg/m^3)
Aggregate	3–15[b,e,f,g,i,k]	0.08–0.2[e,i,k]	6–13[a,b,c]	740–920[a,b,d]	50[a,b]	60–130[a]	2320–2700[j]
Cement	5.3–10[b,h,i]	0.48[i]	18–20[b,c]	1550–1600[a,b]	25[a,b]	21[a]	1290–1540[j]
Water	80[a,k]	12[k]	210[a]	4200[a]	–	–	1000[a]

[a] Engineeringtoolbox.com.
[b] Akbarnezhad et al. (2011).
[c] Youtcheff (2011).
[d] Schärli and Rybach (2001).
[e] Ulaby et al. (1990).
[f] Martinez and Byrnes (2001).
[g] Knight and Abad (1995).
[h] Pokkuluri (1998).
[i] IMS.
[j] Walker (2011).
[k] Metaxas and Meredith (1988).

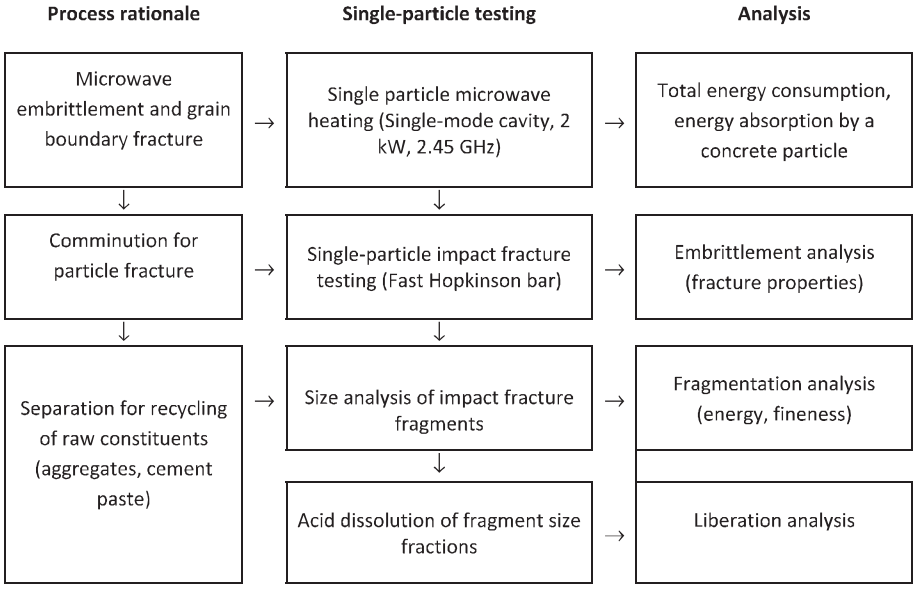

Fig. 1. Concrete recycling rationale and corresponding single particle testing and analysis approach.

In principle, this approach allows changes in material properties and energy consumption to be tracked at every step, thereby giving a firm basis for understanding, improving and developing an industrial process. In the present work, single-particle tests and analyses are presented in detail.

2. Materials and methods

2.1. Concrete samples

The end objective of this work is to produce high purity cement, aggregate and sand concentrates from demolition concrete, thereby achieving complete concrete recyclability. In order to develop an understanding of the mechanisms at play, concrete particles were produced under controlled conditions using CEM 1 52.5 Portland cement. This is a high quality and versatile cement that has been used for many years and complies with the European standard SN EN 197-1, containing at least 95% fine ground Portland clinker. The concrete was prepared with a water-to-cement ratio (w/c) of 0.6, which yields complete hydration of the cement. The aggregate-to-cement ratio (A/C) used was 2.6%, or 72% aggregate by mass on a dry basis, a common value for standard applications. After curing it was confirmed by dissolution of the cement phase that the aggregate phase constituted approximately 60% of the concrete mass, which is close to the 62% mass fraction used in the original mix. The concrete was cast in 100 mm thick slabs, allowed to cure for 28 days in water then cut into $10 \times 10 \times 100$ mm rods. These were stored for seven months before being cut using a Buehler HC 15 diamond blade into approximately 10 mm cubes for single-particle testing.

The concrete was prepared using siliceous NA with particle size in the range 2–2.5 mm. Naturally, the size distribution of aggregate in the cubic particles differed slightly from the original one as some aggregates were sectioned during block cutting. The aggregate size distribution after cutting was measured by selective dissolution of the cement paste and it is this that is presented as the aggregate size distribution. The cement dissolution protocol is discussed later in this article.

2.2. Experimental set-up

The two pillars of the experimental program designed to explore the proposed concrete recycling scheme are a 2 kW/2.45 GHz single-mode microwave test rig from SAIREM (www.sai-

rem.com) and a fast Hopkinson bar. The former is used to subject concrete particles to microwaves, whereas the latter is used to both impact fracture the concrete particles and access their fracture behaviour. A 2.45 GHz microwave test rig was chosen as free water exhibits a higher loss factor at this frequency than at 915 MHz, the other standard industrial microwave frequency and so the concrete should heat faster.

The microwave test rig (see Fig. 2) comprises an 86×43 mm rectangular wave guide and a single-mode sample cavity. The cavity is designed to hold a 30 mm diameter silica (microwave-transparent) tube holder inside which concrete particles are placed for testing. In the tests reported here, one single concrete particle is placed inside the sample tube. The test rig allows the microwave power applied to particles to be adjusted so as to produce a continuous standing wave with an intensity of up to 2 kW. Also included in the microwave rig are a timer to control exposure time and a reflected power detector that records the instantaneous energy absorbed during a test.

The comminution properties of individual concrete particles, whether untreated or treated with microwaves, are tested using a short vertical Hopkinson bar, the essential features of which can be found in Bourgeois and Banini (2002). The rod used here is made of 43CrMo4 steel with length 1.5 m and diameter 20 mm. The compression wave is measured using a full Wheatstone bridge with 540 Ω semi-conductor strain gages from Micron Instruments with a gage factor of 140. Bridge balancing and conditioning is achieved with an MGCPlus system from HBM. The 0–10 V signal output by the ML10B amplifier is sampled and digitised at a rate of 1 MHz using a Spectrum PCI Express data acquisition card. Overall, the experimental set-up is a highly sensitive measurement system, which allows precise measurement of the force applied to, and energy absorbed by the particle during a dynamic impact.

The value of the Hopkinson bar testing apparatus is twofold. Firstly, analysis of the output signal yields the total energy absorbed by the particle during the impact and, under favourable conditions, gives indicators of a particle's degree of embrittlement through measurement of fracture-sensitive properties such as energy-at-first-fracture, particle strength and toughness. Secondly, since the impact of a single particle can be considered as an elementary comminution event, analysis of the post-impact fragment size distribution and liberation gives us direct insights into the comminution/liberation/energy relationship for the particles under study.

2.3. Post-treatment data analysis

The main issue with concrete recycling is one of energy consumption. As indicated earlier, the energy absorbed by the particle during impact testing, whether microwave-treated or untreated can be quantified precisely using the Hopkinson bar. Measurement of the energy absorbed by single particles during microwave tests is not so straightforward unfortunately. The microwave test rig used in this work is an open system, as shown in Fig. 2, so that energy absorbed by a single concrete particle during exposure to microwaves is lost to the particle's surroundings through water vapour losses and heat exchange with the air. Temperature measurements of the particle surface, given the small size of the particles tested in this work, could be used to estimate the average particle temperature, hence the energy absorbed during exposure to microwaves. In this work mean particle temperature was estimated by combining measurements of mass loss during microwave tests and thermo-gravimetric analysis (TGA) mass loss curves. Combining the energy absorbed during impact testing and estimates of absorbed microwave energy gave a value for total specific energy consumption.

The size reduction and liberation analysis is the other side of the problem that needs to be quantified. Size reduction is measured by dry sieving the product of the single-particle Hopkinson bar tests through a series of narrow sieve fractions. Strictly speaking, liberation can only be measured by electron microscopy and image analysis, using highly dedicated equipment such as the MLA (Gu, 2003) or the QEMSCAN (Gottlieb et al., 2000). In this study, for budgetary and time constraints, liberation is quantified with a simple technique that takes advantage of the material being made of phases with different chemical activity. Individual size fractions produced by the first sieving step is dissolved separately using 25 ml of a 2 M hydrochloric acid solution per gram of concrete. This is done at room temperature in a glass beaker with a magnetic stirrer rotating at 300 rpm. Sufficient time is allowed for all the cement to dissolve, which varies between 20 min for small fragments to 2 h with >5 mm concrete fragments. At any rate, calibration tests were carried out to prove that the siliceous aggregates did not dissolve significantly under such conditions. Once a size fraction has been dissolved, it is re-sieved. Aggregate liberation in that size fraction is calculated by comparing the mass of aggregates in the size fraction before and after dissolution, with the assumption that the aggregates that stay in the size fraction before and after dissolution were liberated. The technique and corresponding liberation calculation formulae can be found in Kiss and Schönert (1980).

3. Results and analysis

3.1. Single-particle microwave testing and analysis

As per Fig. 1, the single-particle testing process starts with subjecting the particle to microwave heating. Due to the interrelationship between electric field, the input power of the microwave

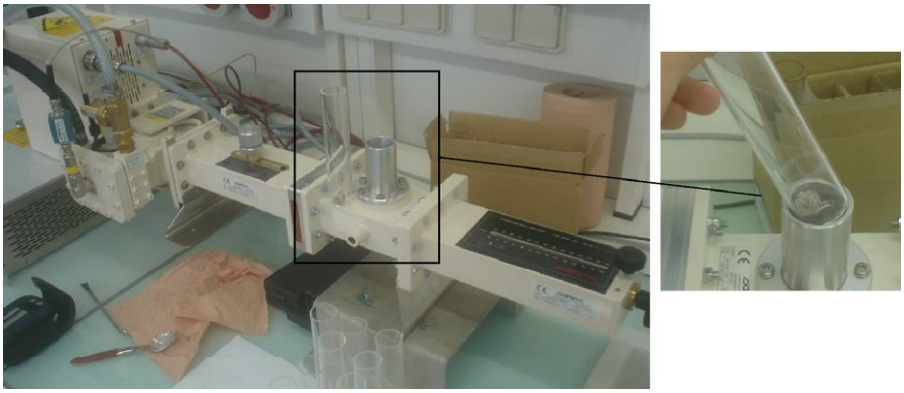

Fig. 2. Left: single-mode cavity microwave test apparatus from SAIREM (www.sairem.com); Right: sample holder with a 10 mm concrete particle.

system and the sample, optimum settings for the iris and short-circuit piston were found manually using a typical sample before treating test samples. Once these conditions were determined, they were used with all the single-particle tests, so that all samples would receive as near as possible to maximum and equal amounts of energy. Samples were treated for 10, 30 or 50 s or left untreated.

Both the input and reflected power during a single particle microwave test are measured at a sampling rate of 1 kHz during a single-particle microwave test. They are recorded as a 0–10 V analogue signal, whose range corresponds to the 0–2000 W power input range of the microwave system. The measured raw voltages are filtered in two steps, first using a Fast Fourier Transform with a 50 Hz cut-off frequency, then with a simple moving average of width 100 points or 0.1 s. The actual power absorbed by the system during the test is then calculated by difference between the smoothed input power and reflected power signals. Fig. 3 shows one example of input, reflected and absorbed power signals, for a 10 mm concrete particle with a mass of 2.10 g exposed to a power input of 1900 W or 95% of the system's nominal power input for 43 s. It can be seen that this system reaches the set power level in approximately 3 s.

The energy absorbed by the system during a microwave test is calculated by integration of the power signal. In the case of Fig. 3, we find that the integral of the power input yields 81.3 kJ. This value is just under the nominal power input, 1900 W $\times$ 43 s = 81.7 kJ, as the power input takes a few seconds to reach its nominal 1900 W setting. In this case, the system absorbed 18.4 kJ or 22.6% of the power input. This value is typical of all the tests that were carried out, for which it never seemed possible to input more than 20–25% of the input power into the system.

3.2. Estimation of absorbed microwave energy by TGA

As discussed earlier, the microwave system used here is an open system, so that the value of the energy absorbed does not correspond to the energy really absorbed by the particle.

Estimation of the energy absorbed by a single particle during a microwave test is inferred from thermogravimetric analysis (TGA) of the cured cement paste, performed using a TA Instruments Q600 thermal analyzer. Cement was mixed and cured in exactly the same way as the concrete but using no aggregate, then cut to yield 10 mm cement cubic particles. Cement particles were subjected to microwaves using the exact same method as the concrete treated for 50 s, such that TGA curve could be measured for both untreated and microwave treated cement samples. The TGA curves, shown in Fig. 4 are almost parallel from approximately 160 °C onwards. From this it is concluded that the temperature of the treated cement reached 160 °C during microwave exposure. The difference in mass lost between untreated and treated cement, 9.3% in this case, is due to be water loss only. Indeed, the temperature did not reach the 425–500 °C temperature range at which portlandite decomposes (Lee et al., 2009), which is further confirmed by the fact that the same mass loss is obtained in this temperature region in both cases. This mass loss, which equals 5 wt%, gives the amount of portlandite in the cement. The small hump that is seen around 700 °C corresponds to the decomposition of calcium carbonates.

Accounting for the 62 wt% aggregate in the concrete, the TGA curve for the cement phase was converted to a TGA curve for the concrete as a whole, which is shown in Fig. 5. The mean temperature reached by microwave samples was estimated by assuming that the cement in concrete loses the same mass fraction of material at the same temperature as pure cement phase under TGA analysis and no mass is lost from the aggregate during TGA or microwave treatment. The mean mass lost from concrete treated for 10, 30 and 50 s is 0.6%, 6% and 7% respectively. From the adjusted TGA curve this corresponds to a temperature of 52 °C, 125 °C and 160 °C, Fig. 6. From the TGA curve and supported by the 10 wt% water used in the original concrete mix this would seem to confirm that all mass lost during microwave heating was water and the temperature of portlandite degradation, approximately 400 °C, was not reached. There was visual confirmation in all single particle microwave tests that a significant amount of water was released, some of which would condense on the upper part of the silica sample holder (see Fig. 2).

An alternate technique would have consisted in analysing the whole concrete by TGA. Given that TGA requires only 50 mg of material, this would have meant a very fine grinding of the concrete prior to TGA analysis, to ensure a representative concrete sample. Analysis of pure cement is simple and was deemed suitable for analysis by TGA as aggregate does not show any measurable mass loss until very high temperatures.

A first approximation of microwave energy absorbed by the sample was determined from the known fractions of aggregate to cement, typical values of specific heat from Table 1, 830 J kg^{-1} °C^{-1} for aggregate and 1550 J kg^{-1} °C^{-1} for aggregate and the enthalpy of evaporation of water and the mass lost during microwave treatment. For 10 s, 30 s and 50 s this equals 14, 70 and 87 kWh/t of microwave energy, approximately 4% of the energy absorbed by

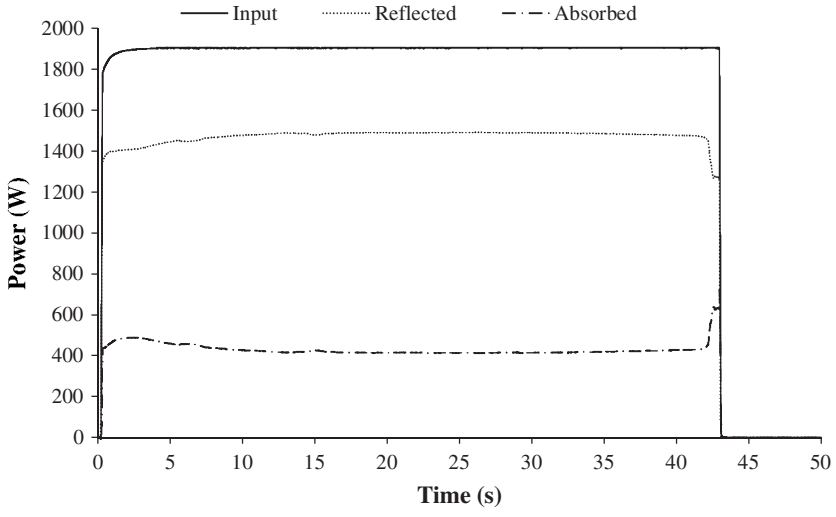

Fig. 3. Example of processed microwave power measurement for a single particle microwave test.

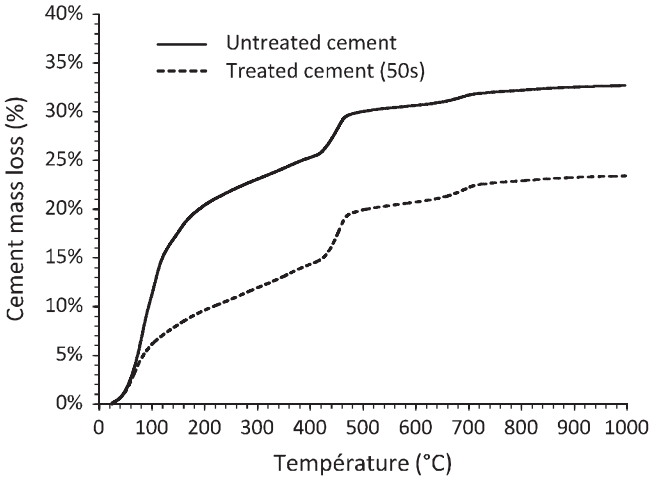

Fig. 4. TGA curve for cured cement, untreated and microwave treated for 50 s.

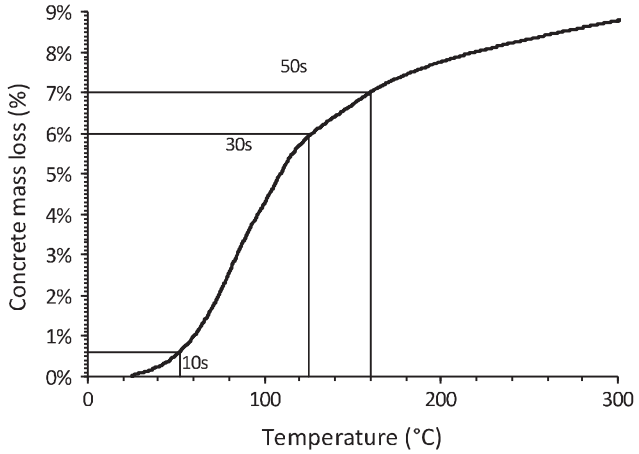

Fig. 5. TGA curve for concrete, showing measured mass loss and maximum temperature estimations for 10 s, 30 s and 50 s microwave exposure.

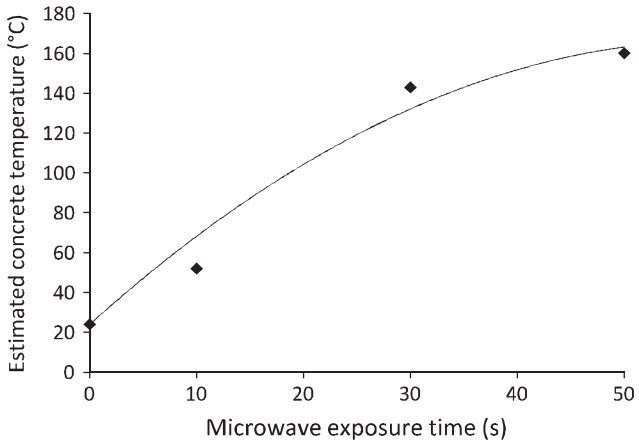

Fig. 6. Estimated temperature of single concrete particles as a function of microwave exposure time.

the system. These values are 1 to 2 orders of magnitude higher than the 1–3 kWh/t reported in the literature with ores (Ali and Bradshaw, 2009). Notwithstanding the errors in the above calculations, the energy values seem reasonable. Indeed, when considering that the electric field applied here is only one tenth that used by Ali and Bradshaw with a 30 kW generator and exposure times of a few milliseconds only, recalling that heating rate, the key factor in stress formation, is proportional to the square of the electric field strength, it is not surprising to obtain higher mass specific energy consumption.

As some concrete samples were observed to glow and others showed evidence of melting, burning and spalling it is probable that local temperatures were significantly in excess of the average maximum temperatures ascertained from the TGA curve.

3.3. Single-particle impact fracture testing

Single-particle Hopkinson bar testing yields impact size reduction and liberation data by analysis of the fragments produced after impact, along with measurement of the level of damage of a concrete particle, before and after microwave treatment. Fig. 7 shows typical impact traces measured with the fast Hopkinson bar for untreated and microwave-treated 10 mm concrete particles, using a 40 mm bearing ball dropped from 100 mm. For sake of comparison, all impact tests reported here were carried out using the same impact conditions. Of the whole trace, only the first 500 μs are shown here in order to emphasise the particle's compression phase during which visible fracture events may occur, yielding measurements of energy-at-first-fracture and particle strength.

Under the conditions of the impact test, the untreated concrete particle exhibits a Hopkinson bar impact behaviour that is typical of elastic brittle materials, showing a rapid linear force rise that leads to a sharp first fracture event. The particle in this case first fractured at a force of 768 N, after having absorbed 7.1 mJ, giving a specific fracture energy of 3.6 mJ/g and particle strength of 7.7 MPa.

The gradual change in mechanical behaviour with exposure time is best seen when zooming on the first 20 μs, as shown in Fig. 8. Indeed, we see a monotonic decrease in the slope of the force rise during the compression before the first fracture event, which is a direct measure of the reduction in stiffness (alt. increase in damage) of the concrete particles with exposure time.

Under the impacts conditions used, which were kept the same for all concrete samples in order to compare their subsequent fragment size distribution and liberation, the Hopkinson bar signal does not reveal any identifiable fracture event for the particle treated for 50 s (see Fig. 7). Particles have undergone such a high level of damage that it no longer behaves like an elastic-brittle material. The mechanical behaviour of microwave treated concrete particles is particularly interesting. Impact tests with very low amounts of energy were carried out to assess whether some residual elastic-brittle behaviour could be detected with microwave particles treated for 50 s. On rare occasions only did microwave treated particles exhibit any visible fracture event; hence it is difficult to measure fracture energy or particle strength with the Hopkinson bar test for particles treated under such conditions. For this reason the maximum force experienced by the concrete particles during an impact is used as a direct indicator of the mechanical strength.

Fig. 9 and Table 2 give measurements obtained from analysis of Hopkinson bar tests that quantify the change of embrittlement between untreated and treated concrete particles. Fig. 9 was included here to give the reader some idea about the measured variability from one concrete particle to the next. All this quantitative data demonstrate that microwave treatment was able to alter concrete particles in a profound way, with all reported properties being reduced by a factor of 3 or more.

It is noted that particle strength values reported here, which are calculated using an approximation proposed by Tavares and King (1998) for single-particle impact test analysis cannot be compared with standard values of stiffness reported for concrete. The values can however be compared in relative terms.

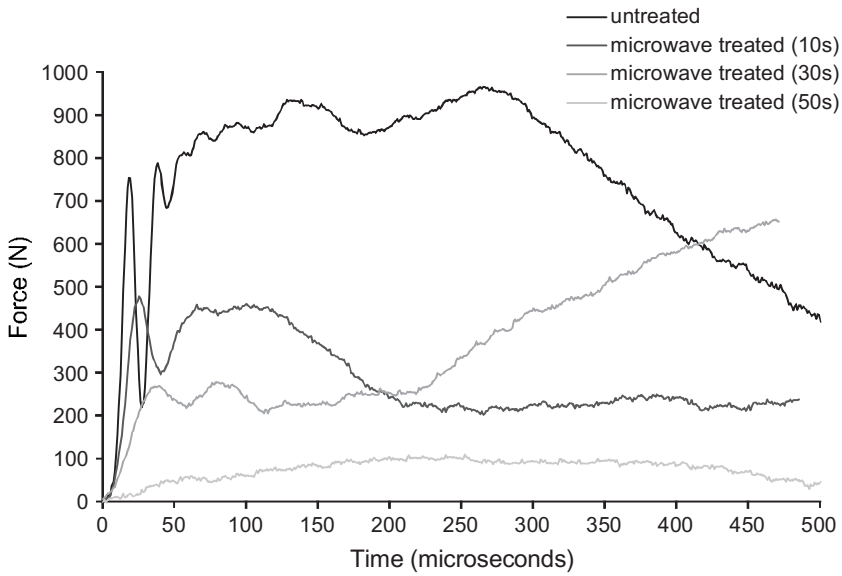

Fig. 7. Example of force–time data for an untreated 10 mm concrete particle (40 mm bearing ball; 100 mm drop height).

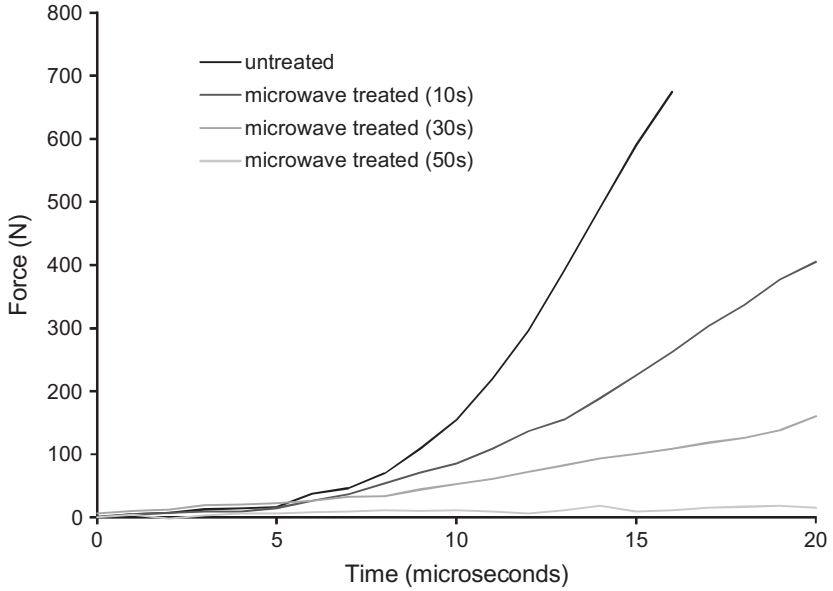

Fig. 8. Direct measure of concrete embrittlement increase with microwave exposure time. Decreasing slope of force–time curve is a direct evidence of the reduction of concrete's modulus of elasticity.

3.4. Fragmentation of concrete particles and liberation of constituents

Fig. 10 gives the fragment size distributions obtained with both untreated and treated concrete particles after Hopkinson bar impact testing. Impact tests were carried out with a 40 mm (260 g) bearing ball dropped from 100 mm. Fragmentation of untreated concrete generated large particles, 83 wt% of the fragments having a size coarser ($\geqslant$2.8 mm) than the largest aggregate particles. In fact, untreated particles mainly yielded fragments larger than 5 mm, which correspond to the 10 mm concrete particle being split in two nearly equal halves during impact. In contrast, only 14 wt% of concrete fragments from 50s tests are larger than the largest aggregate particles. The fineness of the fragments obtained with the concrete particles treated for 50 s is significantly greater than that obtained with the untreated particles. Concrete treated for 10 s and 30 s demonstrate an intermediate fragment size but the rate of change is not constant. The increasing fineness of the fragment size distribution adds to the earlier observations about the dramatic change in fracture properties with microwave exposure time. It permits conclusion that the microwave process produces extensive microstructural damage, creating significant amounts of new surface area, which results in a strong change in comminution behaviour of the concrete.

Liberation is measured by the aggregate and cement distributions after acid dissolution and can be seen in Figs. 11 and 12. Fig. 11 shows that nearly 80% of the aggregates remain embedded in the +5 mm fragment size fraction for untreated particles, which reflects the near absence of liberation of the aggregate phase. In contrast, the 50 s treated particles exhibit a size distribution that is close to that of the aggregates. Similarly, Fig. 12 gives the amount of cement on a size-by-size basis after impact testing on the Hopkinson bar. What can be seen here is that the longer exposure time produces a very large amount of fine cement particles, with nearly 50 wt% finer than 1.8 mm.

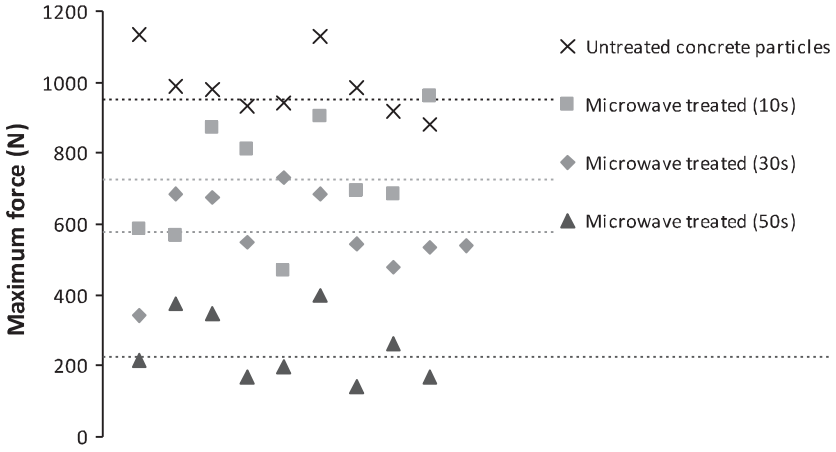

Fig. 9. Maximum force measured with Hopkinson bar with untreated and treated 10 mm concrete particles (40 mm bearing ball; 100 mm drop height).

Table 2
Mean fracture properties measured with the fast Hopkinson bar for 10 mm concrete particles, with and without microwave treatment (N.B.: With 50 s exposure, values of energy-at-first-fracture and particle strength are not representative of the average behaviour of corresponding particles as only very few particles yielded distinct fracture events).

	Maximum force (N)	Energy-at-first-fracture (mJ/g)	Particle strength (MPa)
Untreated concrete particles	948 (min: 538, max: 1423)	2.7 (min: 1.7, max: 4.4)	4.3 (min: 1.3, max: 7.6)
Treated particle (10 s)	727 (min: 468, max: 1156)	2.7 (min: 0.8, max: 3.4)	3.7 (min: 0.8, max: 5.7)
Treated particle (30 s)	573 (min: 334, max: 1150)	4.1 (min: 2.3, max: 11)	2.2 (min: 1.5, max: 3.5)
Treated particle (50 s)	226 (min: 100, max: 644)	1 (min: 0.4, max: 2)	0.6 (min: 0, max: 1.3)

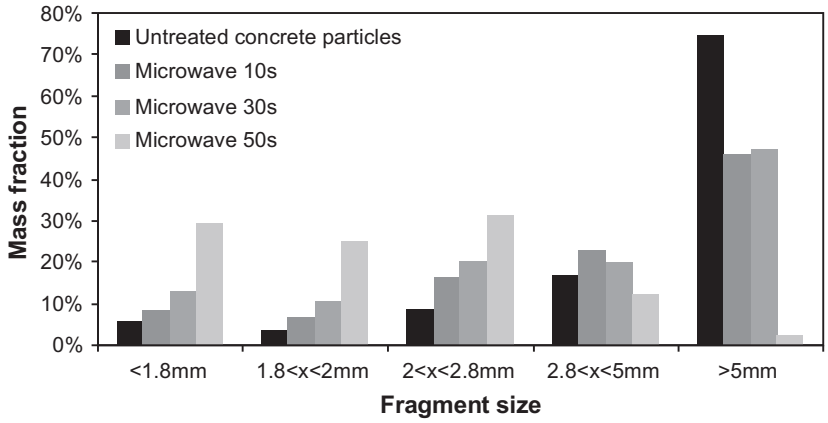

Fig. 10. Fragment size distribution from single-particle impact tests with untreated and treated 10 mm concrete particles (40 mm bearing ball; 100 mm drop height).

Although one may argue that the fine cement fragments were produced by the impact, it is more likely that the microwaves were responsible for shattering the continuous cement phase throughout the concrete particle volume. Such a reasoning would tend to indicate that the microwave process is not as selective as originally thought in that it does not target aggregate-cement grain boundaries specifically, otherwise cement fragments would be expected not to be so drastically shifted towards the fine particle size classes. This is supported by the minimal similarity between the aggregate distribution in the concrete and that in the concrete treated for 10 s and 30 s. From such limited data, and without looking at the texture of fragments after fracture, it is premature however to make a conclusion regarding the selectivity of microwave induced fracture of concrete.

The overall aggregate liberation is plotted in Fig. 13. There seems to be a small gain in aggregate liberation from 10 s to 30 s exposure time, however the gain is significant between 30 s and 50 s. The nature of this change is unknown at this stage; however it is clear that this change is targeting some of the phases that are present at the interface between aggregates and cement paste due to the large increase in liberation. Untreated concrete particles did yield very low aggregate liberation, with a value of 3.4%. Liberation is therefore found to increase with exposure time; however the increase is not linear. After an exposure of 50 s approximately 60% of the aggregate particles were liberated after impact. The greatest increase in liberation occurred between the 30 s and 50 s exposure time, which echoes the change in fragmentation behaviour discussed earlier between these exposure times.

3.5. Combining microwave and impact comminution

As indicated earlier in the paper, the single-particle approach was implemented as it permits investigation of individual processes, for which energy absorption can be quantified in principle. Adding to the energy absorbed by single particles during microwave tests, which was discussed in Section 3.2., the fast Hopkinson

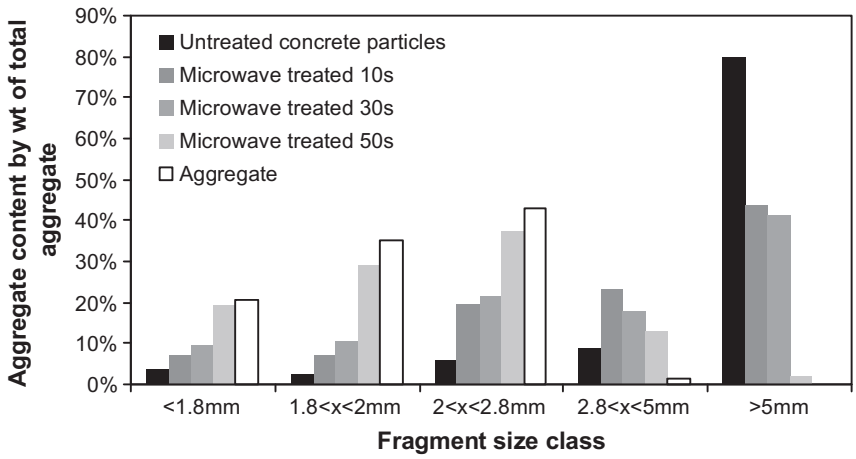

Fig. 11. Comparison of aggregate distribution between microwave treated and untreated 10 mm concrete particles after single-particle impact testing.

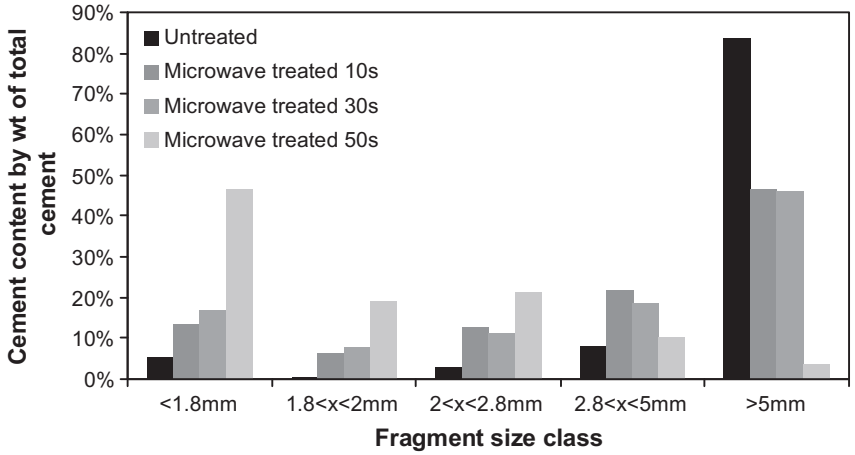

Fig. 12. Comparison of cement distribution between microwave treated and untreated 10 mm concrete particles after single-particles testing.

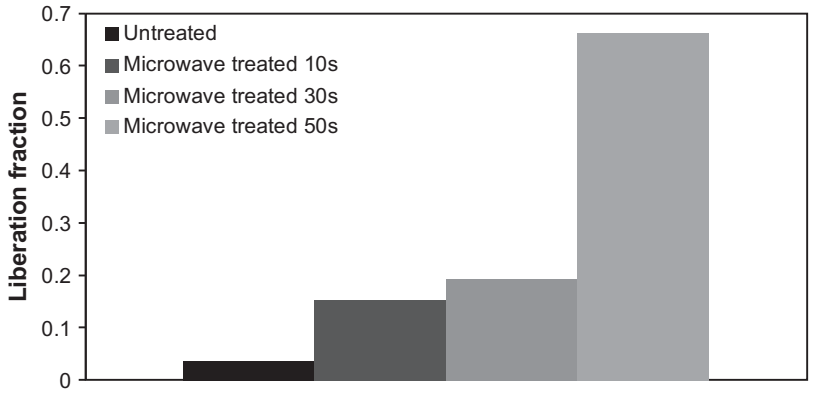

Fig. 13. Liberation of the aggregate phase.

bar yields measurement of the energy actually absorbed by the particle during impact tests. The impact conditions used here corresponded to 31 kWh/t. The fraction of impact energy absorbed by concrete particles decreased from close to 100% of the impact energy for untreated concrete to close to 55% for concrete treated for 50s.

The energy absorbed during microwave treatment plus impact fracture can therefore be added for every particle, such that the overall energy absorption can be quantified. Fig. 14 then shows the aggregate liberation as a function of the average energy absorbed by concrete particles during microwave and comminution tests, under the test conditions used in this work.

The balance of energy absorption changes with the length of microwave exposure, but in any case both microwave and size reduction processes both make significant energy contributions. Optimisation of the proposed process, which includes microwave

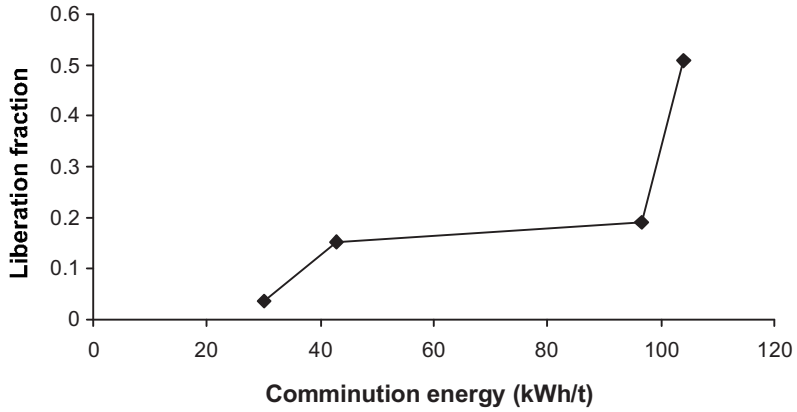

Fig. 14. Measured aggregate liberation as a function of the overall microwave and comminution energy.

heating followed by comminution, will come down first to an optimum end state for the material, whether or not the cement phase is to be recycled and how fine the fragments should be, then an optimum balance between physical and microwave processes before an optimisation of each process individually. As indicated earlier, due to the low power test rig that was used here, the energy consumption obtained is probably significantly higher than what could be obtained with high power microwave systems, say 30 kW or more. It is also important to note that the size distribution of the aggregates, as found in Fig. 11 is left unchanged, which is quite a valuable observation for the purpose of recycling.

4. Discussion

The nature of the changes in mechanical, comminution and liberation properties of concrete subjected to microwaves is largely unknown. The mechanisms behind such changes, which can be so profound as to remove all traces of elastic-brittle behaviour in concrete, are definitely related to modifications of specific mineral phases inside the cement matrix, in the bulk of the matrix as well as along aggregate-cement paste grain boundaries. More research is required to elucidate the nature of these changes, whose understanding is probably the key to finding the best conditions for applying microwaves to concrete with the aim of enhancing liberation of the phases with minimum energy consumption. As discussed earlier in this paper, one pivotal issue in understanding this process revolves around mapping the spatial distribution of phases inside concrete and measuring their properties at the molecular scale at which microwaves affect matter. From a process perspective, properties of the microwaves applied such as power, frequency, exposure time and application mode (pulse frequency) should also be investigated to improve the concrete liberation process.

The liberation of cement was not directly measured here. This would be an interesting addition to this work; however the method used to measure the liberation of aggregate dissolves the cement making this impossible. Cement liberation should therefore be investigated by image analysis techniques.

Besides the issues investigated in the paper, the proposed process raises many engineering related questions.

One engineering issue not addressed here is the separation of the aggregate and cement phases after the comminution step. If the intention is to also recycle the cement, the fact that microwaves pulverise the cement phase, leaving the aggregate particles unaltered seems to be of great value. Indeed, already powderised cement phase would be of value for recycling into the clinker making process, but it would also simplify the process of aggregate and cement separation, which would require only a simple screening step. Gravimetric separation, as suggested by Tomas et al. (2000) would probably be ineffective here, as the density of the aggregate and cement matrix are similar after microwave heating, approximately 2.7 g/cm^3 for the former and 2.3 g/cm^3 for the latter.

Another process parameter that has not been addressed here is increasing process efficiency by making use of the high temperature of concrete immediately after microwave treatment. One option is to increase embrittlement by quenching (Akbarnezhad et al., 2011). Another option could be to perform physical comminution at this elevated temperature. This is a subject for future work.

A third issue is that presented by steel reinforcement. Even assuming the steel and concrete is separated small amounts of ferric debris will remain in the concrete material. The debris could act as an 'initiator,' rapidly increasing the temperature of the material and leading to an overall increase of process efficiency. It could also pose a hazard to equipment, but this is beyond the scope of this project.

As previously stated significantly more powerful machines than those used in this work would be adapted to adopt this technology on an industrial scale (Ali and Bradshaw, 2009). This could be a simple continuous microwave/conveyor system. One could also imagine mobile systems that separate cement and aggregate onsite, which would revolutionise the demolition of concrete structures. This of course raises more engineering questions and is beyond the scope of this work.

5. Conclusions

Overall, test results show that concrete particles are severely damaged by exposure to microwaves, the greater the exposure time under the conditions tested in this work, the greater the damage. Concrete particles could be so damaged by microwave treatment that fracture behaviour of the treated concrete showed no resemblance with that of regular, untreated concrete.

Microwave treated particles showed improved comminution properties and liberation of both aggregate and cement phases after impact fracture, both increasing monotonically with duration of exposure to microwaves. As much as 60% liberation was obtained with 50 s exposure, as compared with less than 3.5% for untreated concrete. The effect of microwaves was most severe between 30 and 50 s exposure times; however the mechanisms responsible for the observed changes require additional research.

Under the test conditions used here, a comminution step is required to harvest the benefits of the severe damage induced by the microwaves, as particles remain largely as particles after microwave heating. Both the microwave heating and comminution processes contribute to the overall energy consumption of the proposed process. The process produces fine cement particles,

and does not appear to alter the aggregate particles; hence separation of the phases after processing does not appear to be a problem.

Future single-particle test work will be concerned with quantification of the process governing parameters, with the aim of optimisation on the basis of net energy consumption and degree of liberation. The key addition to the single-particle testing protocol presented in this paper will be microscopic investigation of sectioned cement after microwave treatment to reveal microscopic changes that occur within the concrete during exposure to microwaves, particularly fracture growth. Understanding the link between concrete microstructure, particularly the influence of the ITZ and selective embrittlement and liberation by microwaves is clearly a pivotal point for development of this process.

Acknowledgments

This research work is being conducted as part of the COFRAGE project, which is funded by the *Agence Nationale pour la Recherche* (the French National Research Agency) through the ECOTECH program. The authors would like to thank their partners from the *laboratoire de l'Intégration du Matériaux au Système* (IMS) for the work on the dielectric characterisation of concrete components (Table 1).

References

Akbarnezhad, A., Ong, K.C.G., Zhang, M.H., Tam, C.T., Foo, T.W.J., 2011. Microwave-assisted beneficiation of recycled concrete aggregates. Construction and Building Materials.

Ali, A.Y., 2010. Understanding the effects of mineralogy, ore texture and microwave power delivery on microwave treatment of ores, PhD dissertation. University of Stellenbosch.

Ali, A.Y., Bradshaw, S.M., 2009. Quantifying damage around grain boundaries in microwave treated ores. Chemical Engineering and Processing 48, 1566–1573.

Amankwah, R.K., Ofori-Sarpong, G., 2011. Microwave heating of gold ores for enhanced grindability and cyanide amenability. Minerals Engineering 24, 541–544.

Bourgeois, F., Banini, G., 2002. A portable load cell for in-situ ore impact breakage testing. International Journal of Mineral Processing 6, 31–54.

Constantinides, G., Ulm, F.J., 2004. The effects of two types of c–s–h on the elasticity of cement-based materials: results from nanoindentation and micromechanical modeling. Cement and Concrete Research 34, 1293–1309.

Costes, J.R., Majcherczyk, C., Binkhorst, I.P., 2010. Total recycling of concrete. Commissariat à l'Énergie Atomique.

Figg, J., 1974. Microwave heating in concrete analysis. Journal of Applied Chemistry and Biotechnology 24, 143–155.

Klee, H., 2009. Recycling concrete. The Cement Sustainability Initiative. The World Business Council for Sustainable Development.

Galbenis, C.T., Tsimas, S., 2006. Use of construction and demolition wastes as raw materials in cement clinker production. China Particuology 4, 83–85.

Gottlieb, P., Wilkie, G., Sutherland, D., Ho-Tun, E., Suthers, S., Perera, K., Jenkins, B., Spencer, S., Butcher, A., Rayner, A., 2000. Using quantitative electron microscopy for process mineralogy applications. Journal of the Minerals, Metals and materials Society 52, 24–25.

Gu, Y., 2003. Automated scanning electron microscope based mineral liberation analysis; an introduction to jkmrc/fei mineral liberation analyser. Minerals and Materials Characterization and Engineering 2, 33–41.

Kiss, L., Schönert, K., 1980. Liberation of two component material by single particle compression and impact crushing. Aufbereitungs-technik 5, 223–230.

Fischer, C., Davidsen, C., 2010. Europe as a recycling society, the European recycling map. European Environment Agency.

Knight, R., Abad, A., 1995. Rock/water interaction in dieletric properties: experiments with hydrophobic sandstones. Geophysics 60, 431–436.

Kumar, P., Sahoo, B.K., De, S., Kar, D.D., Chakraborty, S., Meikap, B.C., 2010. Iron ore grindability improvement by microwave pre-treatment. Journal of Industrial and Engineering Chemistry 16, 805–812.

Lee, J., Xi, Y., William, K., Jung, Y., 2009. A multiscale model for modulus of elasticity of concrete at high temperatures. Cement and Concrete Research 39, 754–762.

Malesev, M., Radonjanin, V., Marinkovic, S., 2010. Recycled concrete as aggregate for structural concrete production. Sustainability 2, 1204–1225.

Marland, S., Han, B., Rowson, N.A., Merchant, A.J., 1998. Microwave embrittlement and desulpurisation of coal. Acta Montanistica Slovaca 3, 351–355.

Martinez, A., Byrnes, A.P., 2001. Modeling dieletric-constant values of geologic materials: an aid to ground-penetrating radar data collection and interpretation. Kansas Geological Survey.

Metaxas, A.C., Meredith, R.J., 1988. Industrial Microwave Heating. Institute of Engineering and Technology, London.

Nawy, E.G. (Ed.), 2008. Concrete Construction and Engineering, second ed. CRC Press: Taylor and Francis Group.

Pokkuluri, K., 1998. Effect of admixtures, chlorides and moisture on the dieletric properties of portland cement concrete in the low microwave frequency range, Masters thesis. Virginia Polytechnic Institute.

Roy, D.M., Grutzeck, M.W., Shi, D., Lui G., 1993. Cement paste aggregate interface microstructure, Pensylvania State University, Strategic Highway Research Program of the National Research Council.

Schärli, U., Rybach, L., 2001. Determination of specific heat capacity on rock fragments. Geothermics 30, 93–110.

Scrivener, K.L., Crumbie, A.K., Laugesen, P., 2004. The interfacial transition zone (ITZ) between cement paste and aggregate concrete. Interface Science 12, 411–421.

Soutsos, M.N., Tang, K., Millard, S.G., 2010. Concrete building blocks made with recycled demolition aggregate. Construction and Building Materials 25, 726–735.

Tam, V.W.Y., Tam, C.M., 2006. A review on the viable technology for construction waste recycling. Resources, Conservation and Recycling 47, 209–221.

Tam, V.W.Y., Tam, C.M., Wang, Y., 2007. Optimization on proportion for recycled aggregate in concrete using two-stage mixing approach. Construction and Building Materials 21, 1928–1939.

Tavares, L.M., King, R.P., 1998. Single-particle fracture under impact loading. International Journal of Mineral Processing 54, 1–28.

Tomas, J., Schreier, M., Gröger, T., 2000. Liberation and separation of valuables from building material waste. Chemical Engineering and Technology 23, 809–814.

Ulaby, F.T., Bengal, T.H., Dobson, M.C., East, J.R., Garvin, J.B., Evans, D.L., 1990. Microwave dieletric properties of rocks. IEEE Transactions on Geoscience and Remote Sensing 28, 325–336.

Vorster, W., Rowson, N.A., Kingman, S.W., 2001. The effect of microwave radiation upon the processing of neves corvo copper ore. International Journal of Mineral Processing 63, 29–44.

Walker, R., 2011. Density of bulk materials. ⟨http://www.simetric.co.uk⟩, 1998–2011.

Youtcheff, J., 2011. Thermal coefficient of portland cement concrete. ⟨http://www.fhwa.dot.gov⟩, 2011.

http://www.engineeringtoolbox.com, 2005–2011.

4.2 Notes and explanations

This section makes supplementary comments to the published article, and justifies why the remainder of the work presented in this manuscript, in chapter 5, is focused on investigation of the effect of microwave heating at the local or textural level.

The key observations made in the article are that a combination of microwave heating and mechanical breaking can liberate large quantities of aggregate particles (Figure 13), significantly more than mechanical fracture alone. The cement paste was also highly liberated as can be seen by the high cement content in the fine fragment size class (Figure 12). Indeed this is indicative that if concrete waste is weakened by microwave heating before comminution, the only separation method required for cement and aggregate separation may be a dry screening step.

The idea that a key mechanism in the microwave induced embrittlement of concrete is an increased rate of heating in aggregate particles is presented for the first time in the article. While cement and aggregate have similar dielectric properties (Table 1) aggregate generally has a significantly higher density than cement. As microwave heating is a volumetric process this can explain why concrete discoloration after microwave heating, indicative of elevated temperatures is often greatest around aggregate particles (Figure 4.1). This also demonstrates that microwave exposure creates multiple heat sources within materials. Multiple heat sources mean multiple thermal gradients and therefore higher internal stress. Confirmation of the hypothesis of increased stress by quantifying fracture growth was one of the drivers for the development of an SEM image analysis technique, localised investigation.

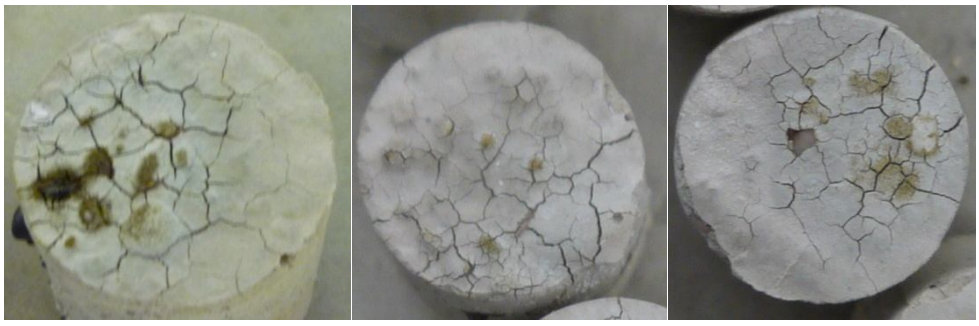

Figure4.1. Increased discolouration of concrete cement near aggregate particles after microwave heating

Microwave heating reduced the strength (Fig. 9) and stiffness (Fig. 8) of the concrete samples tested, so much so that long microwave treated samples, when tested on the HPB showed impact-time signals that no longer resembled brittle-elastic particles (Figure 7). Such particles may not need a comminution process any more intense than that experienced by particles during transportation on a conveyor belt or a fall down a chute. This suggests the possibility of a microwave-based concrete

recycling process completely devoid of a milling or crushing process therefore bypassing the low energy efficiency and wear issues associated with such processes.

The production of cement fines showed a more gradual increase (Figure 12) with microwave treatment than that seen for liberation, however long microwave treatment produced the most fines by a significant margin just as it produced the highest liberation value. This is consistent with the hypothesis that the most efficient concrete based recycling technique could be one based on the input of a lot of energy into the concrete so as to make milling unnecessary. However as the link between the microwave exposure, crushing and liberation has not yet been identified a localised investigation is required to properly justify this hypothesis.

In order to be a sustainable recycling process aggregate needs to remain largely intact through treatment and crushing. The aggregate distribution (Figure 11) shows that fine production never exceeded the fine content of the original aggregate and that aggregate distribution of long microwave treated samples approached the distribution of the original aggregate. This suggests that aggregate particles remained largely intact through the combination of microwave treatment and impact fracture tested, which is yet another valuable attribute of microwave heating for concrete recycling.

This initial work with cubic samples was the proof of concept phase; the technique was still being developed. The prescribed technique for calculation of liberation values described in Chapter 3 was not used for the long microwave treated samples; fewer sieves were used so the size classes were larger. The wide size classes used for liberation of aggregate in long microwave treated samples could place the liberation as low as 36%. This extremely conservative estimate is still significantly higher than the other samples tested. The value quoted is the largest possible value given experimental conditions if it is assumed that the aggregate size distribution matches that of aggregate before being cast into cubes, 66%. This is justified as the aggregate distribution in the fragments of long microwave treated samples so resembled the size distribution of the raw aggregate and the fragments contained so little visible cement (Figure 4.2). This choice also makes the progression of liberation values consistent with the observed progression of concrete strength.

Figure 4.2. Fragments of long microwave treated concrete broken on the Hopkinson bar. Fragments show very low cement content. Left; 2-2.8mm, right; 1.8-2mm sized fragments.

It should be noted that as the cubes were cut from a slab the aggregate in cubic samples must be smaller than that exhibited by raw aggregate so the stated value of 66% might be considered conservative.

The temperatures of microwave treated samples were estimated using the mass loss experienced by untreated samples during thermo gravimetric analysis (TGA). The mass lost was calculated using the mass before treatment and approximately 24 hours after treatment. Considering the colour of treated materials and the temperatures measured on samples S1-S5 the quoted temperature values (50-160°C) should be considered an underestimate. This can be explained primarily by water re-absorption after treatment and secondarily by the shallow slope of the temperature – mass loss curve above 180°C (Figure 5) were a small difference in the mass measurement corresponds to a large difference in temperature. In fact plasma formation and melting would suggest temperatures were above 500°C for long microwave treated samples, at least for some parts of some treated samples. The focus of the article was on what changes are observed when a concrete sample was treated with microwaves and temperature was just one of the ways used to describe the treatment, there is also power absorbed, exposure time and therefore energy absorbed. An incorrect temperature does not change the observations or conclusions in this case.

The force – time signal for untreated concrete in Figure 7 may show a signal perturbation similar to those seen in cylindrical samples described in Chapter 3. It is interesting to note that the impact signals of treated concrete cubes did not seem to exhibit this phenomenon. This is probably a product of the size and strength of the samples relative to the impact energy. In fact it is probably their small size, meaning shorter perturbation period that prevented the phenomenon from being identified first in cubic samples.

The fundamental conclusions of the article are clear. Microwave exposure can and does produce liberated aggregate particles when they are subsequently crushed. To understand the embrittlement mechanisms and the consequent strength loss, fragmentation and liberation requires a local investigation technique. Results of the local technique used in this work, SEM image analysis and the conclusions drawn from those results can be read in Chapter 5.

4.3 Bibliography for Chapter 4

[4.1] Lippiatt N & Bourgeois F. (2012) Investigation of microwave-assisted concrete recycling using single-particle testing. *Minerals Engineering* 31: P.71-81.

Chapter 5

THE EFFECT OF HEAT ON THE FRACTURE POROSITY OF CONCRETE

The manual highlighting method of SEM image analysis specifically developed for this work illustrated the effect of microwave heating on concrete. As the duration of microwave treatment was increased so did the extent of fracture growth within the concrete. Quantification of the fracture growth shows the link between the textural properties of fracture porosity and the mechanical properties of strength and stiffness, as fracture porosity increased the strength and stiffness of concrete samples decreased.

Principal component analysis is used to relate changes in textural properties with the original assumptions of fracture networks and their link to changes in mechanical properties. The fracture energy and fragmentation in particular were linked to the growth of what was labelled the secondary fracture network, which supported the explanation that the disparity between physical and textural liberation lays in the level of embrittlement and fracture growth in the cement paste phase. The principal component analysis also showed physical liberation and textural liberation had almost identical relationships to the principal components. This is clear evidence of the value of a textural perspective on mechanical and comminution properties.

TABLE OF CONTENTS FOR CHAPTER 5

5. THE EFFECT OF HEAT ON THE FRACTURE POROSITY OF CONCRETE

As described in Chapter 3 the SEM image analysis technique used in this work was designed with the specific purpose of describing the growth of heat induced fractures, described as fracture porosity that occurred in the macro and micro size range after heat treatment. This fracture porosity causes changes in mechanical properties of concrete and is directly linked to the liberation of aggregate particles after fracture. This makes fracture porosity the key textural property from the perspective of concrete recycling.

5.1 Development of image analysis scheme and the concept of fracture porosity

The SEM image analysis technique described in Chapter 3 was first presented in the KONA Powder and Particle article *Recycling-Oriented Investigation of Local Porosity Changes in Microwave Heated-Concrete* [5.1], from here on referred to as KONA2014. The key underlying concept of the analysis technique is that of fracture porosity.

It is well known that the strength of concrete is related to its porosity [5.2]. Figure 5.1 shows that the largest fraction of pore volume, as measured by MIP, is greater than 1µm in size. Fracture porosity describes the fractures observed by SEM in cement paste after heating. This distinguishes fracture porosity from porosity in general by its size, shape and origin (Figure 5.2).

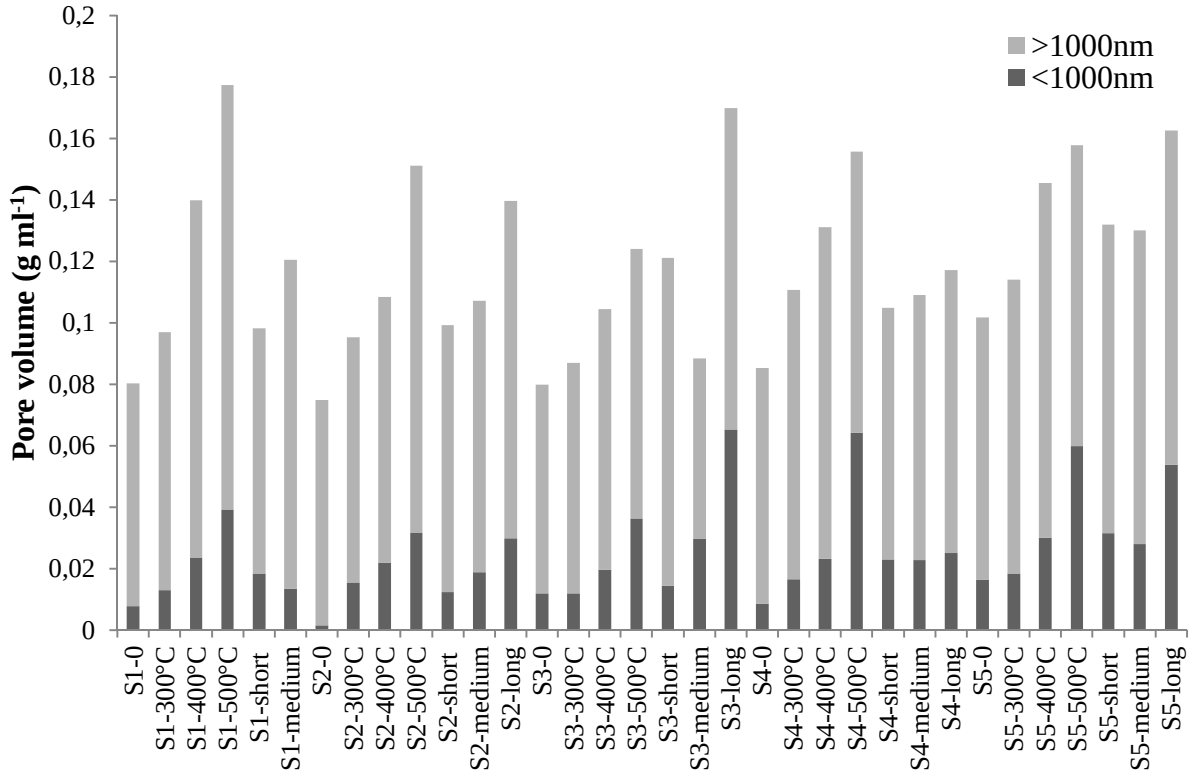

Figure 5.1. Porosity of raw, microwave and oven heated concrete samples measured by MIP showing that the larges fraction of pore volume is made up of pores above 1µm in size

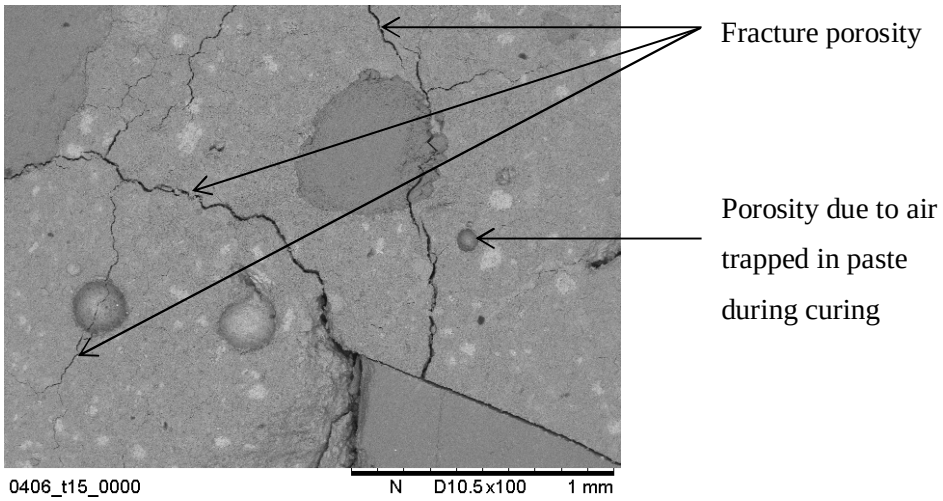

Figure 5.2. SEM image of short microwave treated S1 concrete sample showing interconnected heat induced fracture porosity.

5.2 Measurement of fracture porosity by SEM

The fracture porosity of concrete was measured in overall terms such as total fracture length and total fracture area but was also classified into two different types. By identifying individual branches as being in the primary and secondary networks it became possible to make measurements of connectivity and speculate on the mechanisms of microwave induced fracture growth in concrete.

5.2.1 Primary and secondary fracture networks

While the growth of the primary network (Figure 5.3 and Figure 5.4) was mostly similar between conventional and microwave heated materials the growth of secondary fractures progressed differently (Figure 5.5 and Figure 5.6), with microwave treated samples displaying greater secondary network growth at lower temperatures.

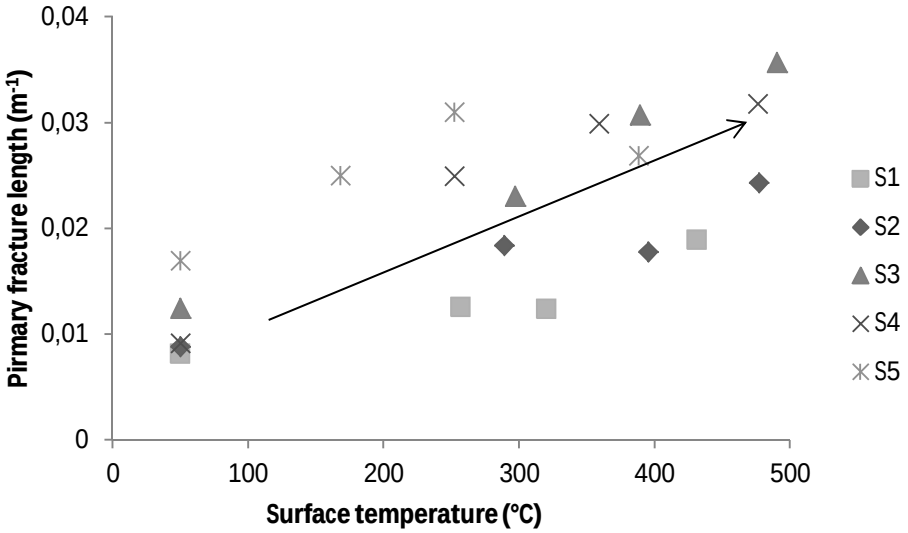

Figure 5.3. Consistent increase in the primary fracture network with microwave treatment, described by post treatment surface temperature

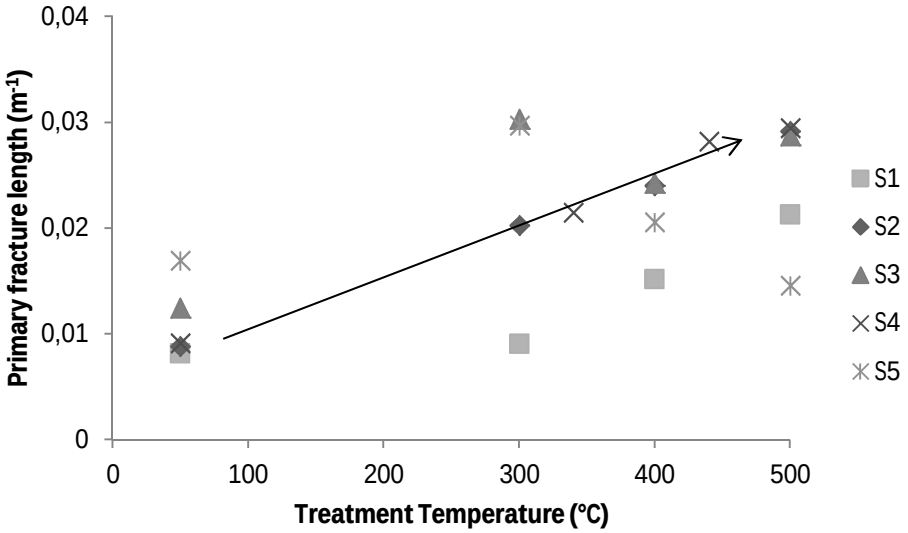

Figure 5.4. Externally heated concrete showed consistent growth of the primary fracture network as the treatment temperature was increased

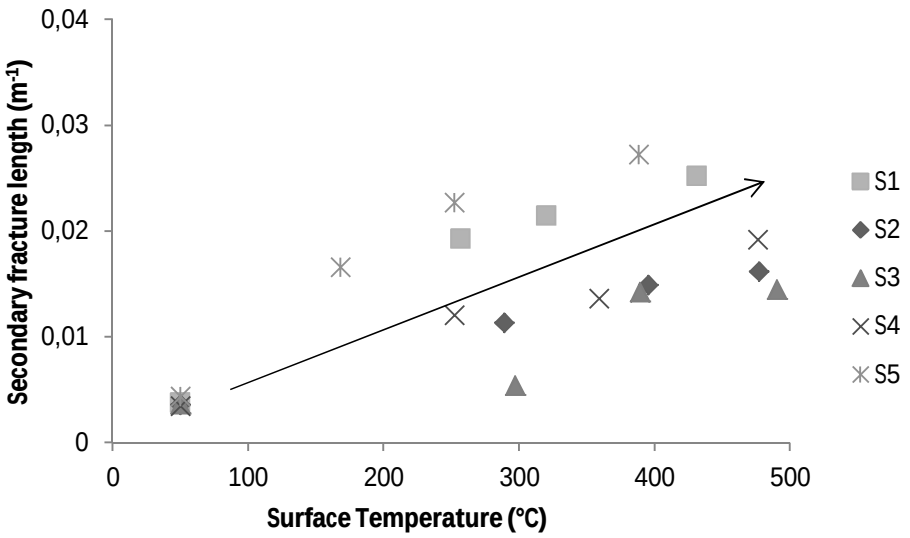

Figure 5.5. Illustration of the growth of secondary fractures in microwave treated concretes showing a consistent increase with the duration of microwave exposure, measured by surface temperature after treatment

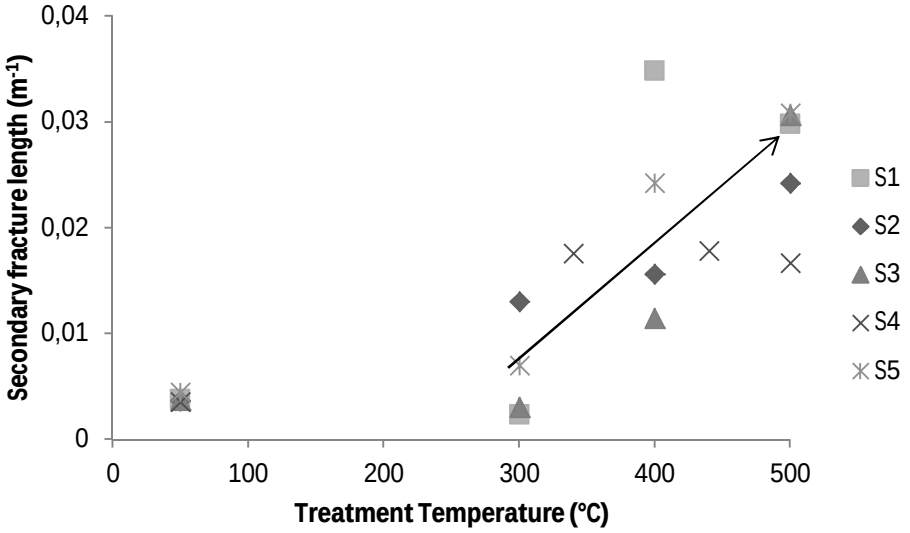

Figure 5.6. The secondary fracture network in conventionally heat treated concrete only sees significant growth after treatment temperatures have exceeded 300°C. This is in contrast to the growth of the primary network in conventionally heated concrete and both networks in microwave treated concrete.

The change in mechanical properties and fracture growth appeared to follow a strong inverse relationship. The secondary network (Figure 5.7) was linked to the fracture strength (Figure 5.8) of concrete and the primary network linked to the stiffness (Figure 5.9). Recall from Chapter 3 that the primary network is associated with fractures at the aggregate – cement interface and those that branch from this interface. By comparing Figure 5.5 and Figure 5.6 it can be shown that microwave and conventional heating processes do not generate the same fracture network in concrete samples.

Conventional heating does not produce the same level of secondary network fracture at lower temperatures as microwave heating.

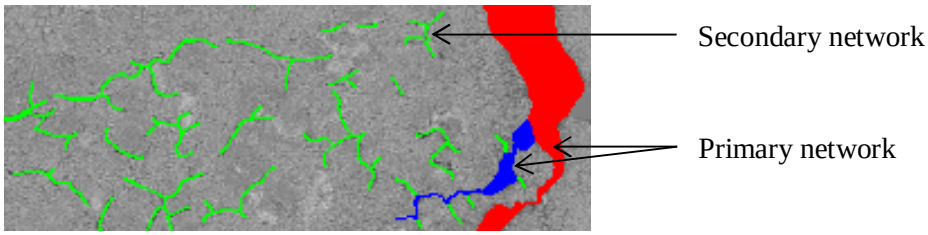

Figure 5.7. Concrete cross section illustrating the definition of primary and secondary network fractures

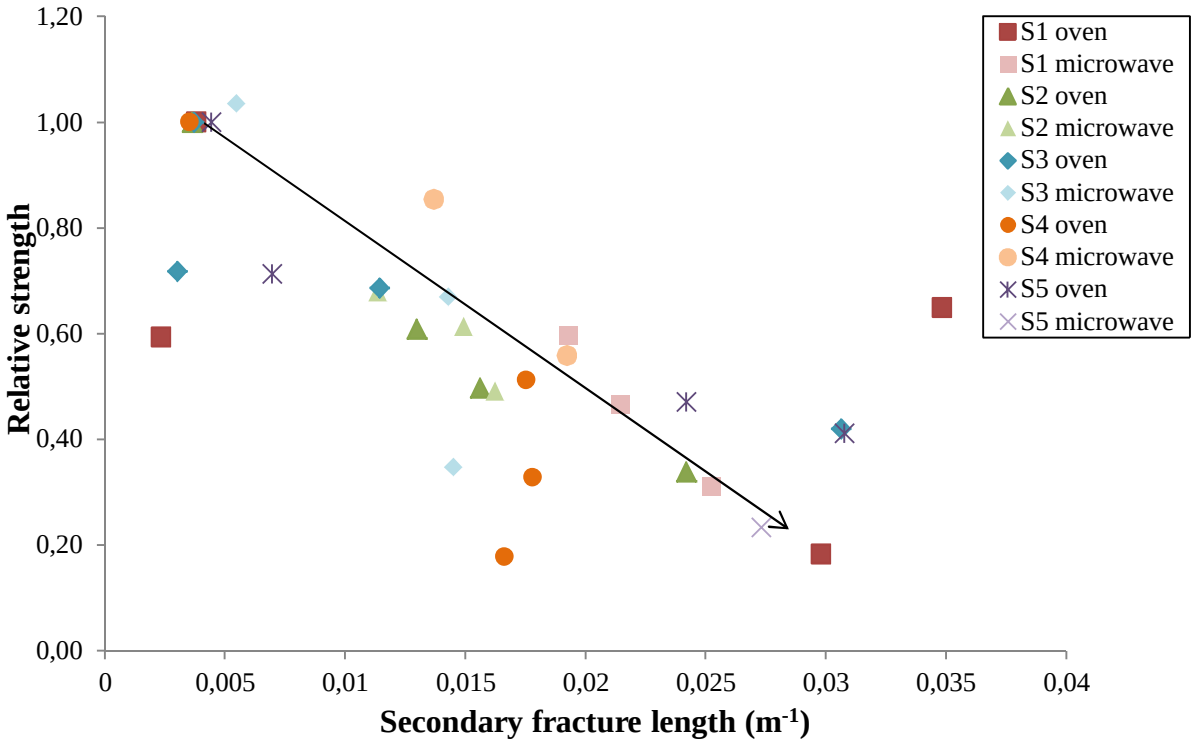

Figure 5.8. Illustration of the progressive decrease of concrete strength with the growth of secondary fracture networks in heat treated concrete samples.

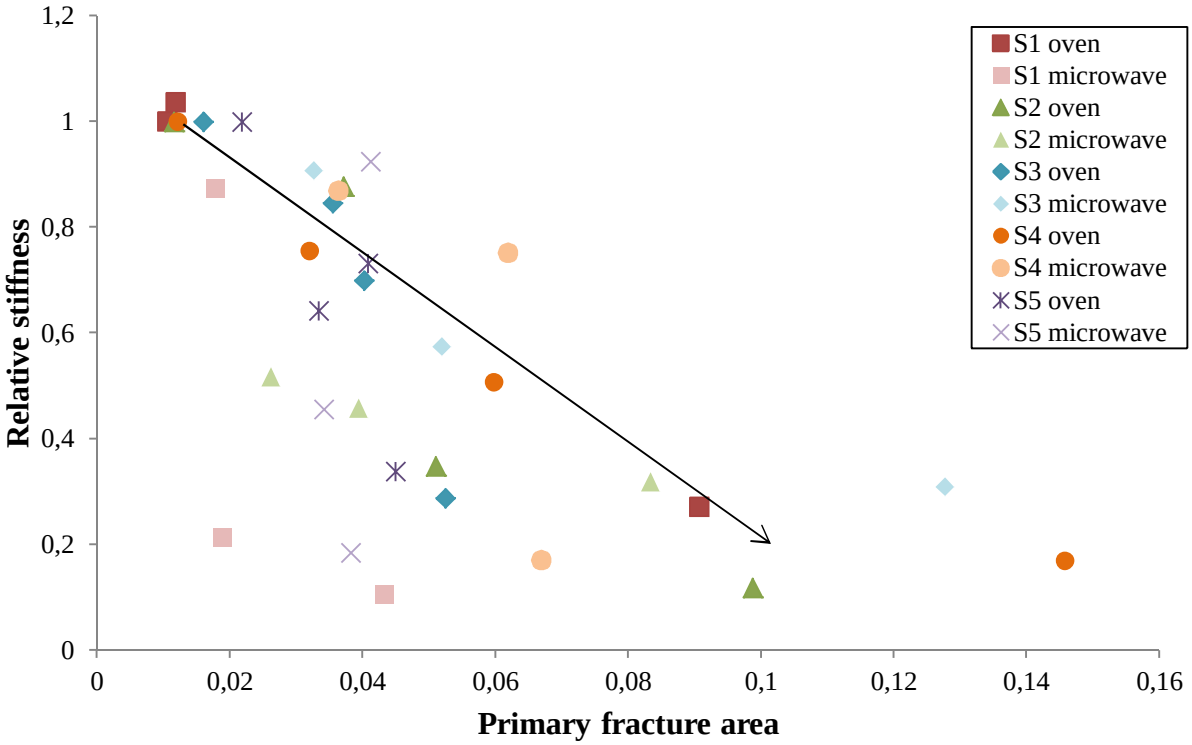

Figure 5.9. Decreasing concrete stiffness, as calculated by relative speed of sound method with the growth of primary fracture networks in heat treated concrete samples

Microwave treated concretes (KONA2014, Figure 25) all exhibit similar fracture porosity size distributions even while the volume of fracture porosity and the number of fracture branches increases. This suggests that the fracture porosity growth mechanism is applied evenly to concrete samples in their entirety. As the stresses due to differential thermal expansion could be assumed to be focused around single points, in this case the aggregate particles, once fractures have formed an increase in differential thermal expansion stresses can be expected to expand existing fractures. Drying shrinkage on the other hand affects the entirety of the cement paste phase so can be expected to both grow existing fractures and cause the formation of new ones. The effects of drying shrinkage most mirrors the observed changes in fracture distribution in both conventionally heated and microwave treated samples. One could conclude then that above 300°C for conventional treatment and for microwave treatments longer than short microwave treatment the principal embrittlement mechanism is drying shrinkage. On the other hand the difference between the branch size distribution of untreated and short microwave treated samples is substantial which requires the formation of many new fracture branches. For the case of microwave heating fracture growth due to differential thermal expansion can not be ruled out.

5.2.2 Textural vs physical liberation

The relationship between textural liberation, the apparent disconnect between aggregate particles and the cement paste and physical liberation, the fraction of aggregate particles liberated from the cement paste after impact fracture has already been discussed in the published work KONA2014. Figure 5.10

shows the range of physical and textural liberation values for all concrete samples. Importantly while both physical and textural liberation increased with microwave treatment and the temperature of conventional heat treatment the actual values of textural and physical liberation were very different. Even long microwave treated S1-S5 concrete samples saw significant differences between the textural and physical liberation values. This is in contrast with the physical liberation seen in concrete cubes (KONA2014, Figure 20). This can be explained by the significant size differences of the samples, which once again highlights the importance of an appropriate comminution technique, both before and after microwave treatment.

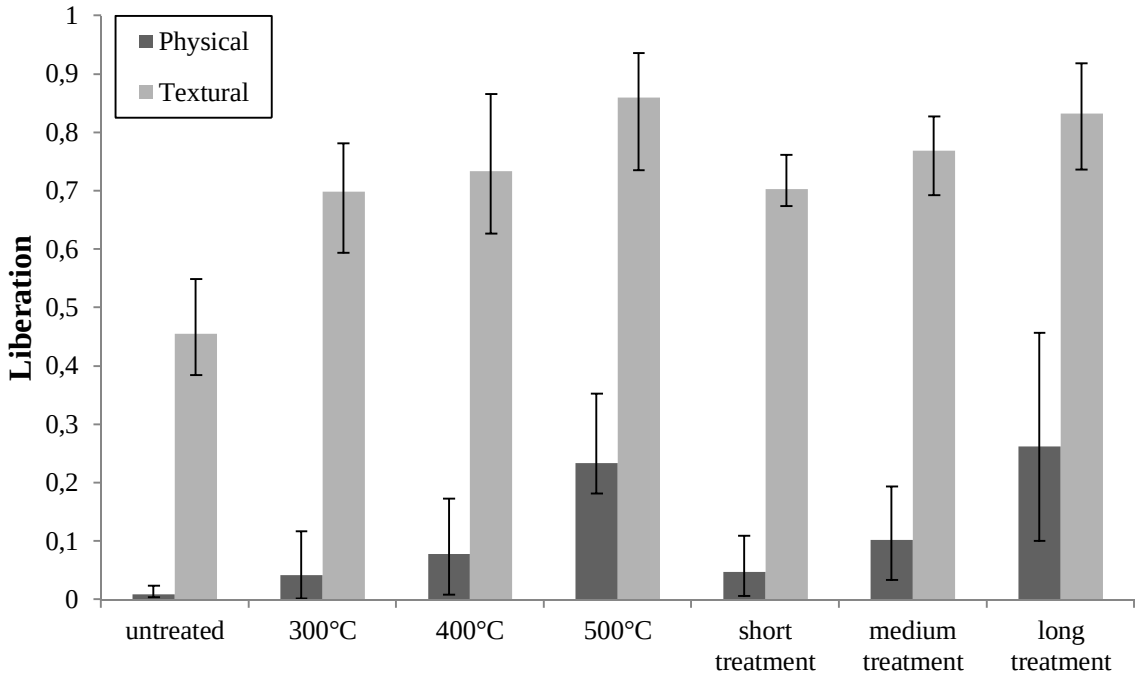

Figure 5.10. Physical and textural liberation of concrete samples with range and mean of tested concrete types S1-S5

The proposed explanation for this in KONA2014 is that while the textural liberation of samples increases quickly with treatment the samples remain relatively strong as they have not yet experienced extensive growth of the secondary network. When a concrete particle is struck by single impact the stress distribution through the sample is a vertical plane of high tensile stress (Figure 5.11.a). While there is sufficient energy to break the samples there is not enough energy to break the samples into small pieces (Figure 5.11.b). As the sample is still mainly a few large pieces the aggregate, while disconnected from the cement paste, remains encased within the cement so that the textural liberation created by the heat treatment cannot be utilised. High physical liberation can only be achieved after significant strength loss (Figure 5.11.c and Figure 5.12).

Figure 5.11. HPB fracture of concrete cubes showing a) Concrete cube displaying fracture mode indicative of a vertical plane of high tensile stress b) Fragments of untreated concrete samples after HPB impact. Concrete samples remain largely intact as 2-3 large fragments and c) Fragments of a long microwave treated concrete sample after HPB impact. Fragments are very small and the largest are mostly liberated aggregate

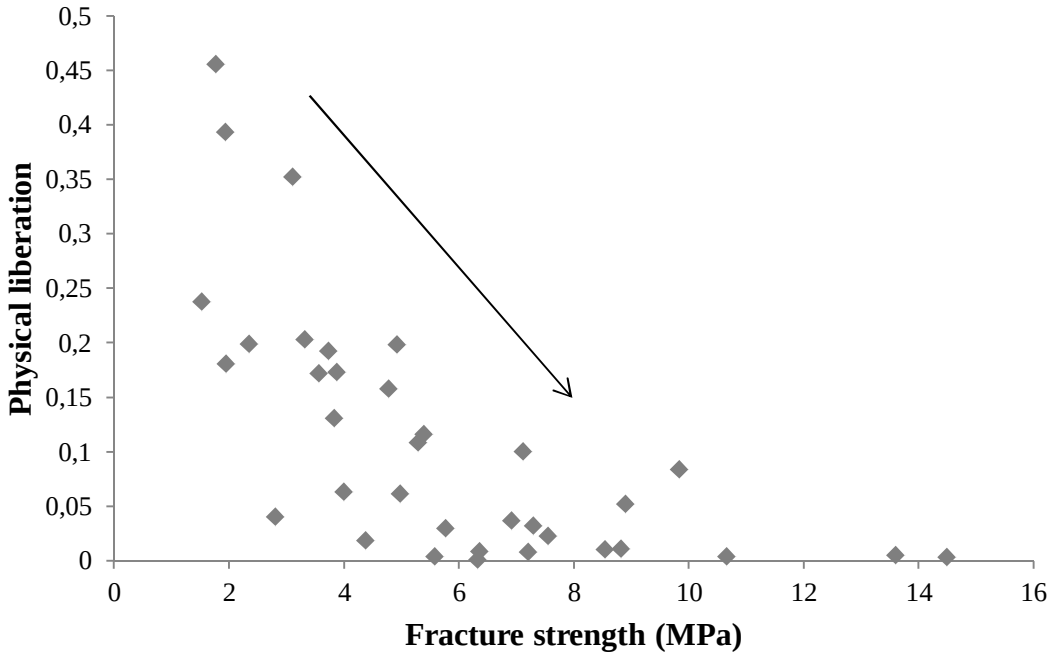

Figure 5.12. Illustration of the decrease in physical liberation of aggregate particles from concrete as the strength of the concrete sample increases

The physical liberation of aggregate particles increased steadily with both microwave and conventional heat treatment (Figure 5.13). It is interesting to note that while the average temperature reached by short microwave treated samples was less than 300°C and the average temperature reached by medium treated samples was less than 400°C the liberation achieved by the microwave treated samples was similar to or higher for eight out of the ten short and medium microwave treated concrete samples than for their conventionally heated counterparts. This suggests for the same treatment temperature and therefore roughly the same energy input microwave treatment is better at liberating aggregate particles than conventional heat treatment.

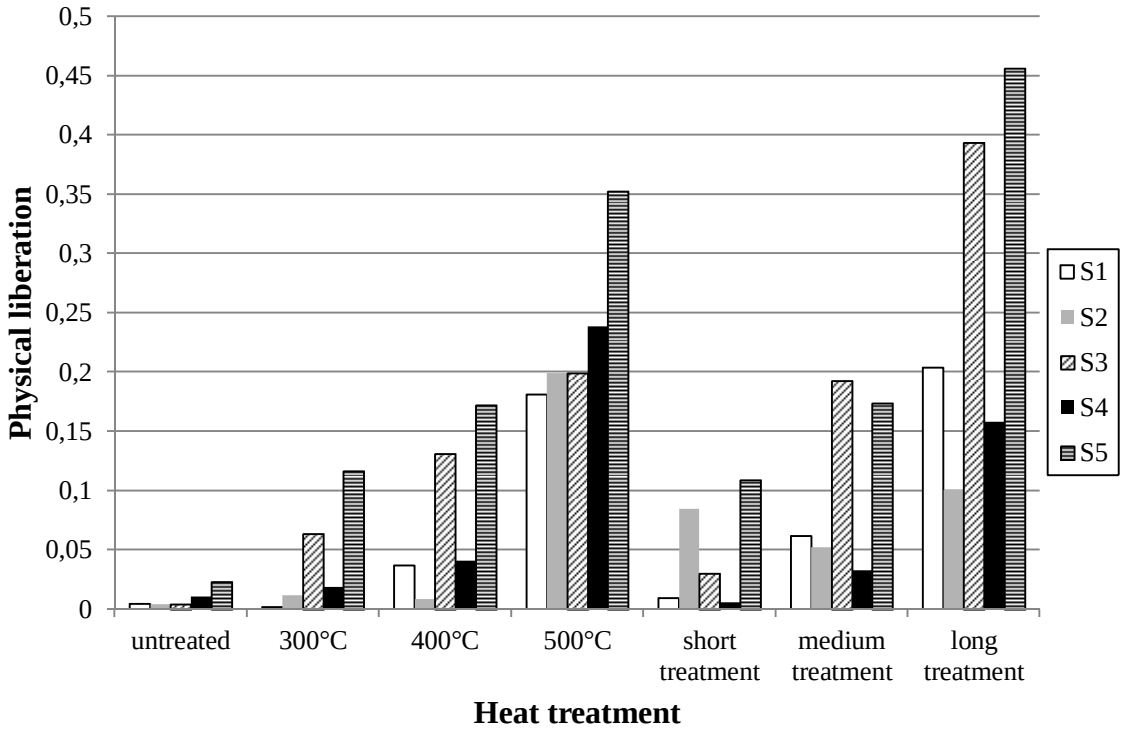

Figure 5.13. Physical liberation of aggregate particles from concrete samples treated conventionally and using microwaves showing the increase in liberation with heat treatment and the relative superiority of microwave heating for aggregate liberation in most cases

The greatest difference between the liberation achieved after short microwave treatment and that achieved after a 300°C conventional heat treatment was seen in S1 and S2, the concretes with the lowest a/c ratio. The high physical liberation of low a/c concretes after short microwave treatment is not particularly surprising given:

- that the average surface temperature of microwave treated samples is below 300°C, the temperature when concrete experiences its first clear change of colour (Figure 5.14), so aggregate is unlikely to contribute a magnetic component to microwave heating
- the increased content of hydrated cement paste in low a/c ratio concretes
- the strength of water's dielectric response

Low a/c concretes contain more water which will contribute to a higher rate of microwave heating and therefore thermal stress.

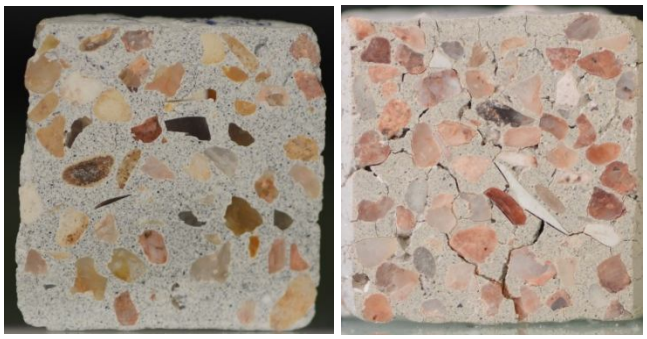

Figure 5.14. Cut surface of w/c 0.6 a/c 1.6 concrete left: untreated and right: treated showing the change in colour to one dominated by red and visible fracture porosity due to microwave treatment

The highest level of physical liberation observed was in long microwave treated S3 and S5 samples, which may be partly because of their high aggregate content. Elevated levels of aggregate content mean an increase in the intensity of microwave heating at elevated temperatures and an increased level of mechanical restraint to the change of volume of cement at all temperatures. An increase in the number of aggregate particles per volume can be expected to alter the stress distribution and therefore crack growth in microwave treated concrete and this contribution likely merits further study. However the high liberation seen for S3 and S5 concretes may also be simply because those were the weakest concretes tested (Figure 5.15). This hypothesis can be applied consistently as the lowest liberation values seen after long microwave treatment were in S2, the strongest concrete tested and S4, the toughest concrete tested which was made with the same a/c as S3 and S5.

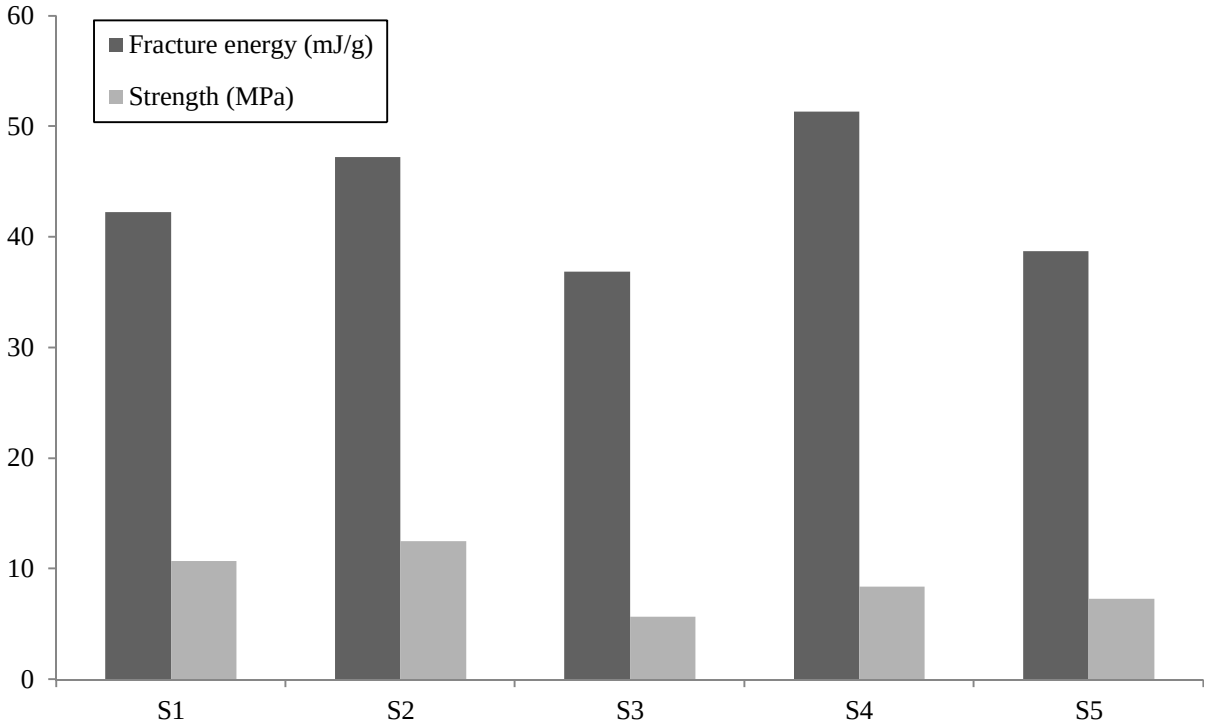

Figure 5.15. Strength and mass specific fracture energy of untreated concrete samples

Regarding elevated heating rates around aggregate particles in concrete exposed to microwaves, this effect may occur after the concrete sample has already been heated to a high temperature. The textural liberation of aggregate in concrete has already increased significantly after a short microwave treatment and only increases marginally with further microwave exposure (Figure 5.10). If it is necessary that the aggregate particles reach a certain temperature before their heating rate is significantly different than the cement paste than by the time this occurs the interface between the phases will already be damaged. If the phases are no longer firmly attached the amount of further embrittlement that can be caused by differential thermal expansion will be limited as the volume changes caused by increasing temperature need to be restrained for differential thermal expansion stresses to occur. If the phases aren't connected there is no restraint to thermally induced volume change so there will be no thermal stresses. This may also explain why the heavily fractured samples of medium and long treatment see only small relative differences in their textural liberation.

While the relative importance of rapidly heated aggregates to microwave induced embrittlement of concrete remains unclear the importance of aggregate to heat induced embrittlement of concrete does not. Figure 5.16 and Figure 5.17 show how the pore size distribution of cement and concrete change with heat treatment. These figures show that concrete samples have more large pores than pure cement and concrete gains a greater volume of large pores than cement when heated. As the presence of aggregate is the only difference between the concrete and cement samples tested, the presence of aggregate must have an effect, even if it is only restricting the thermal deformation of cement.

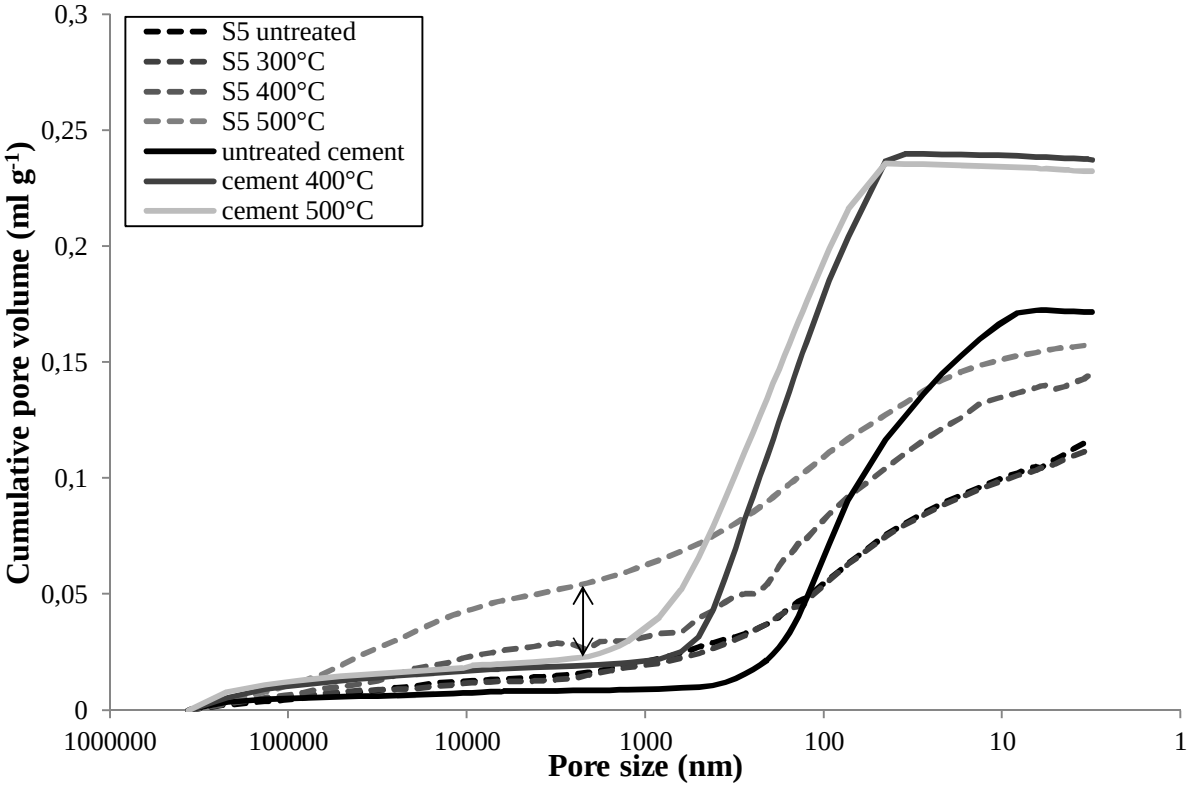

Figure 5.16. MIP intrusion of w/c 0.6 concrete (S5) and cement showing elevated volumes of large pores in concrete relative to cement

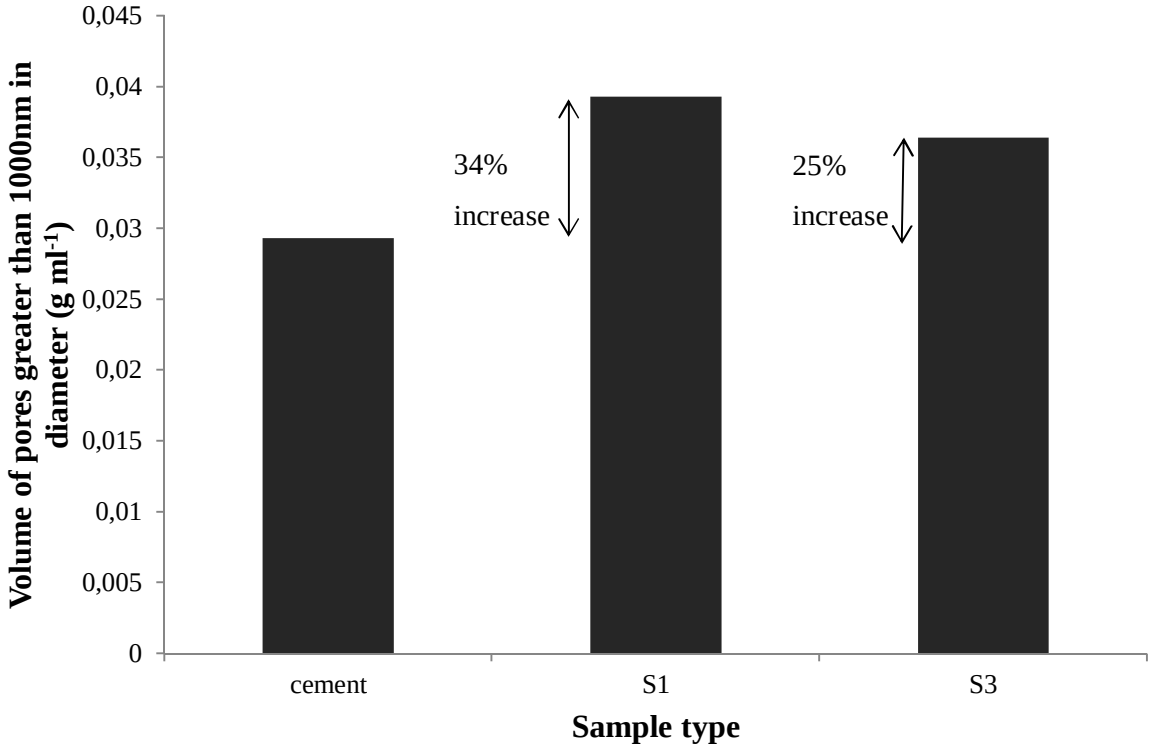

Figure 5.17. Volume of pores above 1µm in diameter as measured by MIP intrusion of w/c 0.4 concrete and cement after 500°C conventional heat treatment showing increased volume of large pores in concrete relative to cement

The liberation due to conventional heating can be explained in similar mechanical terms as microwave induced liberation. Because the heating rate was slow and therefore assumed to occur under equilibrium conditions, the concretes that experienced the highest aggregate liberation at lower treatment temperatures were those least able to resist drying induced stresses and differential expansion, that is to say the weakest concretes. Once the treatment temperature reached 500°C, drying became extreme including the decomposition of CSH [5.3]. At this level of drying the initial strength was no longer important to heat resistance. The volumetric change, specifically how much fracture is necessary to accommodate the volumetric changes, determines the strength loss and therefore liberation. Above 500°C the higher the a/c the more that drying shrinkage is restrained and therefore the higher the level of cement paste fracture is necessary to accommodate the thermally induced deformation. The strength of concrete seems to limit the liberation of aggregate from concrete. Since liberation is required for concrete recycling it is useful to note that the key to overcoming high strength concrete may be higher treatment temperatures.

The relationship between liberation and heat treatment is similar to that seen between heat treatment and fragmentation. To simplify the analysis of sample fragmentation after HPB fracture, the fragments obtained after impact breakage were divided into three size classes (Figure 5.18 and Figure 5.19).

- The first size class was based on the size of raw aggregate particles, 1.6-2.5mm
- The second on those smaller than 98% of aggregate particles, < 1.6mm
- The third were larger than the largest aggregate particles, > 2.5mm

Increasing the intensity of the heat treatment on S1 samples produced a corresponding decrease in the production of large fragments (Figure 5.20) and an increase in the production of small fragments and aggregate sized fragments (Figure 5.21) once the samples were broken on the HPB.

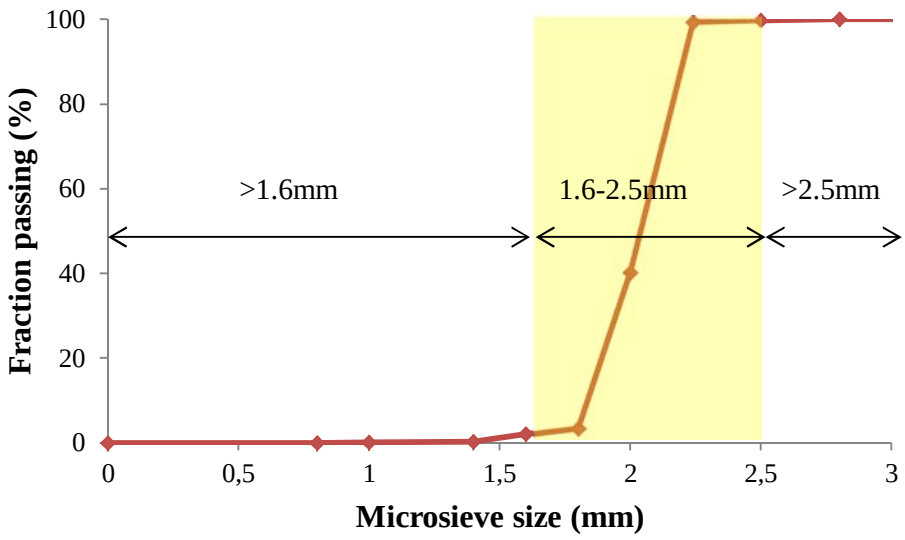

Figure 5.18. Cumulative mass fraction of aggregate particles before their use in S1-S5 concrete including display of fragment size classes showing that 98% of aggregate particles by mass were between 1.6mm and 2.5mmin size

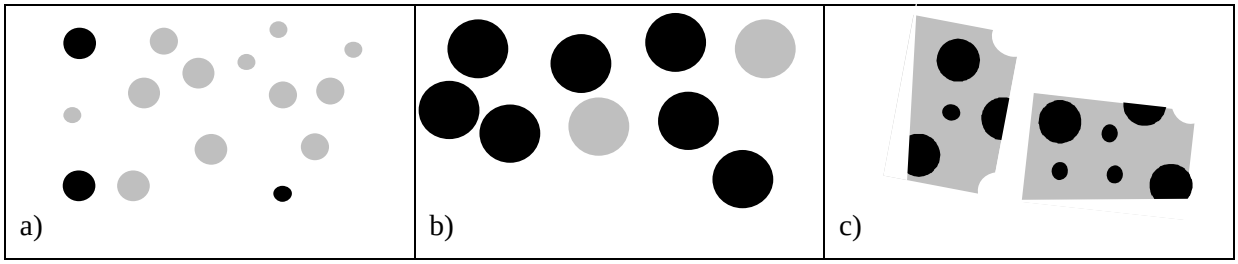

Figure 5.19. Visualisation of the fragment size classes; a) < 1.6mm fragments which are mostly cement b) 1.6-2.5mm fragments which are mostly liberated aggregate and c) > 2.5mm aggregates which are fragments of concrete with aggregate still embedded in the cement phase

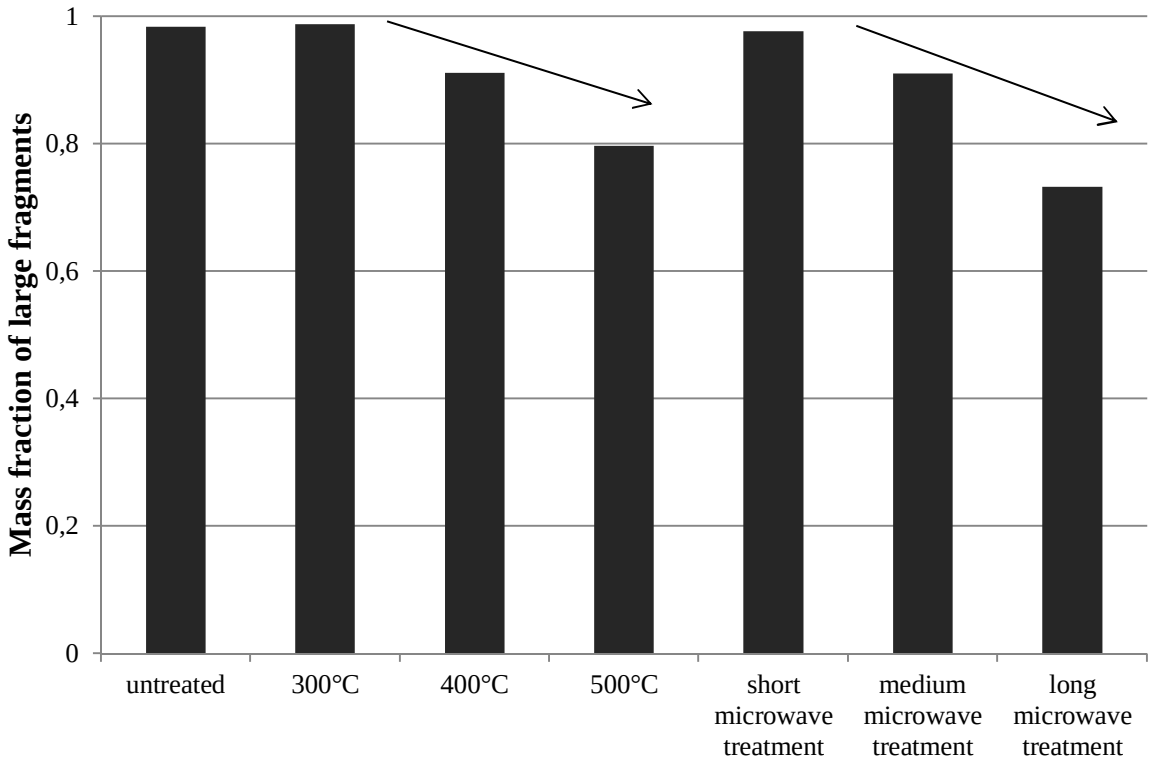

Figure 5.20. Mass fraction of total mass of fragments after breakage on the HPB composed of fragments greater than 2.5mm in size showing decrease in the production of large fragments with heat treatment

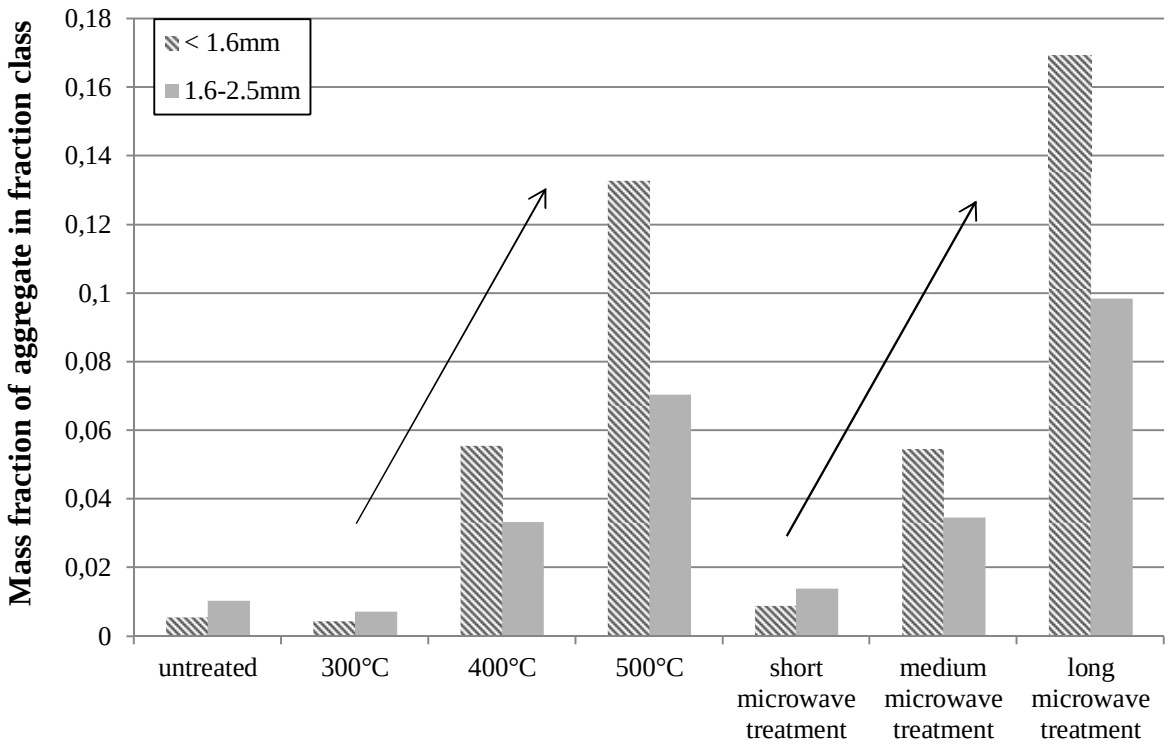

Figure 5.21. Mass distribution of fragments of S1 concrete after HPB fracture by size class showing increased production of small fragments with heat treatment.

The change in fragment size distribution with heat treatment seen in other concrete types is very similar to that seen in S1. In every case microwave treated samples produce more or similar amounts of small fragments than those heated to similar temperatures using conventional external heating. This has significant consequences to processing. Smaller fragments, even if they are not totally liberated aggregates mean the aggregates will have less adhered cement. The less adhered cement on aggregate particles the easier it is to produce totally liberated aggregate [5.4] and thus high quality recycled material. Figures of the same style as Figure 5.20 and Figure 5.21 for other concrete types can be found in Appendix A. The fragmentation results were much the same as those for S1 with the exception of S5 which produced many more aggregate sized and smaller fragments.

The relative fraction of large fragments is similar for untreated, short microwave treated and samples heated to 300°C after each has been fractured on the HPB for S1, S2 and S4 samples. The physical liberation values of S1 and S4 for untreated, short microwave treated and samples heated to 300°C were also very similar. The physical liberation values of S2 did not follow this trend as short microwave treated S2 saw much higher physical liberation than untreated S2 concrete samples. On the other hand the textural liberation of all samples increased significantly relative to untreated samples with all treatments tested. The large absolute difference between textural and physical liberation suggests that the crushing method used does not make effective use of the existing fracture network in treated concrete samples. This has direct implications for the development of a microwave based recycling process and is addressed in more detail in section 5.4.

5.2.3 Recycling-oriented investigation of local porosity changes in microwave heated concrete

The following 18 pages are devoted to the article Recycling-oriented investigation of local porosity changes in microwave heated-concrete published in KONA Powder and Particles Journal volume 31 in 2014. The article is included exactly as it was published.

KONA Powder and Particle Journal No. 31 (2014) 247–264/Doi:10.14356/kona.2014016 Original Research Paper

Recycling-Oriented Investigation of Local Porosity Changes in Microwave Heated-Concrete†

Nicholas R. Lippiatt and Florent S. Bourgeois*

[1] *Laboratoire de Génie Chimique UMR CNRS 5503, Université de Toulouse, France*

Abstract

Large quantities of concrete waste are being produced continuously throughout the world, of which only a fraction are downcycled as construction backfill or as road-base. Seeking total concrete recyclability, this work concerns the development of microwave-based solutions for the separation of individual constituents of concrete. By focusing on the interaction between microwaves and concrete at the microscopic level, the paper makes important connections between local changes in the microwave-heated concrete texture and macroscopic changes in mechanical properties. Through analysis of the concrete texture using SEM imaging, it is found that the microwave heating of concrete causes fracture porosity. The size and shape of fracture porosity can be correlated with recycling performance indicators; namely aggregate liberation, concrete strength and product fineness. In particular, the work finds that only a short exposure to microwaves promotes the formation of a primary fracture network responsible for selective liberation of aggregates. Longer exposure to microwave heating creates a secondary network of smaller fractures that spreads throughout the cement phase, which is directly associated with the changes in mechanical strength of concrete and product fineness.

The work introduces the concept of textural versus physical liberation, and shows that while microwave heating creates a high selective textural liberation of aggregate particles, the comminution of microwave-heated concrete may not necessarily yield high physical liberation. The work concludes that the key to designing a microwave-based process for concrete recycling resides in finding comminution and separation technologies that can best harvest the benefits of the textural and mechanical changes produced by microwave heating.

Keywords: concrete, recycling, microwave heating, fracture porosity

1. Introduction

Concrete is the most-used manufactured product on the planet, as a consequence it also constitutes a large fraction of urban waste. Many countries already make use of concrete waste as backfill and road base. Countries such as the Netherlands and Denmark manage to recycle over 80% of the construction and demolition (C&D) waste they generate (Fischer and Davidsen, 2011; Symonds, 1999). Nonetheless, a large fraction of concrete waste is not used and the concrete that is recycled is invariably downcycled, as can be seen by the ratio of virgin aggregate to recycled aggregate used in concrete production (Klee, 2009). Using crushed concrete as a replacement for coarse aggregate reduces the mechanical performance of the final product in proportion with the fraction of crushed concrete used. This effect is significantly greater when crushed concrete is used as a replacement for fine aggregates, which is why concrete waste is almost never used in this way. The reason crushed concrete reduces the performance of concrete compared to virgin aggregate appears to be due to adhered cement paste and how it reacts to new cement as it cures (Tam et al., 2007). The first step to complete concrete recyclability therefore is finding an effective technique to decrease the volume of adhered cement on recycled aggregates.

Microwave heating is especially applicable to processing multiphase materials as it uses the differences in thermal and dielectric properties between distinct phases to generate fractures and weaken the material. A simple version of this scenario is a strongly dielectric material embedded in a continuous microwave transparent material. In fact, this basic scenario closely resembles what is found for mineral ores, for which microwave heating as a companion treatment step before crushing and milling has been considered for some time and has been shown to weaken the ore and increase mineral liberation, hence mineral yield (Kingman et al., 2004a). The ever-present question is whether the benefit of the increased yield

† Accepted: August 20, 2013
[1] CNRS-Laboratoire de Génie Chimique UMR 5503, 4 Allée Emile Monso BP 84234, 31432 Toulouse Cedex 4, France
* Corresponding author:
E-mail: florent.bourgeois@inp-toulouse.fr
TEL: +33-534-323-633 FAX: +33-534-323-700

exceeds the energy required for the process. As the price of minerals and metalliferous ores and the efficiency of microwave processing technology increase, one might predict that this will soon be the case.

In the case of concrete waste, one could argue that the development of a microwave-based recycling process has perhaps even more potential than with mineral beneficiation. Some arguments to this effect include:

– Recycling concrete has the potential of eliminating a waste stream altogether by recycling all its constituents. Being a high-value man-made material with significant energy and material footprint, the recycling of concrete is a priority.
– Recycled cement can re-enter the clinker-making process (Costes et al., 2010) and thereby contribute to reducing the CO_2 emissions of clinker production by direct substitution with natural carbonates. Reusing cement will also contribute to preserving natural carbonate reserves. Also, the presence of already decarbonated and crystallised phases in recycled cement may also have a positive effect on the energy balance for making clinker, through a possibly reduced heat requirement due to the reduced initial mass and lower required temperatures.
– Recycled aggregate can re-enter the concrete-making process and contribute to preserving natural aggregate resources, which is becoming a scarce resource in developed countries, particularly when dealing with aggregates of alluvionary origin.
– The proximity of concrete waste to consumption areas may contribute to reducing transport associated with the concrete-making industry.

The sensitivity of concrete to microwaves has been known for some time. Using a 5-kW multimode microwave oven and exposure times up to 30 minutes, the possibility of liberating aggregates from hardened cement for concrete analysis purposes was tested over 30 years ago by Figg (Figg, 1974). His pioneering work with 100-mm cubes brought convincing evidence that microwaves could indeed induce boundary fracture at the aggregate-cement interface. At high power inputs, concrete has also been shown to respond explosively, with commercial applications in drilling (Jerby at al., 2002) and controlled spalling (White et al., 1995).

The application of microwave-heating to the issue of concrete recycling is a relatively new endeavour, but one that has already been shown to be effective. Akbarnezhad and co-workers (Akbarnezhad et al., 2011), using a 10-kW generator, showed microwave heating prior to physical comminution to improve recycled aggregate properties, and that this effect is superior to comparable techniques using purely mechanical means or a combination of mechanical means and conventional (external) heating. About the same time, the authors (Lippiatt and Bourgeois, 2012) showed that microwave heating of concrete increases the liberation of aggregate and cement, while decreasing the strength of concrete.

Eventually, impact breakage of these microwave-heated particles of concrete was carried out using a short Hopkinson bar (Bourgeois and Banini, 2002). Liberation was measured using a dissolution technique based on the work of Kiss and Schönert (Kiss and Shönert, 1980).

The results of this previous work validated the hypothesis that the microwave heating of concrete, followed by impact breakage, improves aggregate liberation, thereby opening avenues for recycling concrete. Moreover, the degree of liberation was found to increase non-linearly with exposure time, hence input microwave energy. The short and medium exposures did lead to a similar level of aggregate liberation, which exhibited a significant increase after the long exposure.

Cement liberation was not measured directly but by the mass lost during dissolution. Cement distributions were nearly the same for samples that had undergone short and medium microwave exposures, and cement fines increased dramatically with the longest treatment. It is noted that the sharp increase of cement liberation with the long exposure to microwaves, followed by impact breakage, mirrors the increase in liberation of aggregates by the same process.

Analysis of Hopkinson bar impact tests revealed both a reduction in impact fracture force with increasing exposure, and a progressive loss of elasticity of the concrete with the mechanical behaviour of the most damaged samples resembling that of a loose-packed bed.

These quantitative observations are conclusive indicators of the value of microwave heating for recycling concrete. In summary, when followed by impact breakage, the microwave heating of concrete increases aggregate liberation, increases cement fines and reduces concrete strength.

However, the macroscopic nature of these observations, which result from the combined effect of microwave heating and impact breakage, does not permit understanding what is actually happening inside concrete during microwave heating. The authors argue that some understanding about the microstructural changes that occur at the local scale inside concrete during microwave heating is essential for defining the scope and place of microwave heating in a concrete recycling process. The ultimate goal that this paper aims to move towards is to precisely unravel the elements of reconciliation between variations at the microscopic and macroscopic scales, so as to provide guidelines for the development of an efficient concrete recycling process.

2. Materials and methods

Our ability to relate observations between both scales requires that we quantify the textural changes that take

place inside concrete during microwave heating, especially near the aggregate-cement interface and inside the cement matrix itself. In the process of developing a satisfactory texture analysis protocol, several experiments were performed. This preliminary work led to some appreciation of what had to be quantified for the sake of understanding the link between changes in the microstructure and macroscopic behaviour of concrete. It was concluded that microstructure quantification would have to focus on the properties of cracks, whose patterns were found to change most significantly during microwave heating. Mineralogical changes, as measured by X-ray diffractometry, did not reveal significant changes in comparison. Having decided that the formation of cracks should be the focal point, efforts were allocated during this work to establishing an experimental protocol that would not alter the fractures caused by microwave heating. A non-destructive observation protocol using the scanning electron microscope for texture image acquisition was designed for this very purpose, avoiding altogether any requirement for crack impregnation, cutting or polishing after microwave treatment of the concrete samples.

2.1 Concrete sample preparation

The concrete used in this work was made with cement-enriched mixture (CEM) 1 52.5 Portland cement. Samples were mixed in five different ratios (See **Table 1**) with siliceous aggregate 2–2.5 mm in size. The sample preparation protocol is schematised in **Fig. 1**. Samples were cast in 20-mm cylinders, which after curing, would weigh about 10 g each. After setting in the mould for 24 hours they were removed and allowed to cure in water at room temperature for a minimum of 90 days.

The samples were then removed from soak and separated into lots of 12 units. One sample was reserved for mercury porosimetry analysis, ten for Hopkinson bar impact testing, and one was cut using a water-lubricated diamond saw to give an exposed cross-section. The purpose of this operation was to create a flat surface that could be readily observed after microwave treatment, without requiring any post-treatment cutting or polishing that could potentially alter the fractures induced by the heating process. An alternative would have been to impregnate uncut samples after microwave treatment with a polymer resin or Wood's metal, and then cut and polish to expose an observable flat surface. However, this approach was rejected outright for it had the potential to damage the fractured microstructure. One downside of the protocol that was adopted here over the alternative was that it made the observation of fractures possibly more difficult due to the lack of contrast of the fractures against

Table 1 Properties of concrete samples

Concrete samples	Water/Cement mass ratio	Aggregate/ Cement mass ratio
S1	0.4	0.6
S2	0.4	0.85
S3	0.4	1.6
S4	0.5	1.6
S5	0.6	1.6

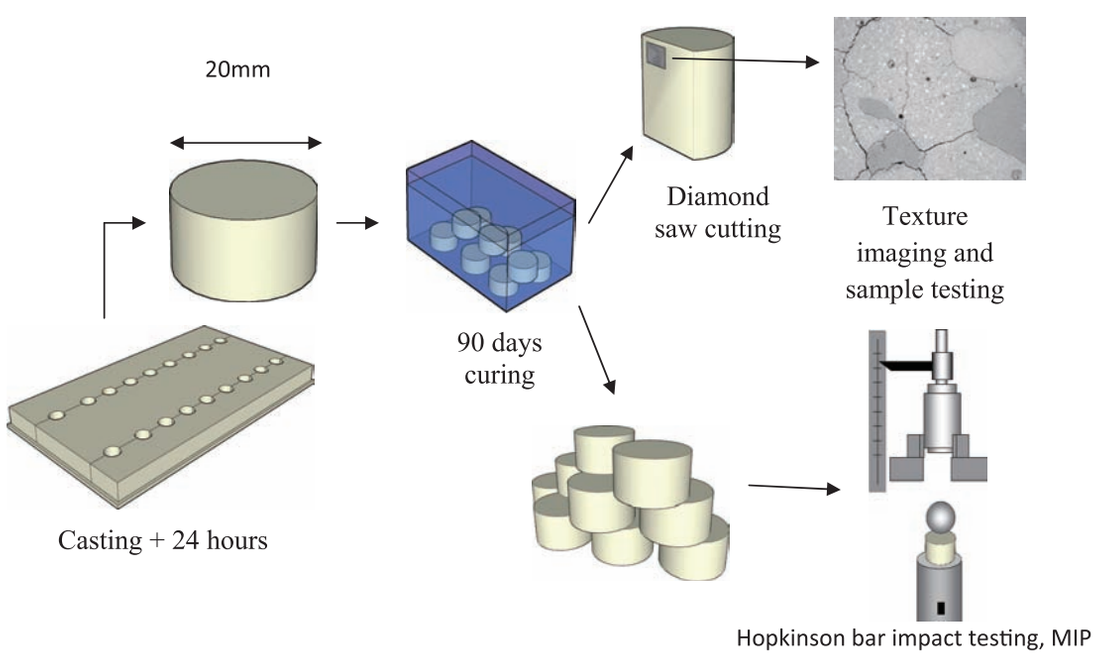

Fig. 1 Illustration of the concrete sample preparation protocol.

the solid phases. This was found to be a problem particularly with untreated samples. The measurement is based on a subjective judgement of contrast and shape. Untreated images showed even less contrast than treated samples.

Some might consider ten samples an insufficient number of samples for mechanical tests of this type. At this stage, the goal is merely to seek patterns so that more extensive testing and results distribution analysis is unnecessary. All results are presented with the mean and full range of measured values.

Prior to testing, samples were systematically dried at 50°C for 24 hours before any microwave treatment or analysis began so that all samples would be equally dry before testing. This was validated by measuring the sample mass changes with drying. After 24 hours at 50°C, the samples stopped losing mass at room temperature.

2.2 Microwave testing and sample post-treatment

Higher power densities are more effective in embrittling multiphase materials (Ali, 2010) and the highest power densities are produced in single-mode cavities (Kingman et al., 2004b). The samples were heat-treated in a 2-kW/2.45-GHz single-mode horizontal waveguide applicator designed by SAIREM. The samples were heated in the microwave system individually; the sample moulds were designed so as to make use of the 30-mm microwave transparent, cylindrical, silica sample holders. The position for the iris and the short circuit for minimum reflected energy were found manually. The iris position was kept constant for all tests. If the initial reflected energy was higher than expected, the short circuit was moved to accommodate. This change in position was never more than a few millimetres.

The samples were treated for 3 characteristic times and the power absorption signal was recorded. These times are seen in **Fig. 2**, and correspond to 15, 30 and 50 seconds called 'short', 'medium' and 'long' treatment, respectively. Short, medium and long microwave exposures are annotated as 'S', 'M' and 'L' so that S1-0, S1-S, S1-M and S1-L represent untreated, short, medium and long treatment times of concrete sample S1, respectively.

They were chosen as they were found to represent three distinctly different stages in the microwave heating cycle for the cast concrete samples under the conditions of the test. The 'short' time comes just after the initial absorption peak, during which 50 to 70% of the sample mass loss occurs, as water evaporates readily. The 'long' time occurs before the absorption starts to peak again, and the 'medium' time corresponds to an intermediate time between these two events. The formation of this microwave absorption peak usually occurred after approximately 50 seconds but was not totally predictable. It is assumed to occur after the formation of local thermal runway and consequently the formation of a plasma. Although the reflected power was measured in real time, the microwave cavity is an open system that can lose mass and energy by convection and evaporation, so the measured energy and power absorbed by each sample is only a guide, and cannot be used as absolute energy absorption by the samples.

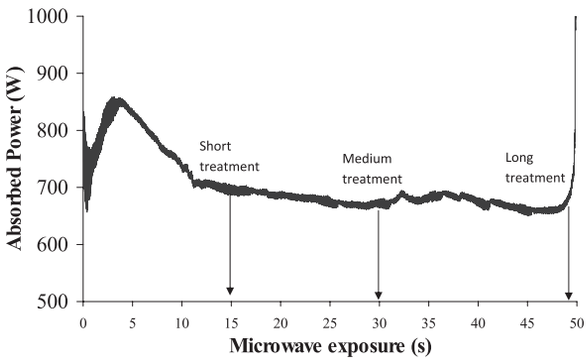

Fig. 2 Typical microwave power absorption record for a 20-mm cylindrical concrete sample (S1).

After cutting the power at the end of the test, an estimate of the average temperature reached by a sample was obtained using a Jules Richards Instruments Flashpoint FX400 infrared thermometer pointed at the sample surface. The temperature was measured on each of the sample's three surfaces. The mean of the highest recorded temperatures of each sample was recorded as the temperature achieved after treatment. Due to conduction with the experimental surface between measurements, the highest temperature measured was usually the first temperature measured. The maximum temperature was chosen as the representative temperature because of the temperatures measured, it exhibited the least variation. The four surfaces of cut samples were also measured but these values were not used in the temperature calculation due to the difference in sample mass. The samples were weighed individually prior to and after microwave treatment, in order to record the mass loss associated with the heating process. Initially, they all weighed about 10 g.

Eventually, a number of tests were systematically performed on the samples. These measurements included:

– Total porosity and pore size distribution by mercury intrusion porosimetry. This was performed using standard 400 MPa intrusion with a Micromeritics Autopore IV.
– Impact breakage testing using a vertical Hopkinson bar. The cylindrical steel bar used was 40 mm in diameter and 1.5 m long. The impactor was a 60-mm diameter, 825-g steel ball bearing dropped from a height of 163 mm and 200 mm. In previous work, a drop height of 163 mm was found to be the minimum required to break an untreated 20-mm concrete cylinder so it was used again for consistency. The 200-mm drop was used

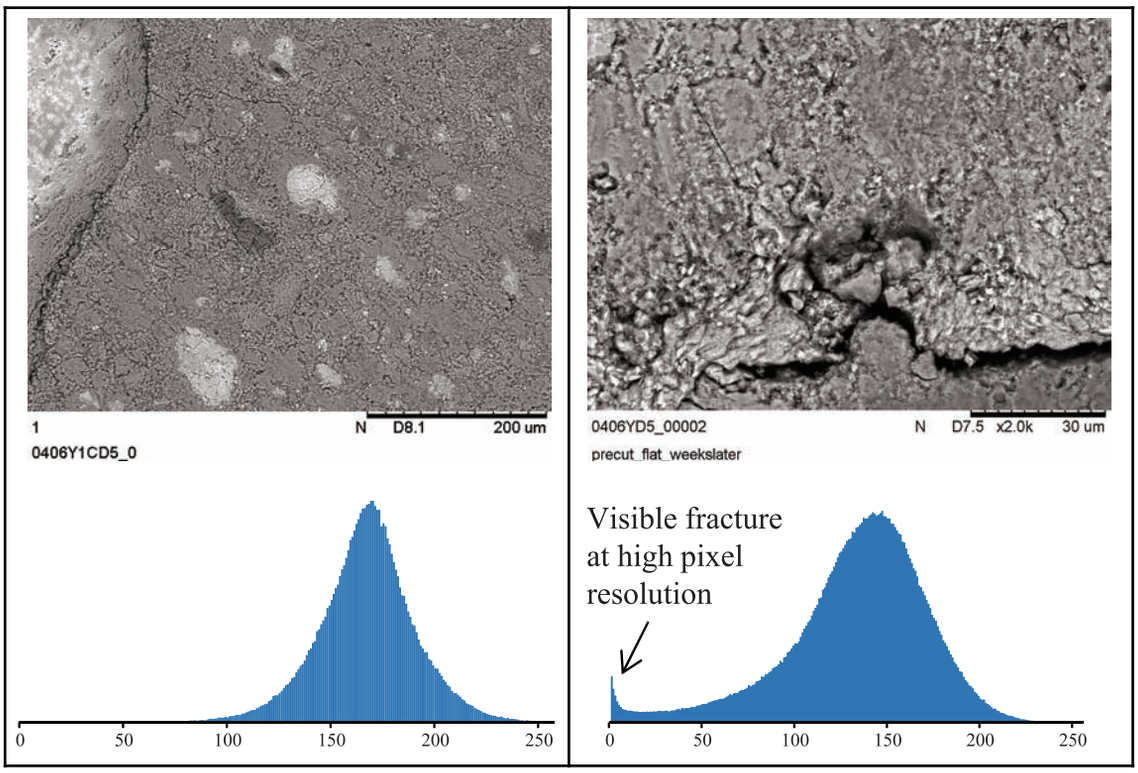

Fig. 3 Standard intensity histogram for SEM images of S1-0 sample. Left: 400× magnification = 0.9 μm/pixel, right 2000× magnification = 0.2 μm/pixel.

to decrease the number of unbroken samples. This does not affect the measure of force required to fracture a sample unless a sample is sufficiently damaged that it no longer displays brittle elastic fracture properties.

– Capture of flat surface images using a Hitachi TM3000 Tabletop Microscope SEM, at different resolutions. The following section is dedicated to this specific part of the sample analysis protocol, which deals with measuring the local effect of microwave heating on the concrete texture.

2.3 Acquisition and analysis of concrete texture images

As indicated previously, the flat surface of the concrete samples, whether treated or untreated, was observed as is by SEM, i.e. without any post-treatment tampering. The SEM images were obtained in this work using a Hitachi TM3000 set to an acceleration voltage of 15 kV. Image analysis of electron microscope images have already been used with success in concrete and cement analysis (Ben Haha et al., 2007; Igarashi et al., 2004; Wong et al., 2006). For the sake of analysing the fractures transecting the flat surface of the concrete samples, the use of SEM images proved to be rather challenging. Indeed the grey-scale intensity of SEM images shows significant overlap between the fractures and the solid phases. **Fig. 3** shows that almost every phase present is included in the same grey level peak.

Given the significant overlap in grey-scale intensity, the binarisation of images is difficult to automate. By careful preparation and observation of samples under sufficiently high magnification, as per the image on the right of **Fig. 3**, the intensity histogram can be separated sufficiently into different peaks so that automated image analysis can be performed on SEM images of concrete and other cement-based materials (Brough and Atkinson, 2000; Yang and Buenfeld, 2001). Examining larger objects such as aggregate particles and the fracture growth that occurs around them requires a lower magnification, meaning greater sample surface area in an image, for reasons of representativity. This lower zoom level has the side effect of condensing the grey-level histogram, making automated image analysis more difficult. Even when highlighted manually, there is the fear that fractures are mislabelled due to low contrast. By repeating the liberation measurement on 40× (9 μm per pixel) images, the uncertainty in the liberation measure was estimated to be no greater than 5% total interface length.

The fractures observed in this work are spaced at distances such that if images were taken at high magnification, say 2000×, then it was very easy to take an image that showed no fracture, even when the sample was highly fractured. When using a low magnification, say 50×, although the high area covered by an image meant the

image was more representative of the sample, it also meant that smaller cracks that were visible at higher magnifications would not be included in the analysis. The minimum zoom possible on the SEM equipment used is 40×, which corresponds to a pixel resolution of 9 μm per pixel. For this work, two zoom levels were chosen, 40× and 200×. Images taken at 40× zoom were chosen to measure the liberation of aggregates as, after cursory examination, a large apparent variation was observed between aggregate particles and this zoom level allowed the largest possible fraction of a sample to be investigated. Another set of images was taken at a zoom level of 200× so that crack networks not visible at a larger scale could be investigated. The number of images was chosen in such a way as to yield a satisfactory compromise between representativity (giving a stable average of textural properties) and keeping the number of images to a minimum, given the strain of the manual digitisation work involved. A scaled comparison of the size of images taken at different SEM magnification levels is shown in **Fig. 4**.

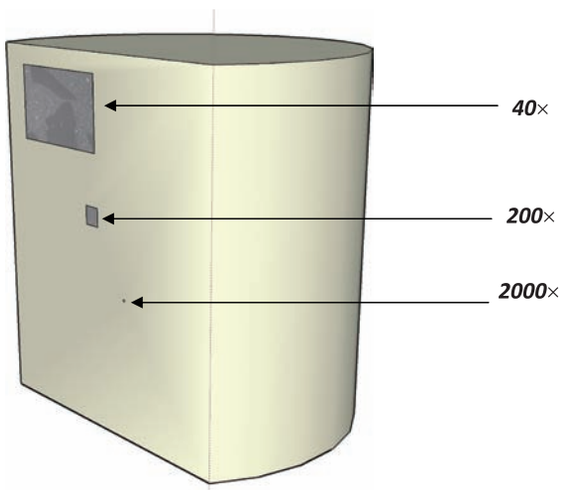

Fig. 4 Comparison of area covered at different zoom levels on sample cut surface.

To overcome the lack of contrast, sample images were highlighted manually. This technique, despite its tediousness, presents a satisfactory way to deal with the aggregate/cement contrast overlap simultaneously with the porosity/fracture contrast overlap. Although the technique has been rightfully identified as imperfect, it has also been used to justify the accuracy of automated image analysis methods (Brough and Atkinson, 2000). In this case, if one of the techniques is accurate, then both must be. **Fig. 5** shows an SEM image before and after highlighting. Aggregates and fractures are easily recognisable. The meaning of the colour-coding of the highlighted image fractures is explained later.

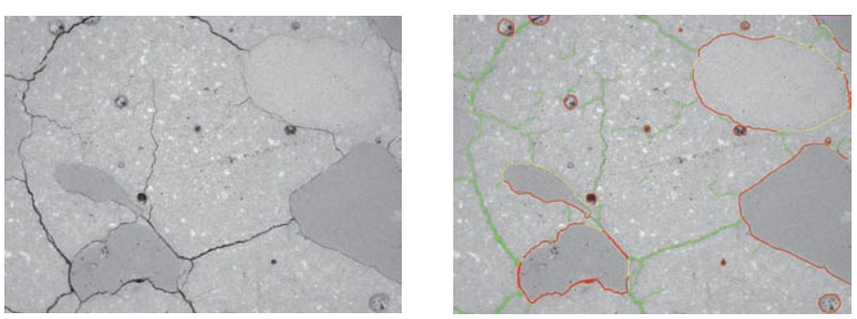

Fig. 5 Example of original and highlighted images taken at 40× zoom for an S1-M sample.

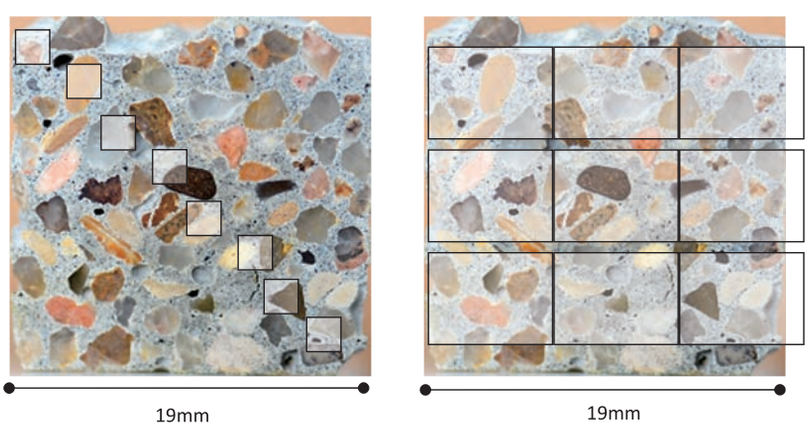

Fig. 6 Illustration of the concrete SEM imaging scheme. Left: images sampled at 200× magnification, Right: images sampled at 40× magnification.

Quantification of fractures being the focal point of the analysis of concrete microstructure after microwave heating, a number of properties were used to quantify fracture porosity.

Straightforward variables that can be measured are the length of, number of and width of cracks present in a given sample area. For the purpose of quantitative image analysis, it was decided to capture 10 SEM images for every sample, 480 pixels by 640 pixels in size, at 9 μm per pixel (40× magnification) and at 1.8 μm per pixel (200× magnification). **Fig. 6** shows the scale and positions of the 10 non-overlapping images for both resolution settings, relative to the 20 mm concrete sample.

Fractures were highlighted manually using a Wacom DTU-2231 interactive pen display. One advantage of this manual image analysis scheme is that it permitted careful hand delineation of different components present in the images, thereby differentiating different classes of fractures. The key highlighted components were:

- Aggregate/cement interface with fracture
- Aggregate/cement interface without fracture
- Fractures within the cement bulk
- Fractures within aggregate particles

As illustrated in **Fig. 7**, every component of interest to the work was highlighted using a distinct colour, which could eventually be used for counting purposes. Six colours, easily distinguished in RGB format, were used (pure green, pure blue, pure red, pure green/red-yellow, pure blue/red-magenta, pure green/blue-cyan), seven including the areas not highlighted (the entire grey-scale from black to white).

Having highlighted different components of interest with distinct colours, a number of insightful quantitative properties, which will be eventually tied to macroscopic variations in concrete properties and operating conditions, could be easily post-treated. They included the properties of fracture per se, as well as the properties that were deemed directly relevant to processing performance.

Starting with the former, the total crack length was measured from skeletonised highlighted images, whereas the total area of cracks, both in the cement bulk and between aggregate and cement paste, and average crack width were measured directly from the highlighted images.

In some images, it is sometimes difficult to tell the difference between a large pore that has formed from an air pocket and one that is the result of an aggregate that is no longer present. Both have a similar shape and appeared to have a similar effect on fracture growth. For initial analysis, all such objects were marked as liberated aggregate. This decision was made to reduce the subjectivity in the analysis process. A side effect of this decision is that all textural liberation values are overestimated. Re-analysis of the S1-0 samples places this variation no greater than 10% of the total aggregate interface length. As all samples were made in the same manner, it can be assumed that the quantity of such large pores is common between samples. Such a systematic error can be ignored in that its biasing the actual values does not change the comparative analyses and conclusions drawn.

Looking now at properties that relate directly to processing performance, the textural liberation of aggregates

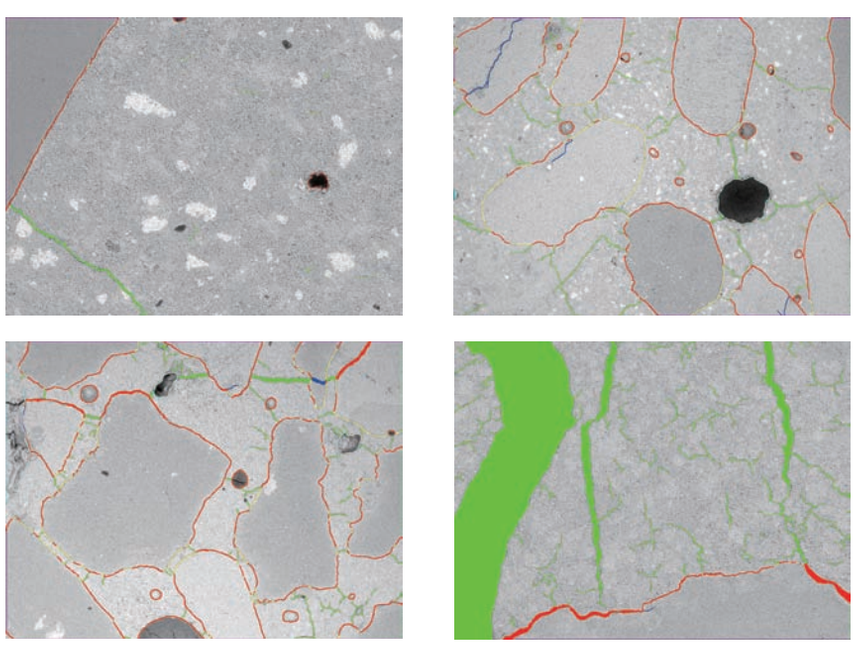

Fig. 7 Examples of highlighted SEM images. Clockwise from top left: S1-0 at 200× zoom, S1-S at 40× zoom, S3-L at 200× zoom, S4-M at 40× zoom.

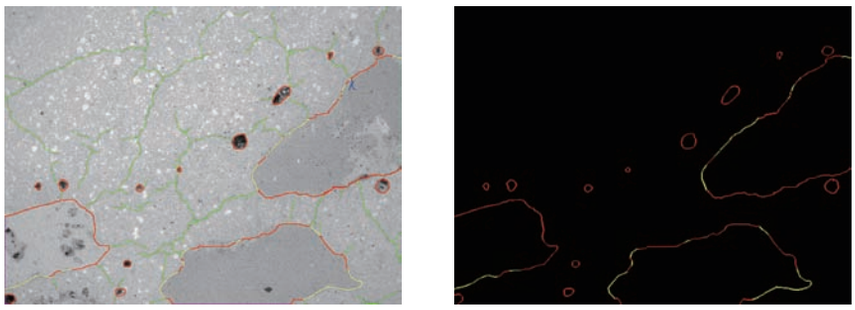

Fig. 8 Example of aggregate textural liberation measurement, S1-M at 40× zoom.

was defined as the ratio between the fractured and total aggregate boundary lengths. **Fig. 8** shows an image with a textural liberation value of 76%.

Aggregate liberation was measured using the 40× zoom (9 μm per pixel) images for the sake of representativeness. The cracks in the cement paste, however, were significantly finer, and were observed using 200× zoom (1.8 μm per pixel) images. During analyses it was found that there appeared to be two different types of fractures forming within the microwave-treated concrete samples. The first group formed the 'primary network', and included all the fractures at the interface of an aggregate particle and the cement paste and all fractures that branched from this interface. This network was visually identified as being made of a few large fractures which ran from aggregate to aggregate throughout the sample. The second group formed the 'secondary network', and included a large number of smaller fractures that spread throughout the cement phase. **Fig. 10** illustrates the 2 families of fractures, which were assigned different colours for quantification purposes. Aggregate fractures occurred also, especially in long-treated samples. However, aggregate fractures occurred to a far lesser extent than cement and grain boundary fractures so were not accounted for in the analysis, which allowed one of the nine colours to be re-assigned so as to permit differentiation between primary- and secondary-network cement paste fractures. In **Fig. 9** and **Fig. 10**, primary network fractures are displayed in yellow.

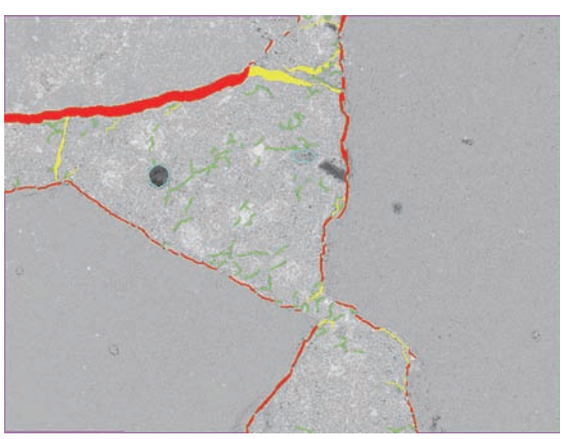

Fig. 9 Example of primary and secondary fracture network highlighting.

Once the images were skeletonised and fractures sorted into primary and secondary networks, the nodes and ends of fracture branches were then counted automatically. A branch is defined as a length of fracture between nodes and/or fracture ends.

Because the post-treatment of highlighted images is

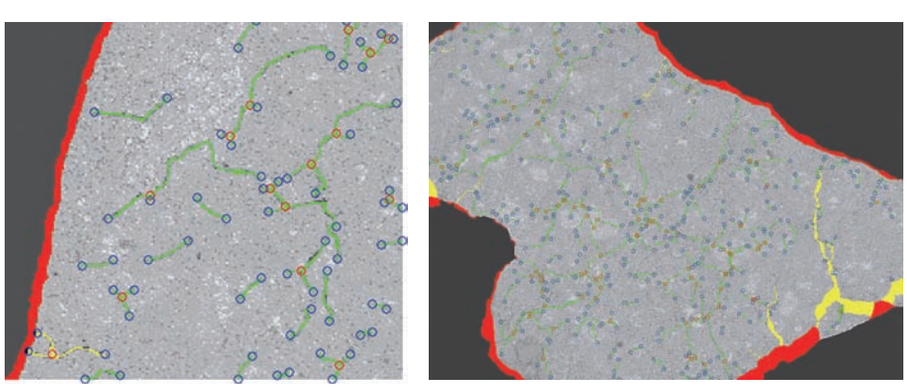

Fig. 10 Example of identification of branches and nodes in the secondary network of fractures. Yellow: primary-network-cement paste fracture, green: secondary-network fracture, red: aggregate/cement interface fracture-primary network, red circle: node, blue circle: branch end.

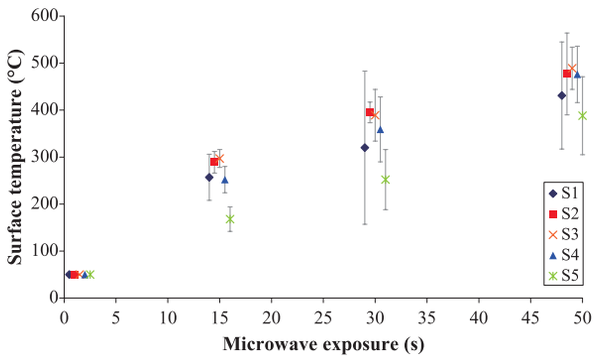

Fig. 11 Measurement of surface temperature as a function of test duration (exposure time offset for clarity).

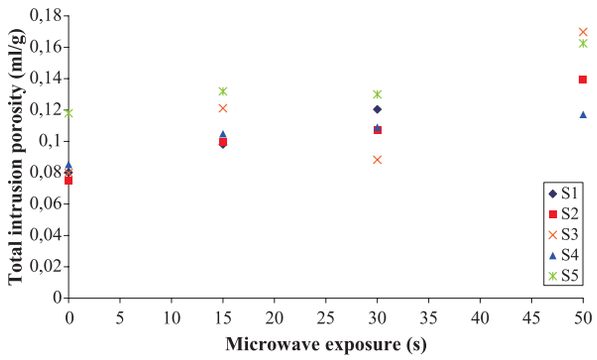

Fig. 13 MIP measurement of total sample porosity for S1 to S5 concrete samples.

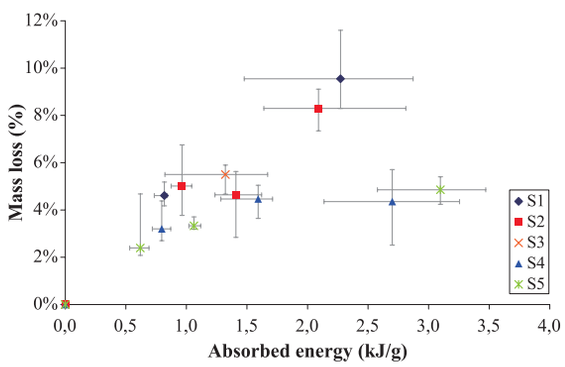

Fig. 12 Correlation between mass loss and energy absorption.

automated, some fractures will necessarily be misclassified, as for example some primary fractures will be connected to aggregates that are not contained in the image, or a primary fracture will branch into two almost identical branches. However, such occurrences are rather rare and do not change the value of the results obtained considering the large number of fractures.

3. Effect of microwave heating on concrete: macroscopic level results and analysis

This section presents the results of measurements made on concrete samples at a macro scale. It shows the temperature, mass loss, fracture strength and the MIP (mercury intrusion porosimetry) porosity changes associated with microwave treatment in different concrete samples. This macroscopic level analysis is used to justify the necessity for local, textural analysis of the effect of microwave heating on concrete.

Microwave treatment increases the temperature of concrete samples, albeit in a different way to that of conventional heating as external heating conducts from the sample surface, whereas microwave heating occurs within the sample. Nevertheless, the longer the application of microwave power, as shown in **Fig. 11**, the greater the temperature measured at the surface of the concrete samples. Despite the S5 sample exhibiting a slightly different trend, it is fair to say that the elevation of temperature, as measured at the samples' surface, is comparable for all concrete sample types tested with short, medium and long treatments.

With the samples tested, it can be concluded that the average temperature reached by the samples does not depend significantly on the variations in concrete properties, at least within the variable range represented in samples S1 to S5 (See **Table 1**). As can be seen in **Fig. 11**, the amount of energy absorbed by each sample is nearly proportional to time once the initial water absorption peak is over. The power input was set to the same 2 kW nominal value for each test. This implies that the differences in thermal properties, dielectric properties and mass compensate for each other and/or they are insignificant in the range tested. As will be seen later, differences in textural properties within the samples are also marginal, suggesting that microwave heating of concrete exhibits a low sensitivity to concrete properties. This is a valuable result from a recycling standpoint as it suggests a concrete recycling process will be insensitive to input properties and no special expense or effort is necessary to accommodate varying concrete waste streams.

The energy absorption by the concrete samples is strongly correlated with the mass loss, as shown in **Fig. 12**, which is itself caused by water loss during heating. It is possible that mass other than water can be lost, however, this effect is deemed insignificant and so all mass changes can be safely assumed to be due to the loss of water. It is also noted that X-ray diffraction spectra did not show any noticeable mineralogical changes between treated and untreated samples, confirming that decomposition of crystallised phases such as portlandite and calcite are marginal at best at such temperatures (Piasta et al., 1984).

By means of MIP, the changes in porosity were characterized with all 5 samples under their untreated and

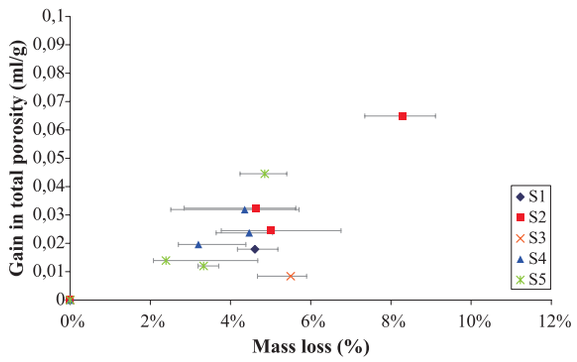

Fig. 14 MIP measurement of total sample porosity as a function of mass loss.

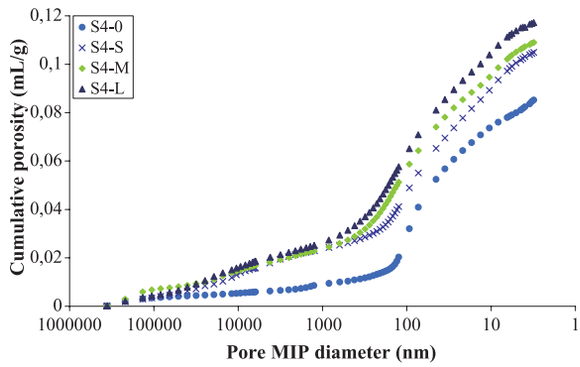

Fig. 15 Measurement of pore size distribution using MIP for sample S4.

microwave-heated states. **Fig. 13** shows the total intrusion porosity, a measure of the total volume of pores in the samples. The data is given on a sample mass basis. There is a consistent increase in total porosity with increased energy input into the concrete samples, for all concrete samples tested.

Although water loss plays a significant role in the porosity gain, as would naturally be expected, **Fig. 14** shows that there is no clear trend between the measured increase in sample porosity and the actual mass loss.

Assuming MIP accurately measures the total porosity, converting the mass loss from **Fig. 14** into the equivalent volume of liquid water shows that bulk water loss could not explain more than 60% of the pore volume that is created. Water loss must come from sources other than free water, such as the decomposition of portlandite and hydrated calcium-silicate (CSH).

This simple calculation indicates that more than 40% of the total porosity created and measured by MIP is associated with mechanisms other than bulk water loss during the exposure of concrete to microwave heating. This trivial analysis illustrates further the intrinsic complexity of porosity changes during the microwave heating of concrete, making a compelling argument for investigation of porosity changes at the local scale, by direct observation of concrete texture.

Fig. 14 seems also to indicate that the higher the water to cement ratio (w/c), the lower the contribution of water loss to the increase in total porosity. This observation indicates that whatever phenomenon other than bulk water loss is causing an increase in microwave-heated concrete porosity, it is associated with the w/c ratio and its effect on concrete microstructure, i.e. porosity. A more porous concrete sample is more prone to evaporation during microwave heating. If we assume the samples made with a higher w/c ratio had less water in their pores (relative to saturation) before treatment, then it makes sense that the evaporation of this type of water contributed less to pore formation. It is also logical that these concretes were more susceptible to other crack formation mechanisms related to drying as they would dry faster and thus be affected by these mechanisms sooner. The results also suggest that there is no significant pore growth due to excessive pore pressure as this would presumably occur more in the lower w/c ratio samples due to their smaller pore volumes. This does not mean that this phenomenon does not contribute significantly to mechanical changes or aggregate liberation. The explosive spalling of some low a/c samples in the first 5 seconds or so of microwave treatment (~100°C) might suggest this is an important phenomenon in terms of concrete recycling, but it does not appear to be an important phenomenon in increasing sample pore volume.

Despite its limitations, the pore size distribution measured by MIP can give some appreciation of the evolution of porosity within concrete samples with microwave heating. One example is given in **Fig. 15** for concrete sample S4. Bearing in mind the limitations of MIP measurement, namely its sensitivity to the ink-bottle effect (Diamond, 2000), what the measurements confirm is that a connected network of large pores, measured to be in the 1–100-μm range, exists in all microwave-treated samples. MIP does not measure this network in the untreated samples. This behaviour was consistently found with all concrete samples tested. One possible explanation is that the connected pores created by a short exposure are becoming larger as a result of heat-induced shrinkage of the cement phase. An interesting observation is that MIP does not appear to see noticeable changes below the 1-μm range between short and long exposure.

Along with changes in porosity, concrete performance is altered in a dramatic way by microwave heating. As reviewed earlier in the paper, the liberation of aggregate and cement was found to increase with exposure to microwaves. Analysis of microwave-heated samples using the Hopkinson bar also revealed strong changes in mechanical properties. **Fig. 16** shows the change in fracture force for the 5 samples considered in this paper, as an illustration of the embrittlement caused by microwave heating. Fracture

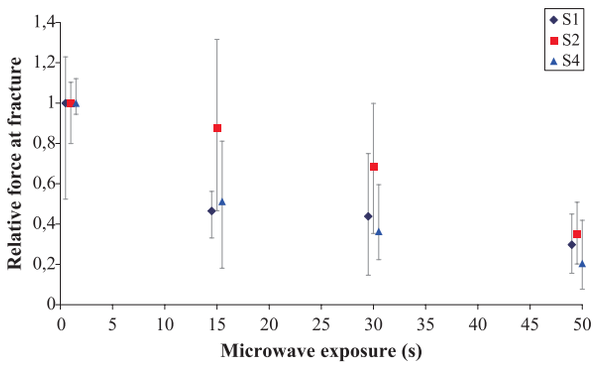

Fig. 16 Hopkinson bar measurements of impact fracture force on microwave-heated concrete samples (exposure time offset for clarity).

force is normalized by the fracture force for the untreated sample, which takes value 100%. This allows a simple assessment of the relative change in fracture force as a function of microwave exposure.

It is consistently found that the relative fracture force decreases continuously with increased exposure to microwaves, possibly with the largest loss in mechanical properties occurring after the short exposure. These are interesting observations, particularly in light of the knowledge that aggregate and cement liberation increases most significantly after a long exposure to microwaves, as seen earlier in **Figs. 1** and **2**. These observations suggest that there is some embrittlement phenomenon that is not effectively observed when using macro-scale measurement techniques, and there is not a direct link between changes in mechanical behaviour and physical liberation.

Overall, the macroscopic analysis has provided us with interesting insights about the changes that occur inside concrete during microwave heating, causing a change in mechanical behaviour, with a loss of resistance to impact fracture that varies continuously with increased exposure, and an increase in liberation of both aggregate and cement phases, albeit significant for the long exposure only. The main change related to concrete microstructure is associated with porosity, which increases continuously with exposure, as seen from both total porosity and pore size distribution measured by MIP. The changes in mechanical behaviour seem to vary as per the changes in total porosity, and a link between porosity and physical liberation of aggregates can be inferred.

The disparity between the evolution of physical liberation and mechanical properties with microwave exposure illustrates the need to further understand the microwave-heating concrete-embrittlement mechanisms with a local technique. For this work, image analysis of SEM images was chosen.

4. Effect of microwave heating on concrete: local level results and analysis

As discussed in the preceding section, the changes in porosity that occur during microwave heating of concrete are possibly numerous and complex, making the observation of porosity at the textural scale a compelling step towards unravelling the mechanisms by which microwave heating alters concrete. As will be shown here, textural analysis of the structure of fracture porosity provides an insightful angle on the mechanisms that take place inside concrete as it is being heated by microwaves, with views on recycling its elementary constituents.

Fig. 17 shows a superimposition of some highlighted images of sample S1. It is noted that the same general pattern applies to all the concrete samples tested in this work, with differences in the magnitude of the observed changes. Looking at the obvious changes in fracture porosity between the images, **Fig. 17** also validates the authors' selection of the 4 characteristic times along the heating process for the sake of quantifying the effect of microwave heating on concrete texture.

- Untreated concrete samples exhibit only few fractures, at both 40× and 200× magnification. Fractures are essentially found around the aggregates, in the region known as the interfacial transition zone (ITZ).
- After the short treatment, the sample having been heated for 15 seconds, a large-scale network of fractures appears, visible with the 40× magnification. These fractures seem to form a network connecting aggregate particles and also appear to run around them, going through the entire sample texture. This network is referred to as the "primary fracture network". As it is associated with aggregate grain boundaries, the formation of this network is directly associated with the liberation of aggregates.
- When the concrete sample is further heated to the medium condition (30 seconds), fractures from the primary network widen. Another network of smaller fractures develops that invades the cement paste. Because it appears to be nested within, and is of a smaller scale than the primary network of fractures, it is referred to as the "secondary fracture network".
- At the long exposure (50 seconds), while the primary network keeps widening, the quantity and length of the secondary network fractures increases significantly.

These generic observations are visible with every tested sample to a varying extent. From a range of observations that were repeatedly made during this study, it was ascertained that a strong correlation exists between the properties associated with the primary network and the loss of mechanical strength and liberation of aggregate particles. The properties of the secondary network further explain the mechanical changes but more importantly provide the

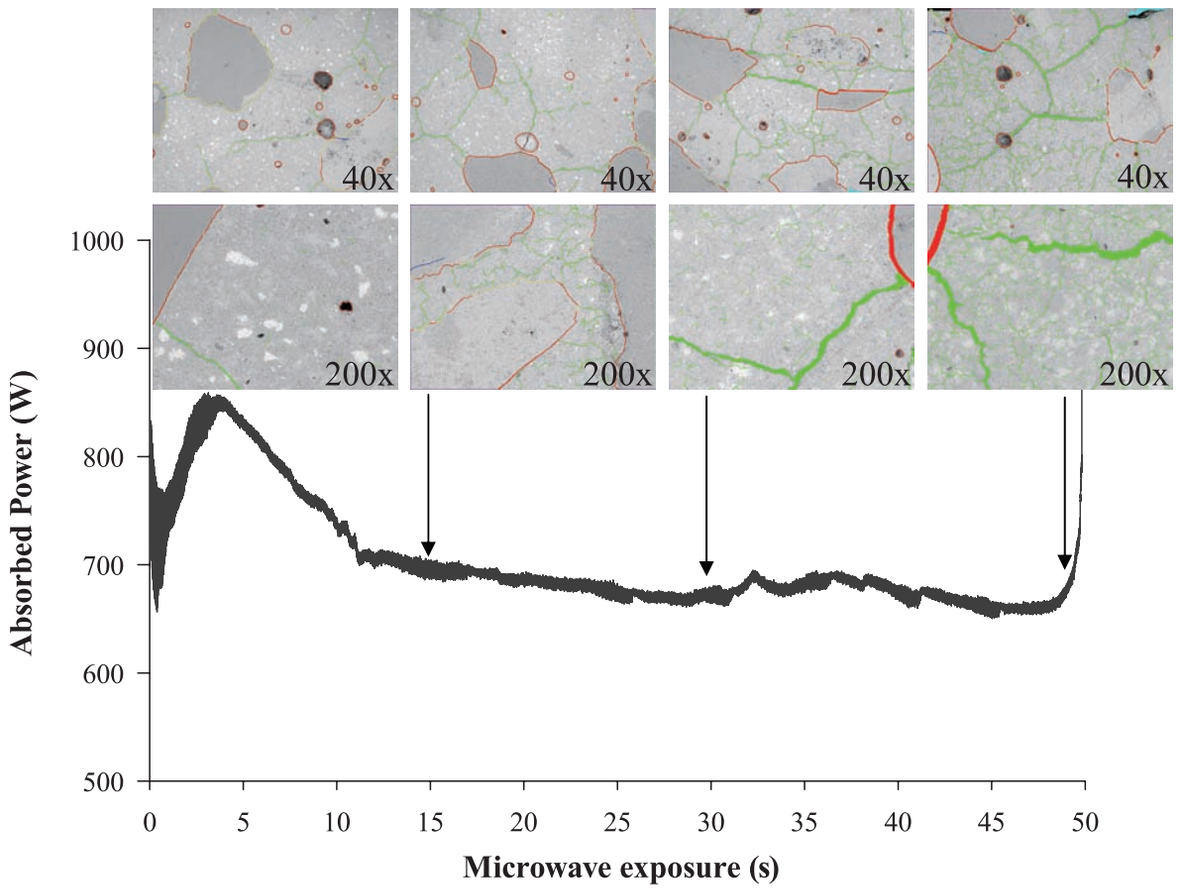

Fig. 17 Local observation of porosity changes with microwave treatment of S1.

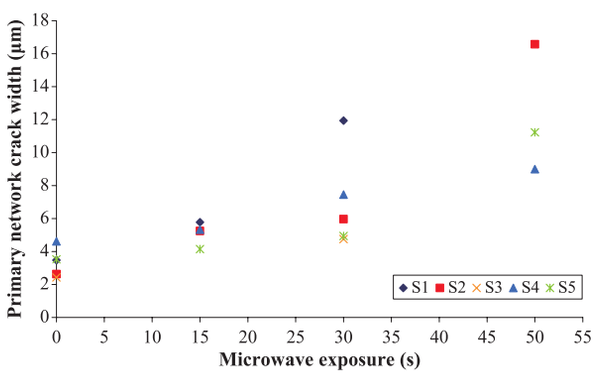

Fig. 18 Variations in primary network fracture width with microwave treatment time.

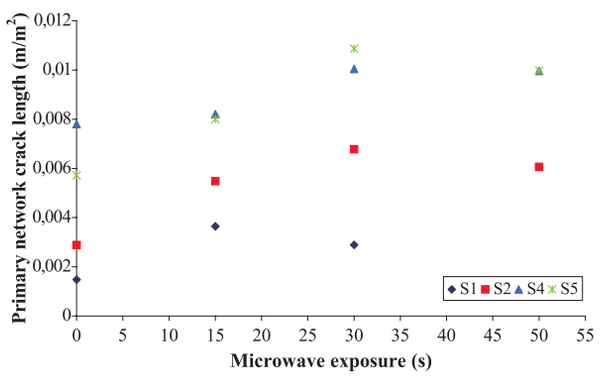

Fig. 19 Variations in primary network length with microwave treatment time.

link between textural liberation and physical liberation, as measured by impact testing, specifically the fineness of the cement paste fragments after impact testing.

Because these networks correlate directly with the macroscopic properties of microwave-heated concrete samples discussed in the previous section, their formation and growth are thought to hold the key to concrete recycling. The following section is concerned with quantification of both primary and secondary fracture networks.

4.1 The primary fracture network

The primary network may be quantified in a number of ways. Accessible properties from two-dimensional images include average properties such as total length, surface area and crack branch number, and statistical properties such as crack branch length and size distributions. As seen in **Fig. 18**, the width of primary network cracks increases very rapidly with microwave exposure. Conversely, as seen in **Fig. 19**, once the network is formed after a short

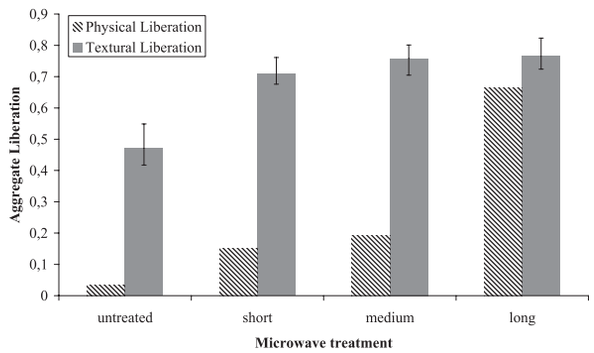

Fig. 20 Comparison between physical liberation (Lippiatt and Bourgeois, 2012) and textural liberation of aggregate particles.

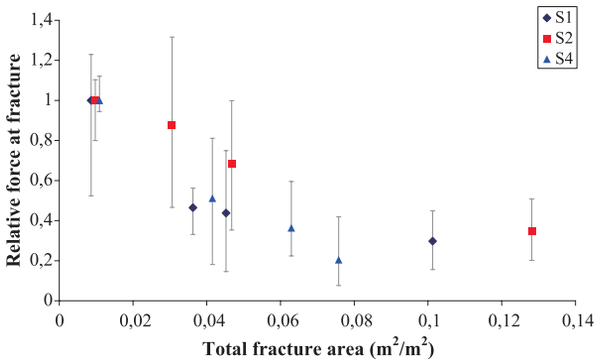

Fig. 21 Relative change in concrete strength, as measured by the relative force at fracture as a function of the combined area of primary and secondary networks relative to the cement paste area.

exposure, the length of the primary network is relatively unchanged. What this indicates is that the fractures that form this network widen with increased exposure, but do not propagate significantly beyond the extent reached after a short exposure to microwaves. The mechanisms associated with the change in thickness of primary-network fractures are deemed to be associated with drying shrinkage of the cement matrix. Because of the specific properties of the ITZ with its high porosity, micro-fracturing and water content (Roy and Idorn, 1993), a strong local reaction to microwave heating is bound to occur around the ITZ during microwave heating, and the formation and growth of the primary fracture network is expected.

By definition, the primary network is associated with what was earlier defined as the textural liberation, which accounts for the fraction of the aggregate perimeter that is liberated in the 2D analysis. **Fig. 20** compares physical liberation, as measured by acid dissolution, with textural liberation. Because the work presented here spans a long period of time, these measurements were not made on the same samples, hence changes in sample properties may contribute marginally to the observed differences. The error bars represent the range of textural liberation values from all the tested samples, the height of the bar representing the average value. The physical liberation values were measured on 10 mm cubes (Lippiatt and Bourgeois, 2012).

Textural liberation is already significant with the untreated sample. The high porosity of the ITZ, often with extensive micro-fracturing, is well documented (Roy and Idorn, 1993). Using MIP, Roy and Idorn estimated values of porosity in the ITZ as high as 37%. Mehta and Monteiro (Mehta and Monteiro, 2005) predict a high level of aggregate boundary fracturing from drying shrinkage during concrete heating, hence the observation of the primary network formation during microwave heating is expected.

Fig. 20 shows that textural liberation reaches a very high value after the shortest of the three measured microwave exposures, and it does not increase significantly after that. Aggregates are highly liberated inside the concrete texture after a short exposure to microwaves only. This is an important piece of information from a processing standpoint, as an increased duration of microwave heating becomes directly an increase in energy consumption. Nevertheless, upon impact breakage testing, the aggregate particles remain trapped inside the cement matrix. Indeed, the 2D analysis finds 70% of the aggregate boundaries being liberated in the concrete sample for the short exposure, when only 15% of the aggregate is physically liberated after single-particle impact breakage of a short-treated sample. It is fair to conclude that single-particle impact breakage cannot harvest the liberation induced by microwave heating. In other words, an alternate form of comminution is required to take advantage of the textural liberation of aggregate particles.

Eventually, for the long exposure setting, the physical and textural liberation of aggregates converge towards the same value. This is explained by the secondary network invading the cement phase, as intense fracturing of the cement phase is necessary for single-particle impact breakage to yield liberated aggregates.

It was shown above that the strength of concrete decreased with microwave exposure, the same can be said of concrete stiffness. Textural image analysis showed an increase in the total crack length, total crack area and average crack width. This increase in crack width was significantly more pronounced in the primary network and specifically the aggregate/cement paste interface fractures. It is impossible to separate the effects of total fracture area and aggregate interface crack width on the mechanical properties as these two values increase together during microwave heating, but it has been noted that concrete stiffness is largely dependent on the ITZ (Mehta and Monteiro, 2005). In this work stiffness is measured with Hopkinson bar impact testing as defined by Tavares and King (Tavares and King, 1998). **Fig. 22** shows that as expected, the stiffness of the samples decreases rapidly with the increase in

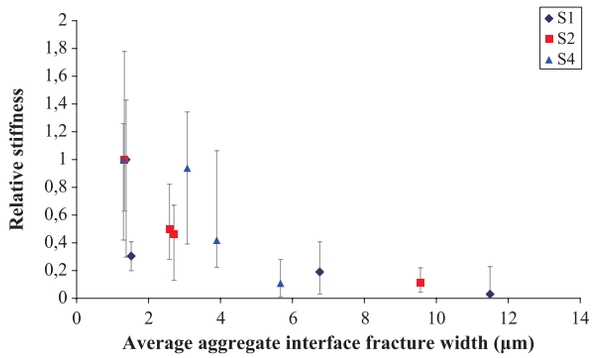

Fig. 22 Change in concrete stiffness with aggregate interface crack width.

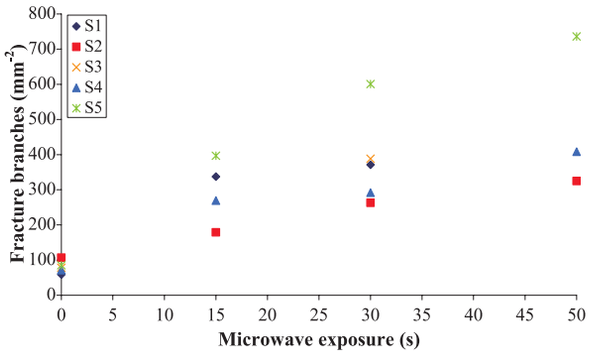

Fig. 24 Number of branches per cement area in secondary network.

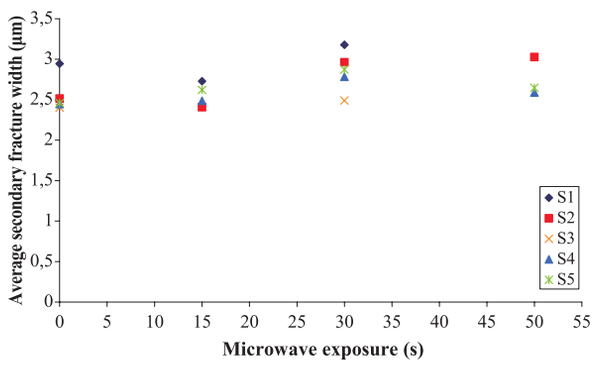

Fig. 23 Variations in secondary-network properties with microwave treatment time.

aggregate interface fracture width. The rate of change slows at higher temperatures, presumably as once aggregate and cement paste is separated the stiffness becomes dependent on the cement phase only, and increasing the size of this separation has no further effect. Similarly, concrete strength has been linked with porosity, the textural measure most analogous with porosity is the total crack area which increases steadily with microwave exposure and shows a strong correlation with loss of concrete strength and can be seen in **Fig. 21**. When compared with **Fig. 19**, it can be seen that the growth of the primary network can not be responsible for the strength loss in samples that have experienced a longer treatment, because while strength continues to decrease, the increase in primary-network fracture length slows with further microwave exposure.

Two-dimensional analysis of the fracture networks has a limited scope for understanding the way by which their properties correlate with operating conditions and with recycling performance indicators. Having clearly established that these fracture networks hold the key to concrete recyclability at the local scale, it appears that three-dimensional observation and analysis is the next logical step. Currently, X-ray tomography has a resolution that is fully compatible with that required to capture the primary network, at a resolution of say about 10 µm per voxel. The authors have started capturing tomographic images of 20-mm heated concrete samples, which confirm that the primary network is a highly connected network that percolates through heated concrete samples. On the other hand, capturing three-dimensional information about the secondary network is clearly more complex because the required resolution must be of the order of a micrometer or less. Nevertheless, the seemingly random occurrence of this network through the cement phase means that 3D properties of the secondary fracture network can possibly be inferred from 2D images using statistical means.

4.2 Analysis of the secondary network

The fracture network that forms during the microwave heating of concrete has been divided in two. The primary fracture network is associated with the aggregate grain boundary, and occurs with short exposure to microwaves, whereas the secondary network occurs randomly in the cement phase and spreads with increased exposure to microwave heating. Just as for the primary network, properties of interest of the secondary network include average properties such as total length, surface area and crack branch number, and statistical properties such as crack branch length, nodes, ends and width distributions. Contrary to the primary network fractures, **Figs. 23**, **24** shows that on average, cracks from the secondary network do not appear to grow wider with microwave treatment, but the total length and number of branches per unit area do increase with microwave heating time. The crack branch length distribution follows a log-normal distribution, as shown in **Fig. 25**, and does not change significantly between samples nor with increased heating duration. Put another way, the growth of individual fractures in the cement paste and the growth of the secondary fracture network as a whole occur together and in constant proportion. This is not unexpected as once the

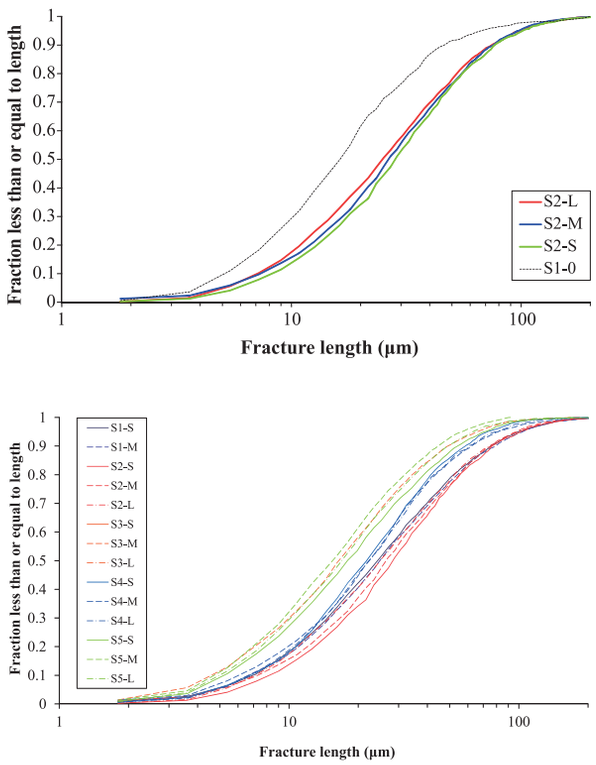

Fig. 25 Branch size distributions, secondary fracture network. Top: for sample S2. Bottom: for samples S1 to S5.

cement paste is disconnected from the aggregate, shrinkage is no longer constrained. This distribution is directly associated with the fineness of the fragments that form after comminution of the microwave-heated concrete samples. Additional research is required, however, in order to correlate the topological properties of the secondary network to the size distribution of the fragments obtained by comminution.

To finalise the discussion about the two fracture networks identified in this work, it was decided to take a look at their relative significance on properties of relevance to the recycling problem. As discussed earlier, the secondary crack length increases with microwave exposure time, i.e. with concrete energy absorption. **Fig. 26** shows the variation between total secondary network crack length relative to the total crack length and microwave exposure time. **Fig. 27** shows that while the total crack length increases steadily with increased microwave exposure, the rate of increase of the secondary-network crack length is faster, and is the key player in the loss of mechanical strength of microwave-heated concrete. As an illustration of this last point, **Fig. 28** shows the measured relationship between the secondary network total crack length relative to the total crack length and the strength of the concrete samples measured by HPB. The correlation is significant, with strength dropping almost in linear proportion to the increase in secondary network total crack length.

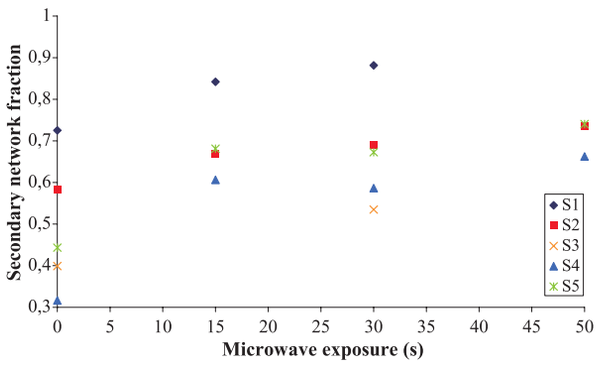

Fig. 26 Fraction of total crack length composed of secondary network.

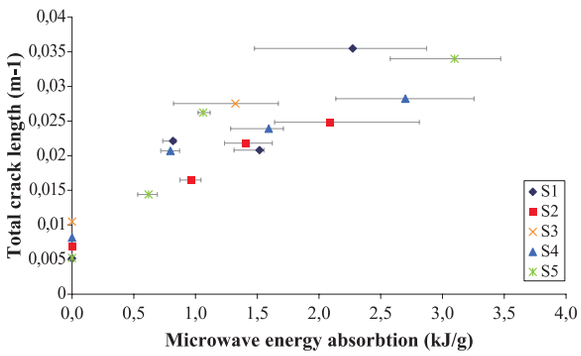

Fig. 27 Total combined crack length of primary and secondary network.

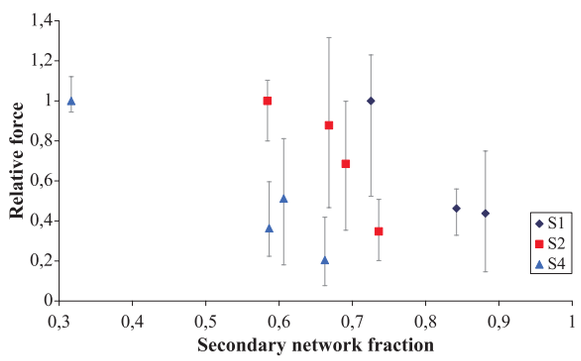

Fig. 28 Relative change in fracture force with fraction of total network length composed of secondary network.

5. Implications for development of a microwave -based concrete recycling process

This work, through local analysis of changes in the structure of porosity that occurs during the microwave heating of concrete, has added additional evidence to the body of existing knowledge about the potential value of microwave heating for the development of a concrete recycling process. The pattern of crack growth is evidence of drying shrinkage as it is the only crack formation mechanism to occur over the entire temperature range observed.

Importantly for concrete recycling, these results show that microwave heating causes fractures to occur at the aggregate/cement paste interface, and importantly for energy efficiency, these are the first microwave-induced fractures to form. Also of note is the observation that the properties of individual concretes are relatively unimportant. This will make the implementation of a microwave-based concrete recycling process easier as it will not require adaptation to different waste sources.

The analysis of fracture porosity has shown that microwave heating interacts strongly with the ITZ to generate a large-scale network of fractures at the aggregate/cement paste interface. Experimental results indicate that this primary network of fractures forms with a short exposure to microwaves. As previously stated, the most efficient microwave generators for embrittlement are those with the highest power output, however, this is based on the assumption that the key embrittlement mechanism is differential thermal expansion. It is still desired that the process is selective, and the higher the power of the microwave generator, the faster heating occurs, the less that conduction can play a role and the more selective the process is. Therefore a high-power generator is most likely still desirable but as dehydration appears to be the key mechanism in the microwave processing of concrete waste, one may expect the point at which increasing power output is no longer economical is lower than it would be for a similar application in mineral processing. In any case the technology needs to be perfected and the appropriate compromise found.

It was noted in a previous work (Lippiatt and Bourgeois, 2012) that the liberation of aggregate particles is seen only after extensive microwave treatment. This was measured using macro techniques, sample fracture then selective dissolution. Conversely, local techniques, i.e. SEM inspection of treated samples used in this work, show that fracture at the cement/aggregate interface occurs much earlier in the treatment process. What occurs later under extended microwave exposure is more extensive fracture growth throughout the cement paste. This extended cement crack growth greatly reduces the strength of the concrete sample and causes the sample to break into much smaller fragments when crushed under impact. It was due to this fragmentation in the cement paste that liberation was measured by impact fracture at such a high level for long-treated samples in this previous work, rather than any actual increase in the separation of the aggregate particles and cement paste.

The SEM results suggest that the aggregate and the cement were well separated, but unless an appropriate mechanical comminution technique is selected, the aggregate samples will remain encased within larger cement paste fragments. Development of an industrial solution would also require identification of an appropriate comminution process to exploit this primary network so as to close the gap between physical and textural liberation with minimum energy consumption.

The above discussion considers optimisation of the liberation of aggregates, and ignores other important dimensions of the process, towards which results from this work bring answers. Once comminution has taken place, a concrete's aggregate and cement paste would have to be separated. One possibility that can be inferred from this work's results would be to induce a dense secondary fracture network by microwave heating prior to comminution in order to generate cement fines, which could then easily be separated from liberated aggregates by dry screening. Moreover, reducing the cement paste to a fine powder would help facilitate the recycling of the cement paste. From these considerations, there is significant scope for development of a microwave-based recycling process, however, given that the microwave heating step is necessarily part of a processing chain that includes comminution, separation and transport, finding the right operating conditions is going to require additional research and development work.

6. Concluding remarks

The applicability of microwave heating to the recycling of concrete is an important issue, given the increase in demand for concrete, the scarcity of natural aggregate resources and the environmental footprint of clinker production. While a number of published works have shown the potential of developing a microwave-based recycling process based on macroscopic measurements relevant to concrete recycling performance, namely aggregate liberation, product fineness and mechanical embrittlement, this work establishes links between fracture porosity and observed macroscopic effects through local texture observation and analysis.

The work associates the formation of two fracture networks with specific recycling issues:

– The primary fracture network is constituted of large connected fractures that are associated with the aggregate grain boundaries, and occurs with short exposure to microwaves. This network, by essence, is responsible for the textural liberation of aggregates. The primary network appears to occur at the early stage of microwave heating.
– The secondary network is constituted of seemingly randomly occurring cracks which spread through the cement phase with increased exposure to microwave heating. This dense network of smaller fractures is strongly linked to the loss of mechanical strength of concrete, and the degree of actual physical liberation of aggregate particles obtained after impact fracture of microwave heated concrete samples.

Mechanisms responsible for the formation and growth of both primary and secondary fracture networks are undoubtedly complex, but the evidence from this work indicate that they are controlled by local drying shrinkage, which starts at the interfacial transition zone around aggregate particles and eventually spreads throughout the bulk of the cement matrix.

Capitalising on the high degree of textural liberation of aggregate particles obtained after a short microwave heating time only, meaning lower energy consumption, requires identification of a suitable comminution solution. The inefficiency of single-particle impact fracture to physically liberate aggregate particles that were texturally liberated suggests that impact-based comminution equipment is not the best option. It is thought that shear-inducing comminution technologies such as high-pressure grinding rolls should be investigated in conjunction with microwave heating.

The longer exposure to microwaves, however, yields extensive growth of secondary network fractures in the cement matrix and subsequent production of cement fines through comminution. Increased cement fines may be valuable for the separation of aggregates from cement and recycling of the cement itself as part of the overall recycling scheme.

In the end, it can be concluded that finding the best position and operating conditions for the microwave heating step in the concrete recycling chain is not a clear-cut situation. The setting of the microwave heating process to grow the primary and secondary fracture networks to a specific level depends on the subsequent process steps, including comminution, product separation and possibly transport.

Having looked at the local scale, one important conclusion from this work is that development of a microwave-based concrete recycling process must consider the processing chain in its entirety.

Acknowledgements

The authors acknowledge the financial support of the Agence Nationale de la Recherche (the French National Research Agency) through the COFRAGE project from the ECOTECH research programme. The authors want to acknowledge Dr. Emmanuel Cid, Senior Research Scientist with the Laboratoire de Génie Chimique, for his valuable contribution to the image analysis of the fracture patterns.

References

Akbarnezhad A., Ong K.C.G., Zhang M.H., Tam C.T., Foo T.W.J., Microwave-assisted beneficiation of recycled concrete aggregates, Construction and Building Materials, 25 (2011) 3469–3479.

Ali A.Y., Understanding the effects of mineralogy, ore texture and microwave power delivery on microwave treatment of ores, Ph.D. thesis, University of Stellenbosch, 2010.

Ben Haha M., Gallucci E., Guidom A.,Scrivener K.L., Relation of expansion due to alkali silica reaction to the degree of reaction measured by sem image analysis, Cement and Concrete Research, 37 (2007) 1206–1214.

Bourgeois F., Banini G., A portable load cell for in-situ ore impact breakage testing, International Journal of Mineral Processing, 6 (2002) 31–54.

Brough A.R., Atkinson A., Automated identification of the aggregate–paste interfacial transition zone in mortars of silica sand with portland or alkali-activated slag cement paste, Cement and Concrete Research, 30 (2000) 849–854.

Costes J.R., Majcherczyk C., Binkhorst I.P., Total recycling of concrete, Commissariat à l'Énergie Atomique, online publication, 2010.

Diamond S., Mercury porosimetry an inappropriate method for the measurement of pore size distributions in cement-based materials, Cement and Concrete Research, 30 (2000) 1517–1525.

Figg J., Microwave heating in concrete analysis, Journal of Applied Chemistry and Biotechnology, 24 (1974) 143–155.

Fischer C., Davidsen C., Europe as a recycling society, Report for the European Environment Agency, 2011.

Igarashi S., Kawamura M., Watanabe A. Analysis of cement pastes and mortars by a combination of backscatter-based SEM image analysis and calculations based on the powers model, Cement and Concrete Composites, 26 (2004) 977–985.

Jerby E., Dikhtyar V., Aktushev O., Grosglick U., The microwave drill, Science, 298 (2002) 587–589.

Kingman S.W., Jackson W., Bradshaw S.M., Rowson N.A., An investigation into the influence of microwave treatment on mineral ore comminution, Powder Technology, 146 (2004a) 176–184.

Kingman S.W., Jackson K., Cumbane A., Bradshaw S.M., Rowson N.A., Greenwood R., Recent developments in microwave assisted comminution, International Journal of Mineral Processing, 74 (2004b) 71–83.

Kiss L., Shönert K., Liberation of two component material by single particle compression and impact crushing, Aufbereit.-Tech, 30 (1980) 223–230.

Klee H., The cement sustainability initiative, Progress report for the World Business Council for Sustainable Development, Duesseldorf, Geneva, 4 June 2009.

Lippiatt N., Bourgeois F., Investigation of microwave-assisted concrete recycling using single-particle testing, Minerals Engineering, 31 (2012) 71–81.

Mehta P., Monteiro P., Concrete: microstructure, properties and materials, 3rd Revised edition, McGraw-Hill Professional, 2005.

Piasta J., Sawicz Z., Rudzinski L., Changes in the structure of hardened cement paste due to high temperature, Matériaux et Constructions, 17 (1984) 291–296.

Roy D.M., Idorn G.M., Concrete microstructure, Strategic Highway Research Program, National Research Council, Washington, DC, 1993.

Symonds Group, Construction and demolition waste

management practices and their economic impacts, Report for the European Commission in association with ARGUS, COWI and PRC Bouwcentrum, 1999.

Tam V.W.Y., Tam C.M., Wang Y., Optimization on proportion for recycled aggregate in concrete using two-stage mixing approach, Construction and Building Materials, 21 (2007) 1928–1939.

Tavares L.M., King R.P., Single-particle fracture under impact loading. International Journal of Mineral Processing, 54 (1998) 1–28.

White T.L., Foster D.J., Wilson C.T., Schaich R., Phase II microwave concrete decontamination results, Oak Ridge National Laboratory, 1995.

Wong H.S., Head M.K., Buenfeld N.R., Pore segmentation of cement-based materials from backscattered electron images, Cement and Concrete Research, 36 (2006) 1083–1090.

Yang R., Buenfeld N.R., Binary segmentation of aggregate in SEM image analysis of concrete, Cement and Concrete Research, 31 (2001) 437–441.

Author's short biography

Nicholas Lippiatt

Nicholas Lippiatt holds a masters in materials science (France) and completed his bachelor's degree in materials engineering at the University of Queensland in Brisbane, Australia. He is currently completing a Ph.D. in materials science (Laboratoire de Génie Chimique, Institut National Polytechnique de Toulouse) in France on the use of microwave heating technology for concrete recycling.

Florent Bourgeois

Prof. Bourgeois holds a B.Eng. in materials science (France) and a Ph.D. in extractive metallurgy (University of Utah). He worked as a research fellow for the CRC Mining (Australia) from 1994 to 1996, and as a lecturer in minerals processing with the University of Queensland from 1997 until 2000. Between 2001 and 2005, he worked as project leader for the French Geological Survey's processing department. He now holds a tenured position at the University of Toulouse. His field of expertise is particulate process design and modelling, with emphasis on comminution, liberation, texture modelling, sampling of minerals and wastes.

5.3 Correlation between fracture porosity and relevant macroscopic concrete properties

To simplify the comparison of fracture porosity and concrete fracture properties a single mechanical property was identified as being most indicative of the milling potential of a material. In MINPROC2014 the mass specific fracture energy was identified as this key fracture property because it showed the widest variation and therefore was assumed to be the most sensitive to textural changes in a material. This was found not just for concrete but for many different materials. Fracture energy was then used as a point of reference to determine the key texture properties, characteristics of fracture porosity that determined how the fracture properties changed using principal component analysis (PCA).

5.3.1 Correlation between fracture porosity and fracture energy

Two variables can be shown to correlate by merely graphing one against the other. A principal component analysis (PCA) gives a value to the strength of the correlation and thus gives an idea of the confidence that can be placed on the existence of a link between them.

The process to create a PCA using the textural properties of concrete; the size, length and connectivity of each network then describing other values with the primary components of this PCA are described in *Introducing the concept of mechanical texture for comminution process modeling and design* [5.5] that will from here on be referred to as MINPROC2014. This article has been included in section 5.3.2.

The PCA showed that the characteristics of the primary and secondary network were individually clustered and these clusters were separate. The grouping of the properties of the two fracture networks gave value to the definitions used for each network. Once the principal components were calculated and the properties of each network were graphed in terms of the first two principal components, the properties of the same network were clustered together but properties of different networks were separated into different quadrants (MINPROC2014, Figure 9).

The relationship of individual results to the first two principal components (MINPROC2014, Figure 10) gives an idea of what these components mean in a physical sense. Untreated samples with little fracture porosity and samples that have the most fracture porosity are placed at either end of the x-axis, Principal component 1. Principal component 1 can therefore be said to represent the extent of fracture porosity growth. The samples that fall at each end of the y axis, Principal component 2, are those with the highest and lowest ratio of primary fracture length to secondary fracture length. Principal component 2 can be said to represent the relative quantity of each fracture type that has

formed in the sample. However this implies a difference in processing. The samples at the extreme of Principal component 2 are; low and medium microwave treated S1 at one end and long microwave treated S3 and 500°C oven treated S4. Other concrete types that have experienced the same heat treatment are not clustered in the PCA correlation circle. The only variation between tests besides heat treatment was the type of concrete used so Principal component 2 is assumed to be related to differences in the material. The manifestation of this difference in material properties is whether under thermal strain the growth of fracture porosity is primary dominant or secondary dominant. A summary of this idea is shown in Figure 5.22. It is noted that principal component 1 and 2 together explain 78% of the variation observed in the properties of fracture porosity.

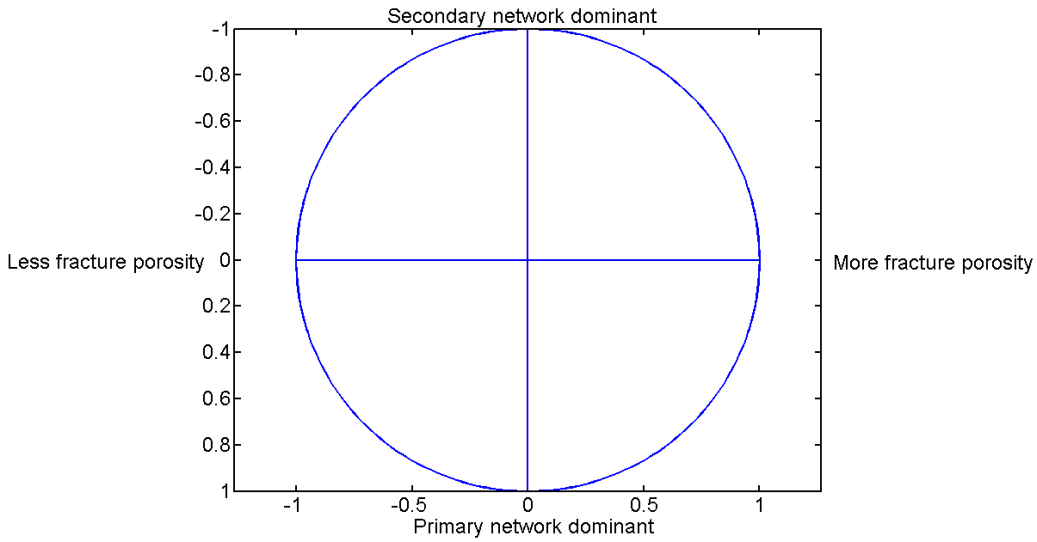

Figure 5.22. PCA circle of correlation for fracture texture properties showing the meaning of the relative position of a point in the PCA space in physical terms

With the principal components identified MINPROC2014 showed a strong link, considering the nature of the measurements, between mass specific fracture energy, the key mechanical property for processing, and fracture porosity. In particular the variation of mass specific fracture energy was shown to correspond to the growth of the secondary fracture network and the mean mass specific fracture energy was shown to correspond to primary network dominance and inversely to the growth of both fracture porosity networks.

All these observations added value to the idea of a textural perspective on material properties.

5.3.2 Introducing the concept of mechanical texture for comminution process modelling and design

The following 18 pages are devoted to the article Introducing the concept of mechanical texture for comminution process modelling and design that is to appear in the International Journal of Mineral processing in 2014.

Introducing the concept of mechanical texture for comminution process modeling and design

Florent S. Bourgeois[a,*], Nicholas R. Lippiatt[a] and Malcolm S. Powell[b]

[a] *Laboratoire de Génie Chimique UMR CNRS 5503, Université de Toulouse, FRANCE*
[b] *The University of Queensland, Sustainable Minerals Institute, Julius Kruttschnitt Mineral Research Centre, AUSTRALIA*

Abstract.
Modern comminution research and development is mainly product driven rather than material driven. An opinion that is gaining acceptance throughout the comminution community is that it is desirable for the comminution field to evolve towards material driven process design. To this end, this paper introduces the concept of mechanical texture, which corresponds to those textural properties of materials that have a direct bearing on their mechanical and fracture properties, which in turn should be the primary target for comminution process research and equipment design. The paper shows that mass specific fracture energy *Ecs* is a fracture parameter that is highly sensitive to variations in material texture, leading to selecting *Ecs* as the best mechanical texture index. The paper then shows that, in the case of concrete, a set of specific features of the fracture porosity that can be measured inside concrete texture correlate highly with *Ecs*, thereby defining mechanical texture for concrete comminution. The demonstration that it is possible to establish a direct link between textural properties of concrete and macroscopic properties relevant to comminution shows that material driven comminution process modeling and design is possible and should be encouraged.

Keywords: *mechanical texture, comminution modeling, ore breakage characterization, concrete recycling*

Highlights:

- New concept of mechanical texture embodies textural properties that control ore fracture.
- Mass specific fracture energy is a sensitive macroscopic ore texture index.
- Fracture porosity defines mechanical texture for concrete.
- Illustration of a direct link between mechanical texture and processing performance for concrete.

1. INTRODUCTION

Size reduction has been a pivotal process in the production of metals for as long as can be remembered, for beneficiation of minerals and waste. Size reduction unit operations are used throughout the minerals industry for the purpose of liberating valuable minerals, creating reactive surface area and producing desirable particle size distributions. As stated by Lynch in his introductory statement to his acclaimed 1977 textbook, "*the extent to which breakage must proceed depends on the fineness of intergrowth or the "natural grain size" of the valuable particle. The natural grain size may vary widely…*" (Lynch, 1977). This statement is perhaps one of the most important statements made in the early days of comminution modeling, as it recognizes the significance of ore texture in the size reduction process, and emphasizes its natural variability.

Surprisingly, despite the strong significance of material properties implied in Lynch's statement, the path which comminution research has followed since has diverged away from the material to be processed. Neither has it been focusing on the process undergone by particles inside comminution unit operations, but has been dedicated to modeling and predicting the product output from the unit operations. This approach to comminution modeling and optimization has permitted formalization of a coherent and

useful framework for what was prior an "empirical art", thus taking mineral comminution to an entirely new level. Over the past 4 decades, comminution research has served the industry well, giving it the means to increase production rates and meet society's needs. Comminution research did produce major conceptual advances, of which the most significant perhaps are the energy specific size reduction relationships, the breakage and selection functions for application of the population balance model to mineral comminution modeling, and the development of advanced simulation environments and control systems. And yet, the focus of comminution research and development has not been the ore itself, which finds itself embedded into sophisticated comminution models through some averaging property, distant from its actual physical properties and the variability thereof.

As a result, Powell et al. (2008) have formed the opinion that this comminution modeling approach has now reached an impasse, in that it can no longer evolve to meet the expectations of a modern mineral industry whose future depends on its ability to juggle scarcer and poorer ore bodies, rising energy costs, increasingly stringent environmental constraints, competition for access to water and fast changing societal needs. In order that the mineral industry can meet such a complex equation, Powell et al. propose a unified vision of comminution modeling, which some may consider as a paradigm shift relative to current practice. This vision focuses on the process itself, with the ambition of describing and predicting every individual event that occurs when comminuting an ore, down to the level of individual particles. This approach repositions the material to be processed to the heart of comminution modeling, which comes back to Lynch's statement cited above. This vision is largely fueled by the recent ability to simulate, with millions of objects, individual events that occur inside comminution machines in operation (Cleary, 2004; Cleary and Morrison, 2011; Cleary, 2013; Weerasekara et al., 2013). In retrospect, it is fair to recognize that such capabilities were nonexistent and inconceivable when modern comminution modeling research emerged, which justifies the path taken by comminution research. Being able to simulate individual stress events inside a full scale comminution machine means, in turn, that physical properties of mineral particles relevant to comminution must be identified and modeled. Hence, relating mineral texture of a particle to the manner in which it fractures under stress is one critical issue in Powell et al.'s vision of the future of comminution modeling.

Prediction of the fragmentation behavior of a mineral particle under stress from knowledge of its texture is one of the key ingredients to Powell et al.'s vision of the future of comminution modeling. There are a number of steps to achieving this, of which the following 3 are perhaps the most significant:

Step 1: Measurement and modeling of the *mineral texture,* which is a spatial description of the components that make up the texture of the ore. Texture modeling for the purpose of enacting Powell et al.'s unified comminution model requires means for quantifying and reconstructing particle texture in three dimensions.

Step 2: Identification of the textural components responsible for the mechanical / fracture behavior of the texture under stress, whose combination define what is here referred to as *mechanical texture*. The concept of *mechanical texture* embodies the direct link between mineral texture and the mechanical/fracture behavior of the ore under stress.

Step 3: Simulation of the fracture of a mineral particle with known mechanical texture under given loading conditions (D. Weatherley, 2013). This 3rd step provides the link between ore texture and DEM modelling for predicting the outcome of comminution processes.

The present contribution focuses on the notion of mechanical texture, which is the pivot between mineral texture and DEM modeling.

2. DEFINITION OF MECHANICAL TEXTURE

As stated above, assigning a mechanical texture to an ore implies that one identifies and ranks the textural features responsible for the physical fragmentation behavior of the texture of interest under stress, and the variability thereof. *The set of textural features that govern the mechanical behavior of the material of interest defines the mechanical texture of the material*. Textural features of interest may be associated with grain boundaries, pores, hard inclusions, etc. This raises the question of how one may identify such textural properties in the first place.

The idea proposed here is to define some simple scheme for identifying such textural properties. When fracturing single particles by impact on a Hopkinson bar, one recognizes that individual particles behave differently from one another. The range of mechanical behavior of the particles is a direct measure of the variability of the mechanical texture of the material. We propose here that identification of mechanical texture components of significance relies on identifying those components which correlate most with the variability of mechanical behavior measured by sensitive equipment such as Hopkinson bars.

This scheme first requires that one identifies the macroscopic fracture property which varies most significantly for a given lot of particles, its variability being taken as an indicator that the property in question best captures the intrinsic mechanical heterogeneity of the material of interest. This property is a macroscopic index for the mechanical texture of the ore. Identification of textural properties which comprise the mechanical texture of the material of interest will be those which correlate most with this macroscopic index.

In this section, we establish that *mass specific fracture energy,* noted *Ecs*, as measured by Hopkinson bar impact tests is a sound macroscopic index of mechanical heterogeneity. It is also interesting to note that *Ecs* has become a parameter of convergence for all current comminution models, which makes it likely that the concept of mechanical texture should eventually interface well with current comminution modeling schemes.

To derive this index, to which we shall eventually correlate textural properties of the ore, the authors decided to test what may be considered a model material due to its extreme level of homogeneity from a mineral texture standpoint. Six millimeter soda lime glass beads (Figure 1) underwent impact testing on a Hopkinson bar (Bourgeois and Banini, 2001).

FIGURE 1. 6mm soda lime glass beads used for single-particle impact testing on a Hopkinson bar

Figure 2 gives the force-time profiles measured by Hopkinson bar impact testing for the 6mm soda lime glass beads. Tests were conducted using a 60mm / 882g stainless steel ball bearing dropped from 80mm. The clean superimposition of the force rise, which is expected given that the particles have the same shape, confirms the repeatability of the test protocol. What is significant here is the range of fracture forces measured for individual particles. This range spans from 2231N to 4253N, i.e. it varies by a factor of 2, which can be described satisfactorily using a Weibull distribution with parameters k = 6.6 and λ =

3433 N. The mass specific fracture energy *Ecs*, which is the energy actually absorbed by the particle before the point of fracture - not to be mistaken for the potential energy of the striker - varies by a factor of 4.5. The broad range of mass specific fracture energies reflects the significant variability of mechanical properties of the soda lime glass beads, despite their being a model material.

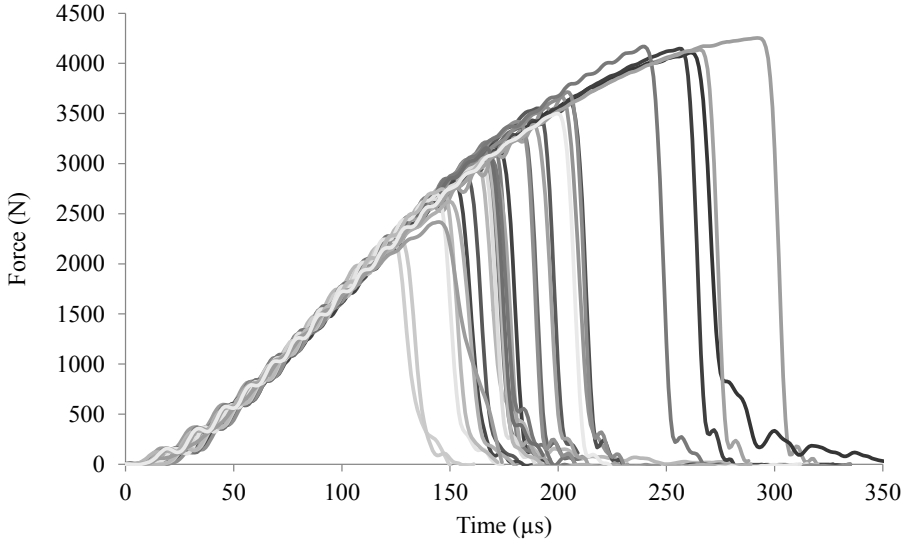

FIGURE 2. Force-time profiles measured on 31 soda lime glass beads

Force-time measurement from Hopkinson bar tests yields estimation of particle strength, stiffness and mass specific fracture energy (Bourgeois, 1993; Tavares and King, 1998). The former relates to the maximum load which the particle can sustain before fracturing, whereas the latter is associated to the amount of deformation of the loaded particle. Distributions of force at fracture and mass specific fracture energy measured for soda lime glass beads are shown in Fig. 3.

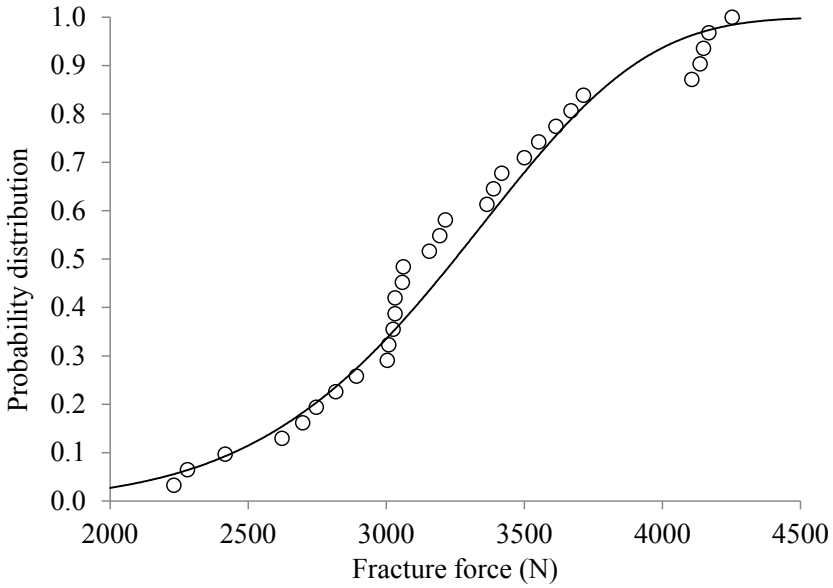

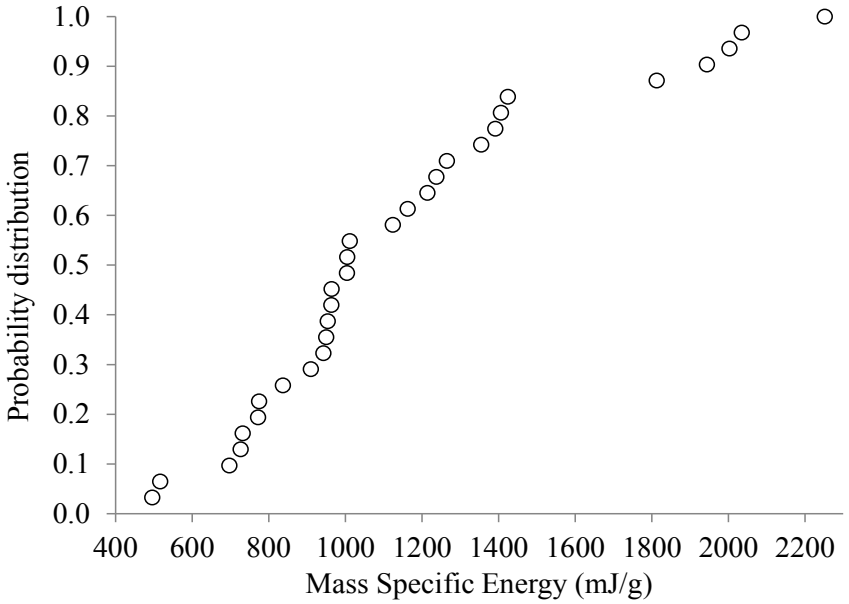

FIGURE 3. Measured distributions of force at fracture and the mass specific fracture energy for 6mm soda lime glass beads

The distribution of fracture properties, which is revealed by the Hopkinson impact test carried out on individual particles, yields a good appreciation of how significant the distribution of mechanical properties is, even for a material seemingly as texturally homogeneous as soda lime glass. Tavares and King (1998) have shown that there is a strong correlation between particle strength and mass specific fracture energy for glass beads, but the issue here is not so much about the correlation between mean values, but more on the variability, i.e. the spread of the distribution of the measured properties.

Table 1 summarizes the measured values of relative standard deviation (RSD) for mass specific fracture energy, strength and stiffness for the 6 mm soda lime glass beads.

TABLE 1. Measured range of Hopkinson bar test properties measured on 6 mm soda lime glass beads

	Mass specific fracture energy	**Strength (or Fracture force)**	**Stiffness**
RSD	0.39	0.17	0.16

Of the 3 properties which are readily available from Hopkinson bar impact tests, the mass specific fracture energy exhibits the largest variability. It is concluded that the mass specific fracture energy is a macroscopic index most sensitive to the variability in impact fracture behavior of the soda lime glass beads; hence textural properties that correlate strongly with *Ecs* should define the mechanical texture of the glass beads.

Taking numerous sources of Hopkinson bar test results from the literature for samples of 25 particles or more, independently obtained on a wide variety of materials, natural ores and manmade materials, Figure 4 shows the RSD for mass specific fracture energy and strength. By and large, the majority of points are located near or above the bisecting line. Indeed, the RSD of the mass specific fracture energy is, on average, 48% higher than that of particle strength. It is concluded that mass specific fracture energy is, on average, the best index for the variability of fracture properties of impact loaded materials.

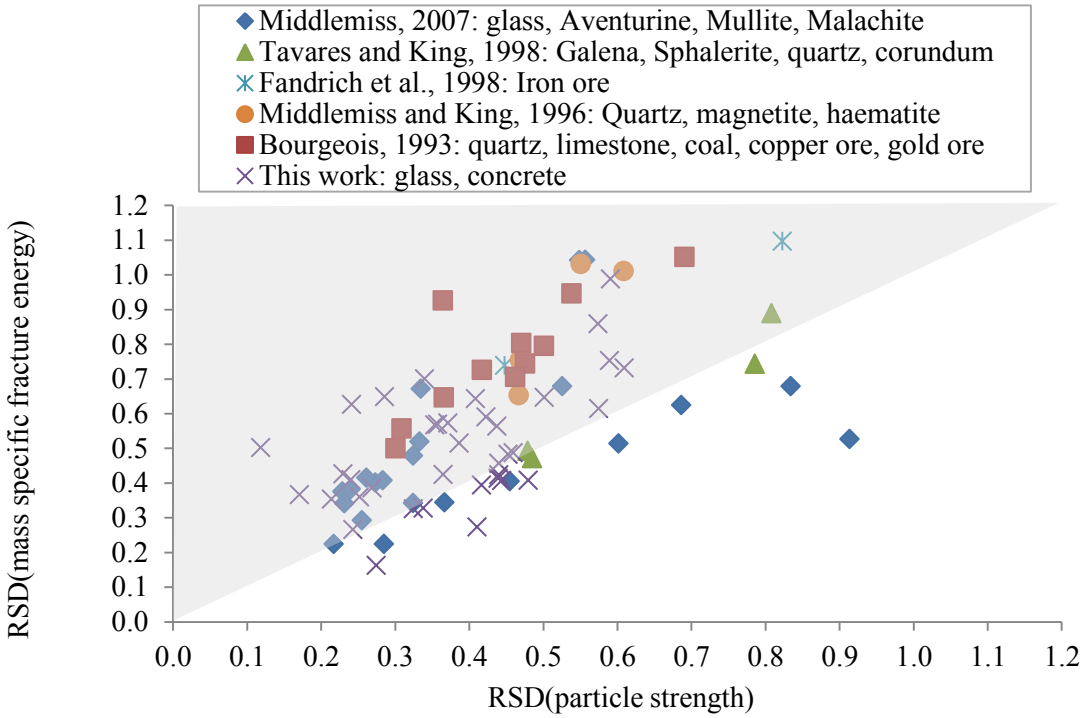

FIGURE 4. Validation of the *Ecs* as the Hopkinson bar test derived fracture property most sensitive to variations in mechanical texture

From this analysis of mechanical texture variability from Hopkinson bar testing, it is proposed to use mass specific fracture energy as the mechanical texture index of the ore. The RSD of the *Ecs* therefore is a macroscopic measure of the variability in mechanical texture of the material.

Using this index requires that a large enough number of particles be tested with the Hopkinson bar. Analysis of textural heterogeneity from an insufficient number of particles would be futile, given the wide confidence intervals for the estimate of the standard deviation. In practical terms, the analysis proposed here requires that 30 particles or more be tested, as it is commonly applied to Hopkinson bar testing.

For the 6mm soda lime beads, Ecs = 292.0 mJ/g and $\mathrm{RSD}(Ecs) = \dfrac{114.1\ \mathrm{mJ/g}}{292.0\ \mathrm{mJ/g}} = 0.4$

For a given material, it is known that *Ecs* obeys a log-normal distribution (Bourgeois, 1993; Middlemiss, 2007). Fig. 5 shows the distribution of RSD(*Ecs*) values from the data plotted in Fig. 4. The distribution can be approximately described by a left-truncated Gaussian distribution with mean = 0.56 and standard deviation = 0.23.

Testing an ore on the Hopkinson bar and positioning its mechanical texture variability index RSD(*Ecs*) in this distribution may be a useful tool for ranking its heterogeneity in mechanical texture against known materials. It is also an interesting manner by which one may readily quantify the effect of a pretreatment on the mechanical properties of ores. Indeed, pretreatment are expected to affect the mechanical texture of the ore, both in mean value and variation about the mean, the former being captured by the proposed mechanical texture index *Ecs* and the latter by RSD(*Ecs*).

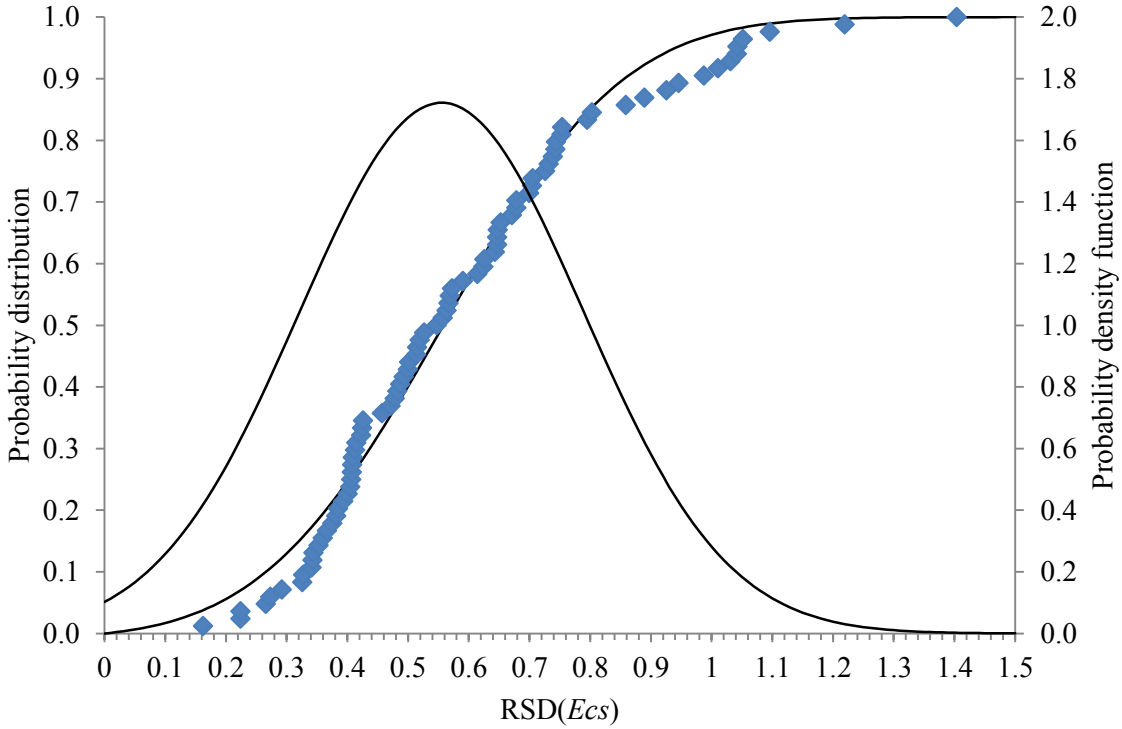

FIGURE 5. Distribution of RSD(*Ecs*) for the data from Fig. 4.

The distribution of *Ecs* and that of RSD(*Ecs*) are statistical fracture properties which can be fed into population balance models (King and Bourgeois, 1993). However, they are not relevant for DEM comminution models which require a model mechanical texture at the particle scale. As a step forward towards such an endeavor, the next section of the paper investigates the textural features responsible for the mechanical texture, which is defined on a macroscopic scale by *Ecs*. Such textural properties are those which correlate most with the proposed mechanical texture variability index *Ecs* and associated variability RSD(*Ecs*). Provided such properties can be identified, they will in turn need to be modeled spatially, which reverts to the mineral texture modeling step presented in introduction, in order to serve as input to DEM modeling.

3. UNRAVELING THE LINK BETWEEN MINERAL AND MECHANICAL TEXTURE

As indicated in the introductory statements, material driven process design requires identification of those textural properties that dictate the mechanical texture of the material. Such properties are utterly material specific; hence it is difficult to imagine some universal way to link mineral and mechanical textures. Nevertheless, the link exists, and it ought to be the focus of material driven process design. The following section explores this link for the case of concrete, with the end objective of designing a material driven process for recycling concrete. In the context of concrete recycling, processability is measured in terms of aggregate liberation, comminution product fineness and mechanical strength of the material. For the purpose of exploring the link between texture and processability, the paper focuses on concrete strength as an example, which, in processing terms, equates to comminution energy. The question therefore is to identify the textural parameters that make up the mechanical texture of concrete, i.e. the textural parameters which correlate most strongly with the proposed mechanical texture index *Ecs*.

The textural property which is considered to be of the most interest is related to porosity. Porosity is a complex textural property in concrete, which can be manipulated in a number of ways. It can be changed at the mixing stage, through varying the water to cement ratio for example, but also by heating. In order to generate different fracture porosity patterns, the properties of which will be correlated to the mechanical texture variability index, the authors chose to heat laboratory-made concrete samples either externally, with an oven, or using microwaves (Lippiatt and Bourgeois, 2014).

3.1. MATERIALS AND METHODS

Concrete samples were cast from a mixture of CEM II/B-LL 32.5N Portland cement and narrowly sized 2-2.5mm siliceous aggregate particles. Five different concretes were made using three different water to cement ratios (w/c) and three different aggregate to cement ratios (a/c). The sample preparation and testing protocol is represented in Fig. 6.

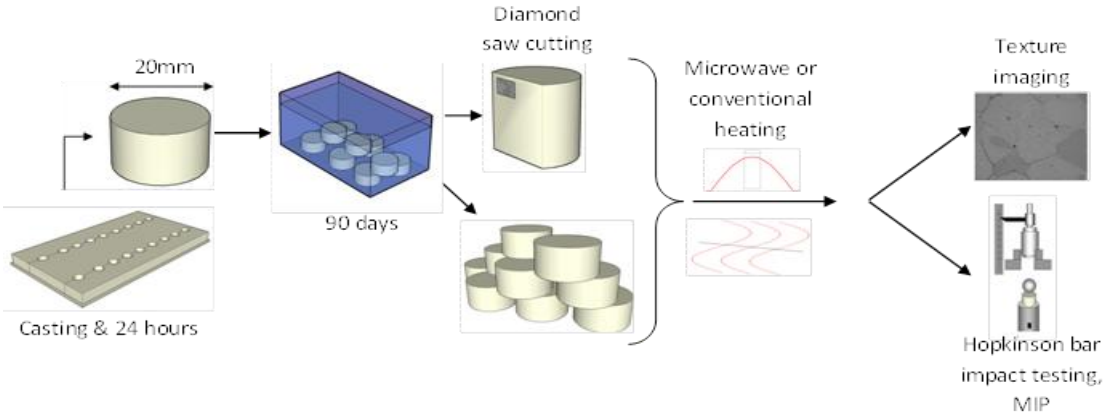

FIGURE 6. Concrete sample preparation and testing protocols.

Samples were cast in 20mm (≈10g) cylinders and were tested in two ways. The first protocol consisted of heating whole cylindrical particles, and then subjecting them to Hopkinson bar impact testing. The second protocol, dedicated to texture analysis, consisted of diamond saw cutting samples to expose a flat surface in the cylindrical samples prior to heating them, and then observing the flat surface by electron microscopy (SEM) after treatment. The primary concern of this protocol was avoiding tampering with the treated sample surface before observation. Porosity was characterized via a number of features measured on SEM digital images. Approximately 20 images were used per sample, of which 10 were taken at a magnification of 40x and 10 at a magnification of 200x, yielding images with resolutions of 9μm/pixel and 1.8μm/pixel respectively. For full details, see Lippiatt and Bourgeois (2014).

3.2. TEXTURE AND EMBRITTLEMENT

On a macroscopic scale, an increase in the porosity of concrete due to heating causes concrete to weaken. This is a key problem associated with the fire resistance of concrete (Willam et al., 2005). Fig. 7 shows the mass specific fracture energy obtained for a set of 33 concrete samples with varying aggregate to cement ratios (a/c). Mass specific fracture energy, as measured by Hopkinson bar testing, exhibits an inverse relationship with total porosity, as measured by mercury intrusion porosimetry (MIP). The correlation is significant, and yet the measurements show a large degree of scattering.

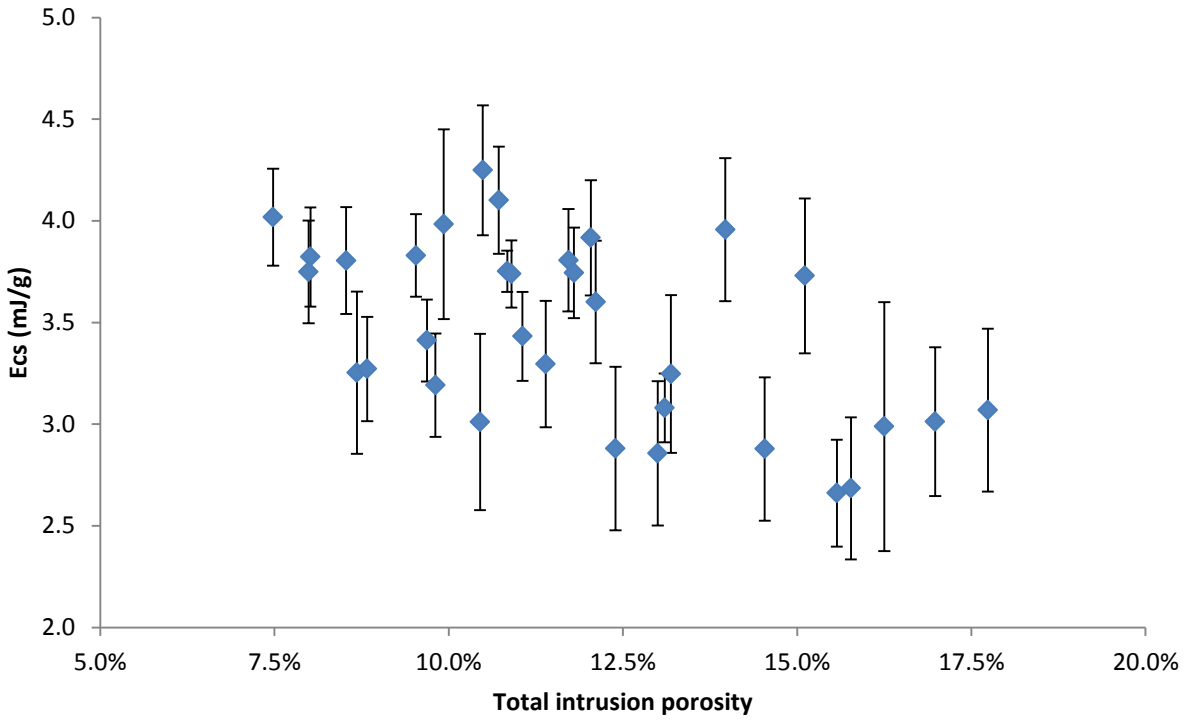

FIGURE 7. Measured variation between mass specific fracture energy and total porosity measured by MIP.

Fig. 7 confirms a direct link between textural (porosity) and mechanical (*Ecs*) properties for concrete. However the macroscopic nature of total intrusion porosity means that it has little power in explaining the fracture behavior, hence the scattering of Fig. 7. It is therefore not an appropriate property to be used as a mechanical texture property. The source of changes in mechanical texture, as measured by *Ecs*, was sought at the local scale by quantifying the properties of fracture porosity. Indeed, defining the term *fracture porosity* to describe the fracture system in concrete, the authors have shown (Lippiatt and Bourgeois, 2014) that distinct changes in fracture porosity occur, albeit at different scales inside the concrete, during heating. Through observation of numerous heated concrete samples, the authors have identified that fracture porosity, which changes with heating temperature and duration of exposure to heat, occurs as two distinct fracture networks. Fig. 8 illustrates the form taken by fracture porosity inside a concrete sample.

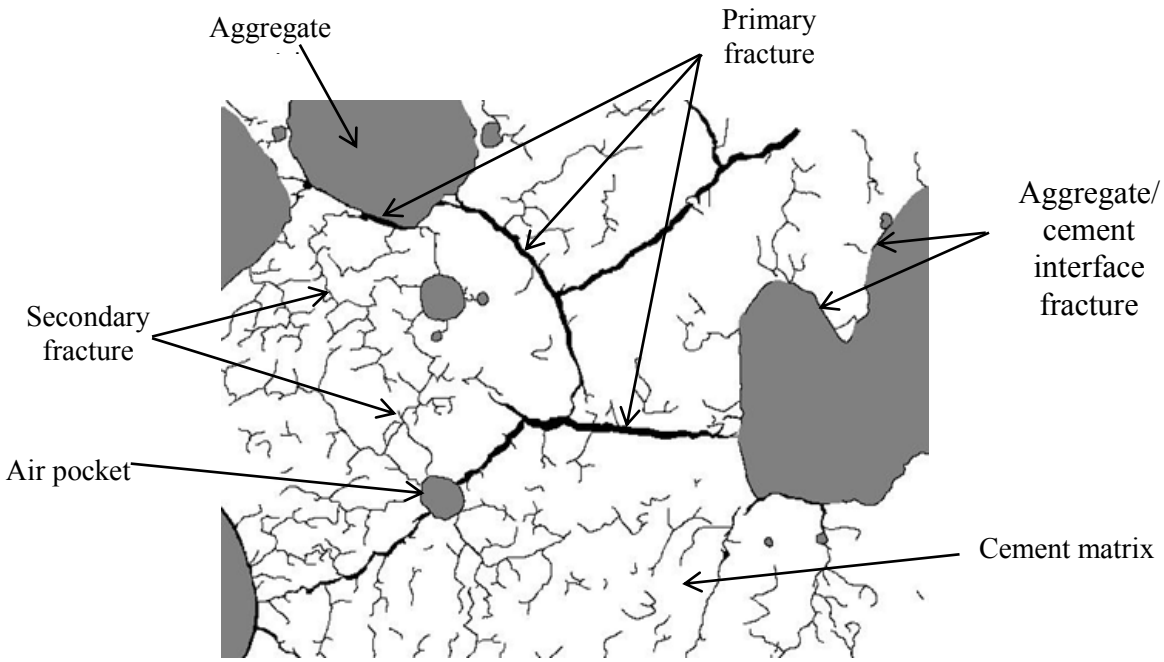

FIGURE 8. SEM photomicrograph exemplifying the formation of heat-induced primary and secondary fracture networks

The first system of fractures consists of large scale fractures that run along grain boundaries, often joining aggregate particles and air pockets present in the cement phase. The formation of this *primary network*, noted N1, is associated with the aggregate-cement interfacial transition zone (ITZ) [4], which is a few tens of micrometers thick. It is known for its high relative water content, steep moisture gradient, high porosity and high portlandite content. Air pockets play a role in dissipating heat-induced stresses inside the cement matrix; hence the convergence of primary network fractures as seen in Fig. 8.

Observation of concrete texture for low microwave energy inputs and low furnace temperature, points towards fractures being initiated near aggregate grain boundaries, hence inside the ITZ and forming a more or less connected network of large fractures that percolates through the concrete sample. X-ray tomographic images confirm the existence and percolation of the primary fracture network.

For the purpose of analysis primary network is defined as all fractures at the cement paste/ aggregate interface and all fractures they are connected to. In the case of divergence only the widest connection is included in the primary network. In the case of two branches of equal width the only the longest was included in the primary network. All other fractures in the cement paste are defined as being of the secondary network. All analysis of the primary network was performed using images at 40x magnification (9μm per pixel). Analysis of the secondary network was performed using images at 200x magnification (1.8μm per pixel). For further details see Lippiatt and Bourgeois (2014).

To understand the textural properties used in analysis first requires an understanding of the division of image areas. Aggregate particles and cement paste could be easily identified so pixels were divided into those that showed part of an aggregate particle and those that did not, the latter defined as cement area for analysis purposes.

The properties which define the primary fracture network are:

- Total fracture length (m/m^2): The sum of the lengths of all the primary network fractures in all highlighted images divided by the cement area in all highlighted images for that combination of concrete type and pre-treatment.
- Fracture area (m^2/m^2): The sum of the area of all the primary network fractures in all highlighted images divided by the cement area in all highlighted images for that combination of concrete type and pre-treatment.
- Textural liberation: The ratio of the total length of fractures at the aggregate/ cement interface divided by the total length of aggregate/ cement interface.
- Nodes per object: How many fractures diverged from the aggregate/ cement paste interface into the cement paste phase.

The secondary fracture category consists of a large number of small fractures that seem to form randomly, or at least more randomly than fractures in the primary network, throughout the cement paste phase. The density of fractures in this *secondary network*, noted N2, increases with heat energy input.

Total fracture length and fracture area were defined in the same way for both the primary and secondary network. The other properties which define the secondary fracture network are:

- Number of branches per object: The average number of fracture intervals (branches) that diverge from every grouping of connected fractures (objects).
- Number of branches per fracture area: Using the same number of branches as the definition above but dividing the value by cement area rather than number of objects.
- Euler number: A measure of the connectivity of the fracture network using the Euler characteristic relating the number of vertices (V), edges (E) and faces (F) (Early, 1999).

  $$x = V - E + F$$

  Which for this case becomes

  $$x = V - b + 1$$

  where b is the number of branches, as F=1 for a two dimensional object.

As it was discussed in the introductory statement, mass specific fracture energy is a macroscopic material property which appears to be most sensitive to textural variation in the material, hence the present focus on chasing the textural parameters responsible for mass specific fracture energy in concrete. This endeavor however should be understood as a specific illustration of the concept of finding causal relationship between textural properties and macroscopic properties of materials relevant from a processing perspective. In this paper, textural properties of concern are those of the primary and secondary fracture networks, whereas the physical fracture property of processing value (and changes thereof) is the mass specific fracture energy.

The principal component analysis (PCA) was selected for identification of causal relationships between properties of fracture porosity, mass specific fracture energy *Ecs* and RSD(*Ecs*). Principal components were calculated using textural variables from the primary and secondary fracture networks only. The mass specific fracture energy and its RSD, measured by Hopkinson bar impact testing, were added to the PCA only after the principal components had already been calculated relative to the textural variables. The rationale behind defining the principal components solely in terms of textural parameters first and then adding the illustrative mechanical properties afterwards was deemed suitable for finding the textural properties that make up the mechanical texture of concrete. This approach is in fact implied by the concept of mechanical texture.

This PCA analysis used:

- 4 textural variables for the primary fracture network N1 (N1_var5 to N1_var8), and 5 textural variables for the secondary fracture network N2 (N2_var9 to N2_var13), so that the PCA analysis was carried out using 9 variables. Table 2 gives the correspondence between the PCA variables and their actual physical meaning.
- The number of individuals was 34.
- The illustrative variables were the mass specific fracture energy *Ecs* (mJ/g) and RSD(*Ecs*). Since this *Ecs* is log-normally distributed, the variable used in the PCA analysis was the natural logarithm ln(*Ecs*), which is normally distributed. It was checked (See Fig. 5) that RSD(*Ecs*) is normally distributed, hence it was used directly.

TABLE 2. Correspondence table between PCA variables and their actual physical meaning

Fracture network	Texture variable name	Texture variable definition
Primary	N1_var5	Total fracture length (m/m^2)
	N1_var6	Fracture area (m^2/m^2)
	N1_var7	Textural liberation
	N1_var8	Nodes per object
Secondary	N2_var9	Total fracture length (m/m^2)
	N2_var10	Fracture area (m^2/m^2)
	N2_var11	Number of branches per fracture
	N2_var12	Number of branches per fracture area
	N2_var13	Euler-Poincaré number

After normalization, the normal distribution of all 9 textural variables was verified. Fig. 9 shows the first two components of the PCA analysis run using the 9 textural parameters of the fracture networks. Principal components 1 and 2 accounted for 58% and 20% of the total variation respectively. These components are noted PC1 and PC2 respectively.

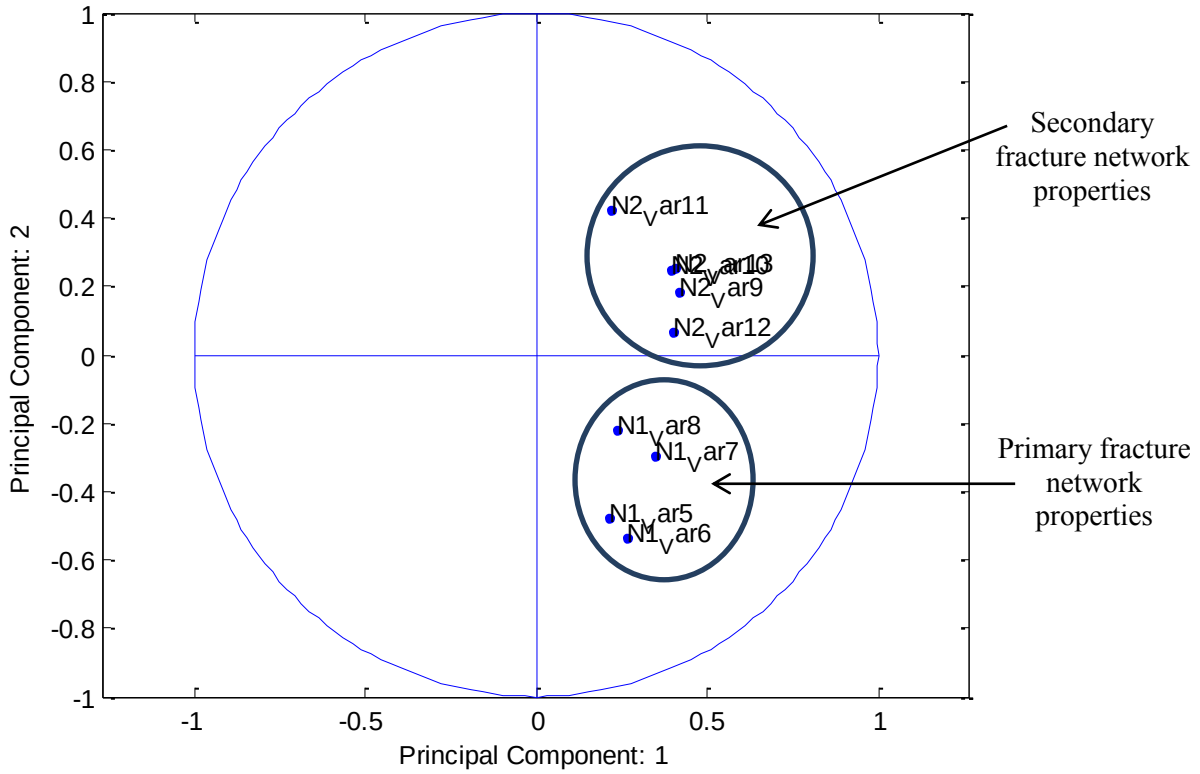

FIGURE 9. PCA analysis results for primary and secondary fracture network properties

On the circle of correlations, we firstly note that there are two clearly separated clusters, each in a separate quadrant, corresponding to the primary and secondary fracture networks. This lends credence to the assertion made from visual observations that there are two distinct systems of fractures occurring in concrete. Secondly, we observe that the primary and secondary clusters are both on the same side of the first principal component (noted PC1) axis.

Positioning the 34 individuals used to carry out the PCA analysis inside the PC1-PC2 plane, as shown in Fig. 10, we find that:

– All unheated concrete samples, ending with the "r" subscript, stand clustered and close to the left side of the PC1 axis, whereas the concrete sample with the least strength, which was obtained by heating to 500°C in a furnace, is directly opposite the PC1 axis. From these observations, it is inferred that the PC1 axis is a measure of the degree of fracturing of the texture.

– Defining the N2/N1 fracture length ratio as the ratio between the total fracture length of the N2 and N1 fracture networks, we observe that the individuals whose ratio is highest stand on the upper part of the PC1-PC2 plane, close to the PC2 axis, whereas samples with the lowest ratios stand directly opposite. The conclusion is that the PC2 axis is a measure of the degree of significance of the secondary fracture network over the primary fracture network.

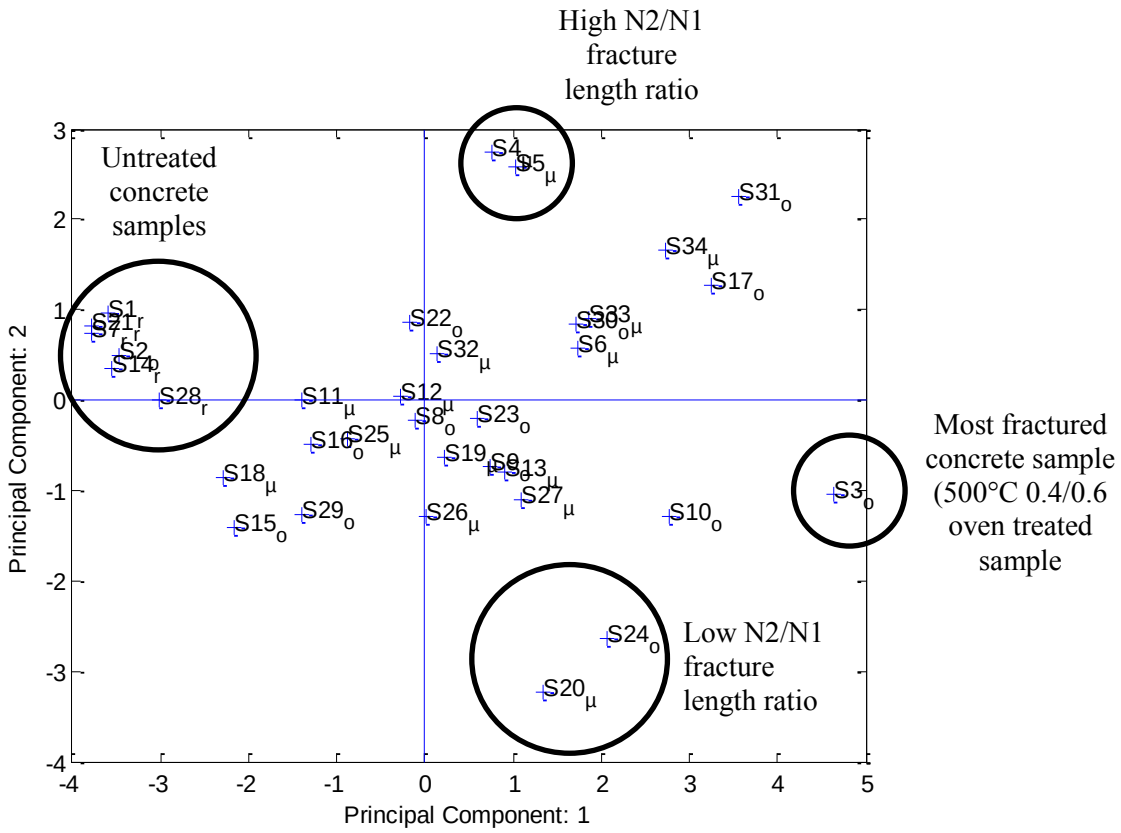

FIGURE 10. Individuals plot, confirming that the 1st principal component axis is a measure of the level of fracturing of the concrete sample, whereas the 2nd principal component axis is a measure of the dominance of the secondary fracture network.

Having given physical meaning to the first 2 principal components, the illustrative variables *ln*(*Ecs*) and RSD(*Ecs*) were then placed onto the circle of correlations. The result is shown in Fig. 11.

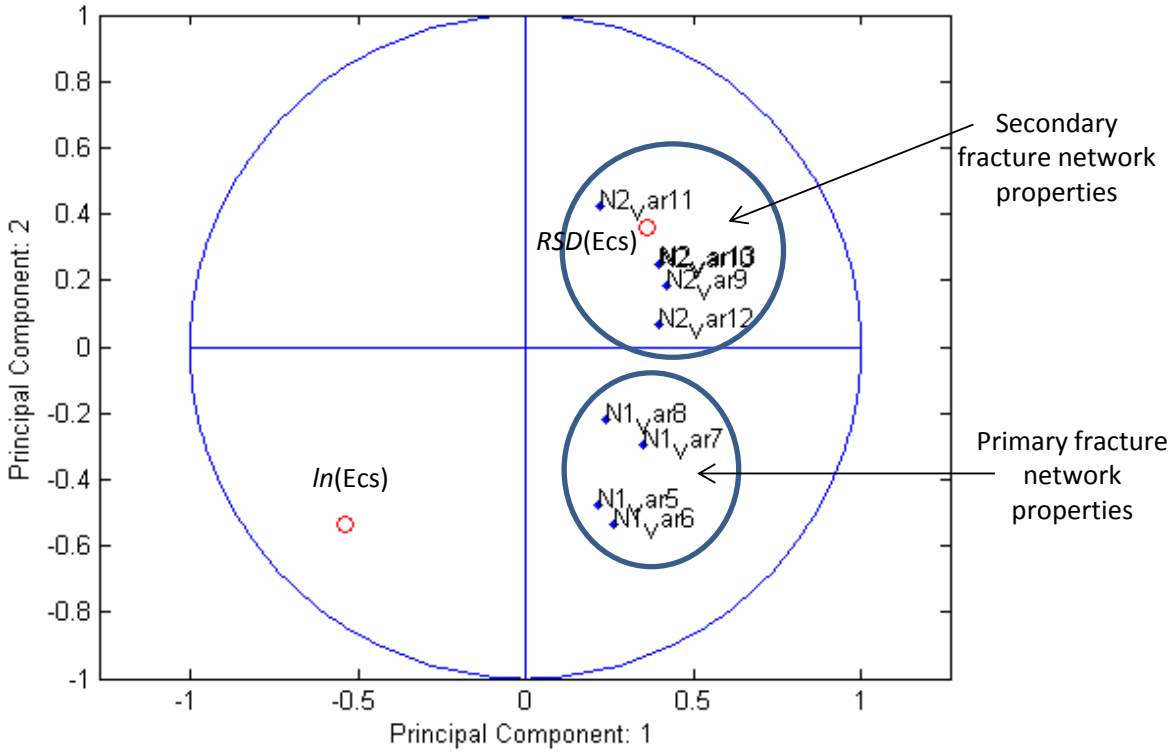

FIGURE 11. Positioning the illustrative variables ln(*Ecs*) and RSD(*Ecs*) on the circle of correlations

We observe that:

- The *Ecs* sits on the same side of the PC2 axis as the N1 properties. This means that the mean value of mass specific fracture energy has a strong positive correlation with fracture networks, dominated by primary network fracture. X-Ray tomography imaging has in fact confirmed the presence of a network of large fractures that percolates through the concrete texture. This analysis establishes the direct link that exists between concrete texture and physical fracture properties in the case of concrete.

- The *Ecs* sits on the side of the PC1 axis opposite to that of the N1 variables. This means, as one would expect, that the greater the primary fracture network variables, the lesser the mean mass specific fracture energy of concrete.

- We observe that RSD(*Ecs*) falls in the cluster of N2 properties. This indicates that for concrete, both the average and variability in mass specific fracture energy are associated with the extent of the secondary fracture network, the former negatively and the latter positively. This reflects a direct interaction between both fracture networks on the fracture properties of concrete, indicative of some continuity between these networks inside the cement paste matrix.

As an increase in *Ecs* is a negative in terms of comminution efficiency from an energy utilization point of view, this analysis indicates that the production of primary network dominant fracture is one key to effectively reducing the mass specific fracture energy of concrete, thereby establishing a direct link between concrete's mechanical texture and processing performance criteria.

From analysis of correlation between properties of the fracture porosity and the mass specific fracture energy in concrete, it so happens that both fracture networks contribute to defining the mechanical texture of concrete. While the extent of both networks appears to govern the mean value of the mass specific fracture energy, whereas the relative dominance of secondary fracture network controls its variability.

4. IMPLICATIONS FOR COMMINUTION MODELING AND PROCESSING OF CONCRETE

Mechanical texture was defined here as the subset of textural properties that govern the mechanical and fracture behavior of particles. Such properties need to be identified, modeled and then fed into DEM comminution models. Having selected mass specific fracture energy as the macroscopic material fracture property of interest, the work established a causal relationship with fracture porosity, a local textural property, in the case of concrete. With concrete, one textural property which is associated with mechanical texture is therefore fracture porosity. This is not saying that other textural properties are not of significance; however additional research is necessary to establish additional correlations between local textural parameters and mechanical properties of concrete.

Definition of mechanical texture however is one step, albeit critical, to feeding material properties into DEM comminution models. The next step consists in deriving a model of the mechanical texture that can be used to simulate the mechanical texture of particles, so that it can be used in DEM simulation environments. This mechanical texture simulation step is a complex issue which requires, in the case of concrete, a spatial description of fracture porosity, in addition to describing the spatial distribution of aggregate particles (Qian and Schlangen, 2013).

Identification of causal pathways between texture and physical fracture property also has direct implications for processing, whether for concrete or any other material subjected to processing for beneficiation. The recognition that fracture porosity variables correlate with the mass specific fracture energy and its RSD for concrete has direct bearing on designing a material driven recycling process. Indeed, processes applied to concrete should be investigated in relation to their ability to alter the growth of both primary and secondary fracture networks in concrete, which to the author's knowledge has not yet been undertaken.

In the case of concrete, the link that was established between the primary fracture network and the mass specific fracture energy indicates that a process which induces an N1-like fracture porosity will be best suited for reducing the mass specific fracture energy of concrete, hence it will be most efficient for minimizing comminution energy. On the other hand, a process that generates an N2-like fracture porosity will yield greater variability in mass specific fracture energy, which may not be desirable from a processing viewpoint.

When microwave energy is applied to concrete samples, the authors have found that low microwave energy input is sufficient to generate the greatest change in primary network growth, whereas longer exposure to microwave yields development of the secondary fracture network. Processing wise, this means that application of low microwave energy is sufficient for weakening concrete, as it targets the textural property most responsible for the mass specific fracture energy of concrete.

Should other processing criteria be used, such as the physical liberation of aggregate or the fineness of comminuted concrete, other textural properties may intervene as additional components of mechanical texture, and hence should be additional processing targets in addition to additional inputs to be considered in texture simulation for DEM modeling. Deriving causal relationships between textural and

macroscopic properties, as confirmed through the concrete example used in relation to mechanical texture, as well as embedding them in texture models for DEM simulation, is expected to show new paths for designing efficient and material specific processing solutions, and for adding realistic fracture models into DEM comminution models.

5. CONCLUSIONS

Design of comminution processes for ores and wastes is largely product driven. It is postulated that more efficient processes could be designed and operated should they be driven by material properties instead. This approach, which operates a significant shift in the way one may approach comminution modeling and equipment design should target the set of textural properties that control the fracture properties of the ore. This set of textural properties is here within defined as mechanical texture.

Through investigation of soda lime glass beads, a model material from the textural standpoint, combined with a large number of published data from the literature, this work justified using the mass specific fracture energy *Ecs* as the macroscopic index for mechanical texture. This result was established on the basis that the relative standard deviation of *Ecs* exhibited the highest value amongst Hopkinson bar single-particle impact test measured properties, directing our choosing *Ecs* as most sensitive to variability in texture as it relates to the comminution behavior of the ore.

Relating textural properties of a material to *Ecs* is very much material dependent. Using concrete as an example, textural properties associated with fracture porosity were convincingly correlated through principal component analysis to *Ecs*. These textural properties included properties of what the authors have identified as the primary and secondary fracture networks, which describe the fracture system in concrete. It was therefore concluded that these fracture networks define the concept of mechanical texture as it applies to concrete. In the particular case of concrete, for the concrete types tested, the primary fracture network was associated with the mean value of *Ecs*, whereas the secondary network appeared to relate more to the variability in *Ecs* values.

For process design, the implication of mechanical texture, as quantified in the case of concrete, was that processes capable of targeting changes in the primary fracture network are desirable for low energy comminution of concrete. The authors found that low energy microwave heating is a process which favors development of the primary fracture network. Other textural variables however may need to be taken into account in the definition of concrete's mechanical texture when considering aggregate liberation and product fineness, so that the information gathered here about fracture porosity networks may not be sufficient to define the terms of reference of a material-based processing scheme for concrete.

6. REFERENCES

Bourgeois, F., and Banini, G., 2002. A portable load cell for in-situ ore impact breakage testing, *International Journal of Mineral Processing*, 65, 31-54.

Bourgeois, F., 1993. Single-particle fracture as a basis for microscale modeling of comminution processes, Ph.D. dissertation, Department of Metallurgical Engineering, The University of Utah.

Cleary, P., 2013. Particle scale modelling of breakage and transport in comminution devices, *Proceedings of the 13th European Symposium on Comminution & Classification*, Eds. A. Kwade, S. Breitung-Faes, D. Steiner, 9th-12th September 2013, Braunschweig, Germany, 39-43.

Cleary, P.W. and Morrison, R.D., 2011. Understanding fine ore breakage in a laboratory scale ball mill using DEM, *Minerals Engineering*, 24, 352–366.

Cleary, P.W., 2004. Large scale industrial DEM modelling, *Engineering Computations*, 21, 169-204.

Early, E., 1999. On the Euler Characteristic, *The MIT Undergraduate J. Math.,* 1, 37-48.

Frandrich, R., Clout, J.M.F., and Bourgeois, F., 1998. The CSIRO Hopkinson bar facility for large diameter particle breakage, *Minerals Engineering*, 11(9), 861-869.

King, R.P. and Bourgeois, F., 1993. A New Conceptual Model for Ball Milling, *proceedings of the XVIII International Mineral Processing Congress*, Australia, 1, 81-86.

Lippiatt, N., and Bourgeois, F., 2014. N. Lippiatt and F. Bourgeois, Recycling-Oriented Investigation of Local Porosity Changes in Microwave Heated-Concrete, *KONA Powder Particle Journal (In Press)*.

Lippiatt, N., and Bourgeois, F., 2012. Investigation of microwave-assisted concrete recycling using single-particle testing, *Minerals Engineering*, 31, 71-81.

Lynch, A.J., 1977. Mineral crushing and grinding circuits – Their simulation, Optimisation, Design and Control, Elsevier Scientific Publishing Company, Amsterdam-Oxford-New York, 1977.

Mehta, P., and Monteiro, P., 2001. Concrete: microstructure, properties and materials, McGraw-Hill Professional (2001).

Middlemiss, S., 2007. Surface damage effects in single particle comminution, *International Journal of Mineral Processing*, 84, 207-220.

Middlemiss, S., and King, R.P., 1996. Microscale fracture measurements with application to comminution, *International Journal of Mineral Processing*, 44-45, 43-58.

Powell, M.S., Govender, I., and McBride, A.T., 2008. Applying DEM outputs to the unified comminution model, *Minerals Engineering*, 21, 744-750.

Tavares, L.M., and King, R.P., 1998. Single-particle fracture under impact loading, *International Journal of Mineral Processing*, 54, 1-28.

Qian, Z. and Schlange, E., 2013. Lattice modeling of fracture processes in numerical concrete with irregular shape aggregates, *proceeding of the 8th International Conference on Fracture Mechanics of Concrete and Concrete Structures*, 1539-1545, March 10-14, 2013 / Toledo – Spain.

Weatherley, D.K., 2013. Numerical investigation relating to lithology and mechanical properties of rock, *Proceedings of the 13th European Symposium on Comminution & Classification*, Eds. A. Kwade, S. Breitung-Faes, D. Steiner, 9th-12th September 2013, Braunschweig, Germany, 221-224.

Weerasekara, N.S., Powell M.S., Cleary, P.W., Tavares, L.M., Evertsson, M., Morrison, R.D., Quist, J. and Carvalho, R.M., 2013. The contribution of DEM to the science of comminution. *Powder Technology*, 248, pp 3-24.

Willam, K., Rhee, I. and Xi, Y., 2005. Thermal Degradation in Heterogeneous Concrete Materials, Journal of Materials in Civil Engineering, ASCE, 17(3), 276-285

5.3.3 Correlation between fracture porosity and liberation

When physical liberation is treated in the same way as mass specific fracture energy is treated in MINPROC2014 it is found to lie very close to the edge of the correlation circle in the quadrant associated with the growth of the secondary fracture network (Figure 5.23). This shows a very strong correlation between the growths of fracture porosity, in particular the secondary fracture network and the physical liberation of aggregate particles.

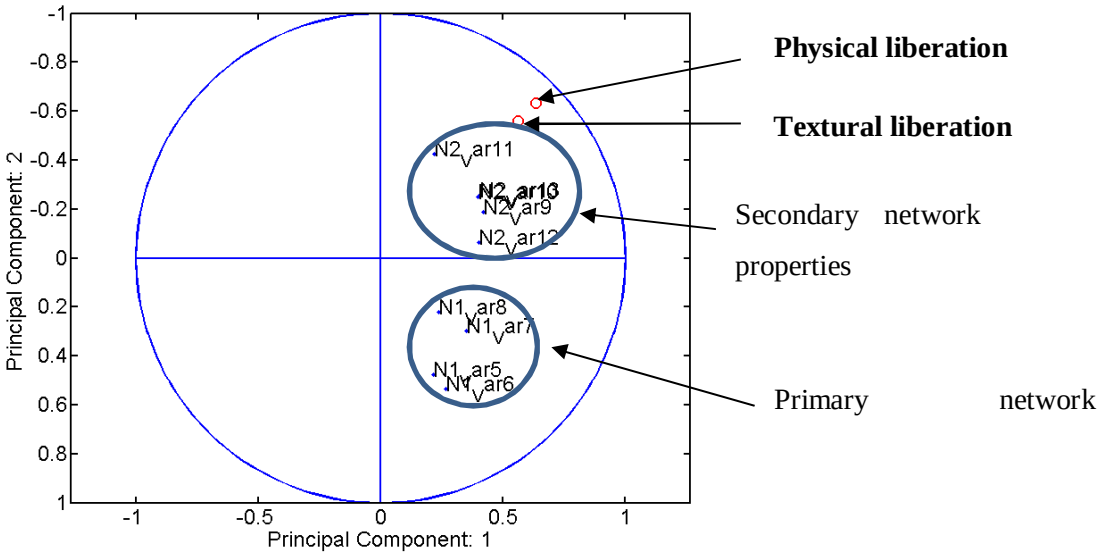

Figure 5.23. PCA circle of correlation showing physical and textural liberation very strongly correlated with secondary fracture porosity growth

Such a strong correlation between physical liberation and secondary network fracture growth is a strong endorsement of the hypothesis proposed in section 5.2.2, that the extent of fracture growth in the cement paste was more important for physical liberation than the connectivity between the cement and aggregate phases, the measurement of which was called textural liberation. The hypothesis that the reason for the large difference in absolute values of physical and textural liberation is a result of the comminution method chosen is supported by the relationship of physical liberation to the first two principal components.

Textural liberation and physical liberation were found to have almost the same position in the PCA (Figure 5.23). This is further proof of the value of the use of textural properties to describe materials for processing. Measuring the same material property mechanically and texturally was found to produce results with the same correlation with fracture porosity so from this perspective they are the same property. Therefore physical liberation is conditional on textural liberation. The strong relationship of liberation with fracture growth and secondary fracture in particular is logical given the need for fracture paste to be broken to liberate the aggregate particles within.

The importance of the growth of secondary fractures for physical liberation, and therefore also the importance of the comminution technique used to capitalise on textural liberation to create physical liberation is further supported by the position of the fragmentation results on the PCA circle of correlation (Figure 5.24). The mass fraction of the three designated fragment size classes produced from concrete after HPB fracture were found to lie on the same diagonal relative to the first two principal components. The growth of secondary network fracture porosity was found to correspond with the production of aggregate sized and smaller fragments and be inversely related to the production of larger fragments. The two smaller fragment size classes were found to lie in the same location as liberation in the PCA correlation circle, which is not surprising given that fragments that are not liberated by definition have cement paste attached and will therefore be larger than the size of aggregate particles.

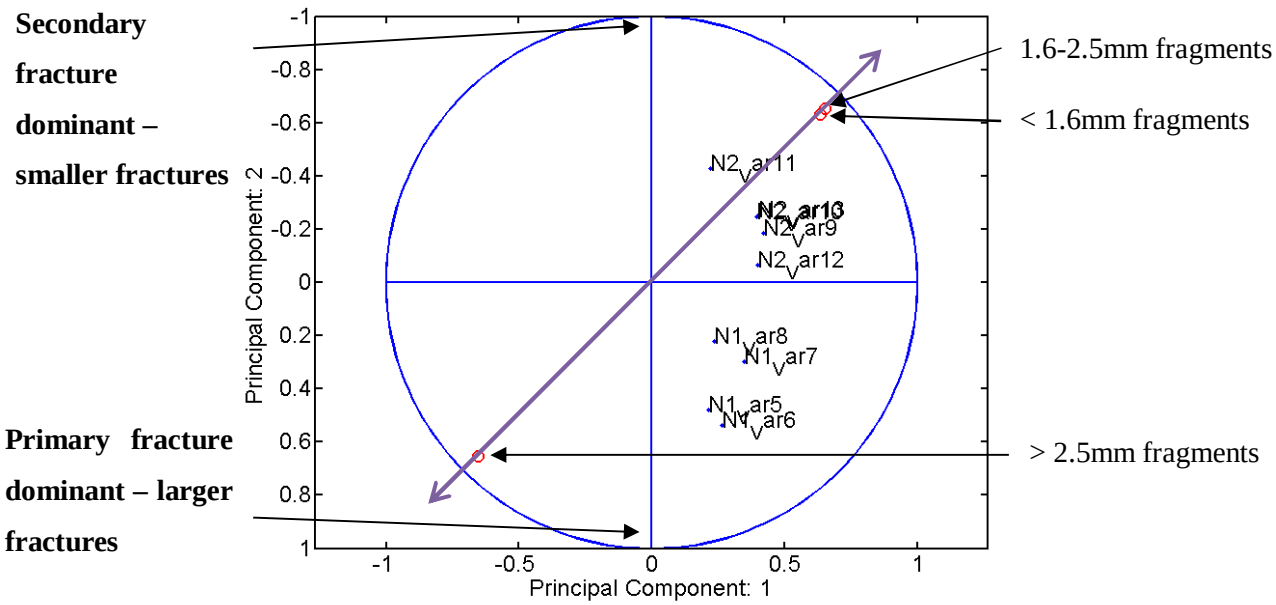

Figure 5.24. PCA correlation circle showing the relationship of the production of different fragment size fractions under impact. Small and aggregate sized fragments are strongly associated with the growth of the secondary fracture network which is inversely related to the production of large fragments.

Principal components are not the goals of heat treatment or concrete recycling; they are merely composites of quantified textural changes, so whether the effects of microwave and conventional heat treatment produce similar results in terms of the PCA is unimportant. Under the conditions tested in this work microwave heating was shown to be more efficient at producing both liberated aggregate particles and small fragments, which is important for milling purposes if the liberation fraction is to be increased further by other means such as mechanical rubbing [5.6]. However, to determine the superiority of one heating type over the other both technical and economic issues must be considered.

5.4 Implications for concrete recycling

This project seeks to contribute to the development of an efficient technique for recycling concrete waste. To that end it has quantified the extent to which aggregate and cement in concrete samples can be texturally and physically separated from each other using microwave heating. It was found that by using microwave treatment on concrete the textural liberation of aggregates can exceed 90%, although whether this level of liberation is achieved depends on the technique used to break the treated samples. This suggests that there are at least two possible avenues for the application of microwave heating to the recycling of concrete waste:

- A low energy microwave pre-treatment to generate interface fracture so as to facilitate aggregate liberation during crushing
- An intense microwave treatment that produces both interface fracture and extensive fracture porosity in the cement paste that facilitates aggregate liberation, increases cement paste fragmentation and reduces the fracture toughness of the concrete and therefore the energy required for crushing

Short microwave treated concrete samples saw an absolute increase in the level of textural liberation by approximately 25% relative to untreated concrete. Since aggregate can be liberated from cement paste even with relatively short microwave exposures a recycling technique could be based on using a short microwave pre-treatment to produce textural liberation. For such a system a suitable crushing technique is required such as high pressure grinding rolls which has been heralded as an energy efficient grinding system. In addition a shear inducing process is probably ideal for converting textural liberation into physical liberation. To optimize a recycling system of this type would require the use of the absolute minimum amount of microwave energy necessary to generate liberation. This would require the study of how the textural properties of concrete are affected by microwave treatments shorter than even the shortest exposures tested here, called short microwave treatment. The optimum exposure time will be dependent on the power of the generator and will be a compromise between energy usage and the quantity of aggregate liberated. A schematic of such a low energy process is shown in Figure 5.25.

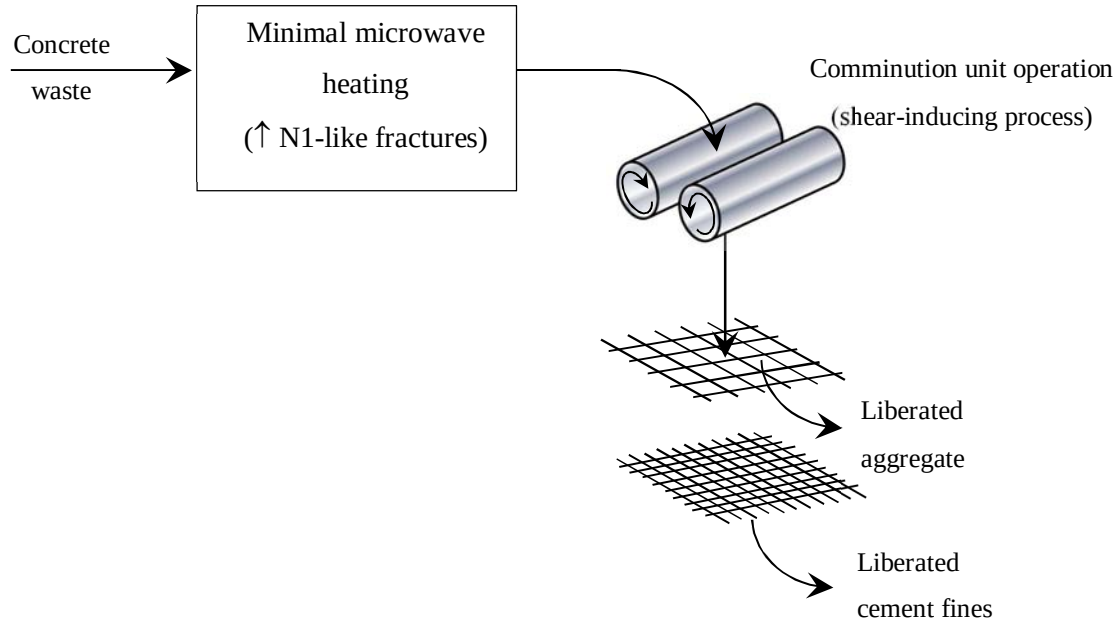

Figure 5.25. Schematic of hypothetical microwave based concrete recycling process highlighting the use of a minimal treatment approach. While the sorting method suggested by the schematic is size based this will depend on the size of the aggregate and the size of the product produced by the comminution process used

Textural liberation values in concretes that had experienced long microwave treatment on average exceeded 80%. Such samples not only presented the potential for a very high rate of aggregate recovery but due to extensive fragmentation saw a very high rate of actual physical liberation after impact fracture. When concrete was exposed to long microwave treatments, samples saw substantial growth of the secondary fracture network which meant the samples lost most of their mechanical strength and tended to generate many more smaller fragments when broken by impact. As an example 95% of the mass of untreated S5 concrete was composed of fragments larger than 2.5mm after HPB fracture, but after long microwave treatment this value dropped to 25%. Samples that had been exposed to long microwave treatment were extremely fragile, many could be crushed by forces no greater than those that would be imposed by a transport process and some could be crushed by hand.

A concrete recycling process could be based on trying to induce the maximum amount of secondary network fracture in samples so as to remove the requirement of an expensive crushing step. The small fragments produced by such a process would also make it easier to recycle cement into clinker as clinker needs to be ground to a fine powder before being used to make concrete. The high temperatures reached during such a process could also be useful for re-clinkering cement. Conserving the heat in the cement paste could prove a technical challenge. It would requiring heating, crushing, sorting and re-clinkering to occur in immediate succession or to be combined by some innovative process into a single process step. If high temperatures are necessary for re-clinkering [5.7] as it is for the decarbonation of limestone when producing raw clinker, then a heating step was already necessary and using a long microwave treatment to promote liberation and the growth of secondary fracture

porosity in this way would remove a treatment step by combing two. The strength loss also means the near-removal of a crushing step from the process and the potential for aggregate and cement separation purely on size. A concrete recycling technique based on long microwave treatment has the potential to be very energy efficient. A schematic of such a process has been included in Figure 5.26. As long as increasing the length of microwave exposure increases liberation and fragmentation than this type of process will most likely be limited by the heat resistance of the aggregate in the concrete.

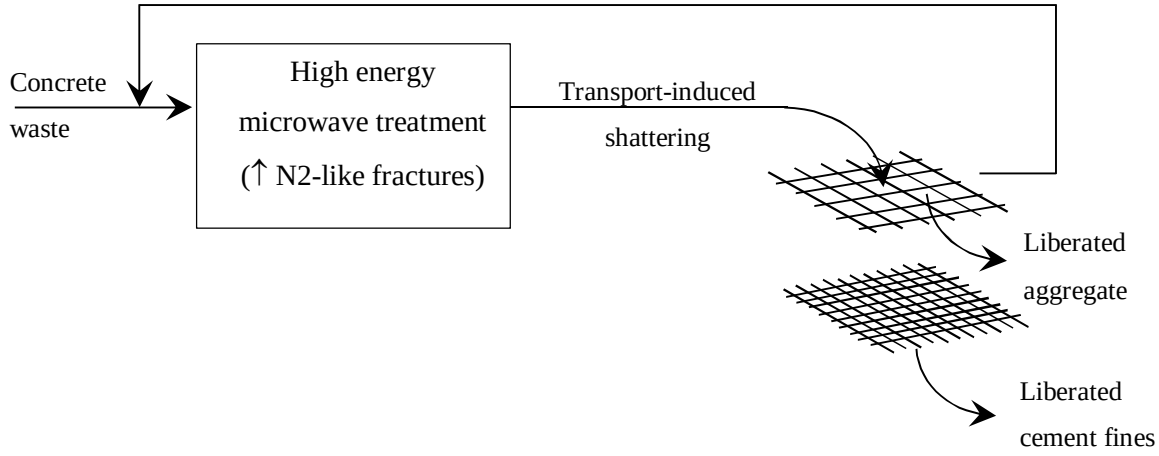

Figure5.26. Schematic of hypothetical concrete recycling process using high-energy microwave treatment. Crushing in such a process would be unnecessary as would be a complex separation process

It should be noted that while the process would be based on 'long microwave treatment' this process would not necessarily require a long exposure. It is the transfer of significant quantities of heat energy into the concrete that is important. The desired outcome is the significant mechanical and textural changes observed after 'long microwave treatment' regardless of what technique or equipment is used.

Conventionally heated concrete samples were shown to be able to achieve textural liberation values that were the equivalent of those achieved by microwave treated samples. If quality was the only factor, that is to say the fraction of aggregate particles that are liberated from concrete then conventional heating could be considered a suitable process but from a processing point of view microwave heating has significant advantages over conventional heating.

Due to the heating rate that can be produced by microwave systems microwave processes require much shorter processing time compared to conventional systems designed to reach the same temperature. Microwave heated concretes were also shown to have more secondary network fracture porosity which meant they produced finer fragments when broken. Smaller fragments require less energy to mill, both to remove excess cement from partially liberated aggregates and to crush cement to produced powdered clinker.

Microwave heating progressively reduces concrete strength by the growth of large fracture pores that also greatly reduce the connectivity between aggregate particles and cement paste. This leads to a decrease in stiffness and toughness as well as an associated increase in fragmentation and liberation of aggregate particles. It is the smaller fractures, those around 1µm in width that appear to be most important in this progression and these require elevated temperatures to occur in large quantities.

Ultimately the choice of process for use in a concrete recycling application is a technical one. The aggregate can only be exposed to a certain temperature before it will start to fracture and no longer be useful for concrete production. To reach that temperature will require a certain amount of energy inherent to the material and putting that much energy into the concrete will require a certain amount of energy depending on the type, size, power of the heating applicator and other design questions. Such questions were not addressed in this work nor were they intended to be but they are important questions in the creation of a concrete recycling process.

While cylindrical samples did not achieve particularly high values of physical liberation even after the most extreme pre-treatments that were tested, the smaller cubic samples physical liberation approached the textural liberation of the larger cylindrical samples. This highlights an important technical issue, the optimum particle size of waste particles before microwave treatment. The cubic samples absorbed energy at a lower rate than the larger cylindrical samples, half as fast at the extreme but as they were approximately one fifth the mass this means the specific energy absorbed (J/g) was approximately three times higher. The size of samples will change the energy efficiency of the microwave treatment and may also, depending on the comminution technique, change the quantity of aggregate that is liberated as it has here.

An alternative microwave processing technique that was not addressed is that of induced spalling. This effect is more difficult to study as a sample that is already broken effectively has no mechanical properties and no longer has a flat surface that could be used to measure textural properties. Even if they did there are no mechanical properties that the textural properties could be used to explain. Tests suggest achieving explosive heating requires:

- a certain minimum level of power absorbed, at least 100 W g^{-1}. This may go up for stronger samples as while explosive heating was not uncommon for S1 samples it was rare for most other concretes tested
- a certain level of humidity, explosions during microwave heating were more common in samples that hadn’t been allowed to completely dry

These explosions occurred after less than 10 seconds of microwave exposure, sometimes as little as 3 seconds. Samples that exploded in this way were heated to approximately 100°C, as measured by infrared thermometer. Spalled samples experienced the same power input as other microwave treated

samples but for shorter periods of time, therefore the process used less energy. The concrete samples were also broken without any kind of milling. It may be found that the most energy efficient technique for liberating aggregate from concrete is to make the samples spall.

Unfortunately as it seems that explosive heating can not be achieved with dry samples, for such a process to be consistently effective would require that samples be hydrated before use such as by soaking. Due to the level of hydration this may also necessitate a drying step after microwave treatment. The combination of a hydration and dehydration step would greatly reduce the mass flow rate through the recycling process and affect the energy balance. In addition the photographic evidence (Figure 5.27) suggests the liberation from this process is quite low. Nevertheless as a concrete process based on spalling presents the opportunity of combining the aggregate liberating pre-treatment and the comminution step into a single process this technique merits further study.

Figure 5.27. Concrete samples that have experienced microwave heating induced spalling

The results of this work suggest that a durable process, one that is capable of processing many different types of concretes waste should be heated with microwaves to at least 350°C so as to produce texturally liberated particles and to see at least the beginning of significant decreases in the size of fragments after breakage.

As the a/c of samples tested were relatively low compared to standard concretes and the aggregate size more similar to mortar than concrete one could expect the results of tests performed on concretes to differ from those observed here. It could be expected that concretes with higher a/c would absorb less microwave energy so heat slower and to lower temperatures under microwave exposure. Considering the high physical liberation of long microwave treated S3 and S5 it could be expected that the increased aggregate/ cement interface and ITZ of higher a/c concretes will compensate for this effect

and microwave treatment of standard concretes will actually be more effective at promoting aggregate liberation than in the mortars observed.

Aggregate liberation of the concretes tested here that had undergone the same process saw absolute variations of as much as 20%. As concrete mixes become increasingly complex, making use of a wider variety of materials, such as masonry to address other recycling problems, the separation of concrete components and therefore recycling of those components will become more difficult and the treatment processes required for recycling will need to become more robust. If recycling was considered before a material was made this would make the process not only easier but would also greatly simplify optimization question regarding energy efficiency and waste.

The major technological competitor to microwave heating for treatment of concrete waste for recycling is the use of high voltage electric pulses. This technique has been shown to be an energy efficient technique for the liberation of aggregate particles [5.8] but requires the particles to be immersed in water. The energy efficiency of microwave heating is a most significant technical issue, as has already been stated, but even so its potential to be a completely dry process is a distinct advantage over comminution by electrical pulse.

Demonstrating microwave heating's potential for concrete weakening and aggregate liberation is only the first step. An appropriate mechanical comminution method that can capitalize on the quantity of fracture that microwave heating generates in concrete and an appropriate method for separating the constituents once they are crushed is also needed. These technical decisions are inter-related and also dependent on how the cement paste will be used after separation and the efficiency of the microwave applicator.

5.5 Bibliography for Chapter 5

[5.1] Lippiatt N & Bourgeois F., 2014. Recycling-oriented investigation of local porosity changes in microwave heated-concrete. *KONA Powder and Particle Journal* 31, P.247-264.

[5.2] Mehta P & Monteiro P., 2001. Concrete: microstructure, properties and materials. McGraw-Hill Professional.

[5.3] Heikal M., 2008. Effect of elevated temperature on the physico-mechanical and microstructural properties of blended cement pastes. *Building Research Journal* 56, P.157-172.

[5.4] Moguchi T, Kitagaki R & Tsujino M., 2011. Minimizing environmental impact and maximizing performance in concrete recycling. *Structural Concrete* 12, P.36-46.

[5.5] Bourgeois FS, Lippiatt NR & Powell MS., 2014. Introducing the concept of mechanical texture for comminution process modeling and design. *International Journal of Mineral Processing* in press.

[5.6] Noguchi T, Kitagaki R & Tsujino M., 2011. Minimizing environmental impact and maximizing performance in concrete recycling. *Structural Concrete* 1, P.36-46.

[5.7] Costes JR, Majcherczyk C & Binkhorst IP., 2010. Total recycling of concrete. Commissariat à l'Énergie Atomique.

[5.8] Menard Y, Bru K, Touze S, Lemoign A, Poirer JE, Ruffie G, Bonnaudin F & Von Der Weid F., 2013. Innovative process routes for a high-quality concrete recycling. *Waste Management* 33, P.1561-1565.

Chapter 6

CONCLUSIONS AND PERSPECTIVES

The following is a collection of the conclusions of the thesis presented here including recommendations for the future direction of technological development in the area of concrete recycling by microwave heating.

6. CONCLUSIONS AND PERSPECTIVES

This project sought to use a texture driven approach to contribute to the development of an efficient technique for recycling concrete waste. To that end it has quantified to what extent the aggregate and cement in concrete samples can be separated from each other using microwave heating. This mode of heating was selected as it draws its efficiency from the heterogeneity of the material, hence the suspected applicability to a material as texturally complex as concrete. This has been achieved by the development of a technique to measure changes in the textural properties of concrete, called fracture porosity using electron microscopy. This measure of fracture porosity describes the most relevant microscopic changes that occur in concrete when it is exposed to elevated temperatures. Changes in fracture porosity can be linked to and explain the macroscopic changes in the material such as changes in mechanical strength, phase liberation and comminution fragment size distribution, which are key factors for recycling.

This work identified that fracture porosity appeared in two different forms, referred to as primary and secondary networks.

- The primary network is composed of large connected fractures which percolate throughout the sample. As the formation of the primary network fractures created significant aggregate-cement boundary fractures, i.e. selective liberation, this work introduced the meaningful concept of textural liberation, as opposed to physical liberation. The primary network was found to develop with short exposures to microwaves, and was associated with aggregate particles. The growth of the primary network was linked to the observed decrease in the mass specific fracture energy of treated concrete samples.
- The secondary network was composed of smaller and more dispersed fractures, of seemingly more random occurrence, whose density increased with the duration of exposure to microwaves. It was shown to have a strong link to the observed decrease in strength and increase in the physical liberation of aggregate particles for heat treated concrete samples.

The formation of both networks was interpreted as being driven primarily by drying shrinkage.

This work opposed textural and physical liberation, showing that aggregate particles could be highly liberated within the material, while the physical liberation that resulted from single-particle impact testing was comparatively low. This important observation validated the soundness of investigating the behavior of concrete at the textural level. By extension, this validates the use of textural level analysis of materials, natural or manmade, in the development of beneficiation processes. It also showed that physical liberation is largely controlled by the comminution environment used. In the case of microwave heated concrete, single-particle impact testing was not capable of converting a high

textural liberation into a high physical liberation. It is believed that shear stress inducing processes would be more suited to harvest the textural liberation associated with the formation of the primary fracture network.

This work relied heavily on the development and use of a dedicated image analysis scheme, which allowed highlighting, categorizing and quantifying fractures inside microwave heated concrete samples. The validity of a texture based assessment of the changes in concrete and by extension the image analysis technique used to measure the textural properties of samples was validated by:

- Correlation between fracture porosity and mechanical changes, measured by single-particle impact testing using a Hopkinson bar apparatus.
- Correlation between fracture porosity and aggregate liberation, which explained the discrepancy between values measured for textural and physical liberation.
- Correlation between fracture porosity and the comminution fragment size distribution. In particular, the increase in secondary network fractures yielded finer fragments, with increased liberation of the cement phase.

The techniques used to measure fracture porosity showed that a concrete recycling technique based on microwave treatment has the potential to liberate and therefore recycle over 90% of concrete embedded aggregate. However questions remain in identifying the comminution step most capable of harvesting the fracture porosity induced by microwave heating. A systemic approach is necessary to pursue this work and derive a recycling process. Indeed, the dependency between the microwave heating step, and the subsequent comminution operation necessary to collect the benefit of the microwave induced fractures, requires that both steps be investigated together. It is believed that shear inducing comminution processes, such as with the high-pressure grinding roll, could be coupled with microwave heating.

A combination of Hopkinson bar impact tests and textural analysis has shown that microwave heating increases aggregate liberation and decreases the mechanical comminution energy required for physically liberating the aggregate. This work, which uses a microwave heating system unsuitable for evaluation of the actual energy consumption, could not yield values for the net energy consumption of a microwave based recycling process. Once the most adapted comminution step is identified, additional work will be required to assess the energy consumed by an overall process coupling microwave heating and comminution, which would then have to use a scalable microwave heating system.

Ultimately the optimum combination of microwave heating and physical comminution is a technical question that will depend not just on how microwave heating reduces comminution energy but things such as the acceptable liberation grade, temperature stability of the aggregate used and the relative cost

of concrete materials and energy. Nonetheless microwave treatment of concrete samples and in particular fracture porosity analysis of concrete samples has highlighted three possible paths for the development of a microwave based concrete recycling process:

- Low energy microwave exposure to liberate aggregates texturally before comminution
- High energy microwave treatment to maximize fracture porosity growth and therefore maximize fragmentation and minimize fracture strength
- High power, low energy microwave treatment that causes explosive expansion

All three of these development avenues could be adapted to concrete recycling. The production of raw clinker uses elevated temperatures. If it is assumed that re-clinkering cement is similarly dependent on elevated temperatures then a high energy process has a particular potential for efficiency. This is because the high temperatures required to re-clinker cement can be used to liberate the phases. By utilising the elevated temperatures required for cement re-clinkering for phase separation, concrete can be recycled with minimal process energy.

Ideally future investigation of processing concrete with microwave heating will include the three processing ideals noted above. A process focused investigation of the relationship between microwave energy input, mechanical energy input and aggregate liberation for each scenario would provide the information required to answer the question of how much energy is required to liberate aggregate as well as providing the information required to optimally adapt microwave heating based concrete recycling to different concretes and markets.

Textural analysis using electron microscopy was effective in demonstrating how microwave heating changes concrete at the microscopic level and how those changes govern macroscopic effects and process performance indicators. The link which this work established between texture and processing performance is a significant achievement, which can be understood as a possible shift in paradigm in comminution process design. Indeed, having demonstrated the possibility of mismatching a comminution operation with the texture of the material, this work makes the claim that comminution process design and operation should be texturally designed.

Returning to the issue of concrete recycling, the texture analysis conducted in this work could be improved by a true measure of the connectivity of the fracture networks, which would require access to the actual three-dimensional properties of fracture porosity, hence the need for a three-dimensional visualization technique. X-ray tomography is a technique that could be used for this task as it was shown to detect fracture porosity. Due to the exponential increase in data included in such an analysis it would need to be automated. Automation would likely require an increase in the contrast between the fracture porosity, cement and aggregate compared to that seen here. This may require an additional

sample preparation step or a particular concrete made specifically for the tests in question that displays a particularly high contrast with fracture porosity when observed using X-ray tomography.

A

APPENDICES

A detailed list of data obtained with cylindrical concrete samples

A. SIZE DISTRIBUTION AND LIBERATION

The following graphs are a continuation of the results shown in section 5.2.2 for other concrete types

S2 concrete: w/c 0.4 a/c 0.85

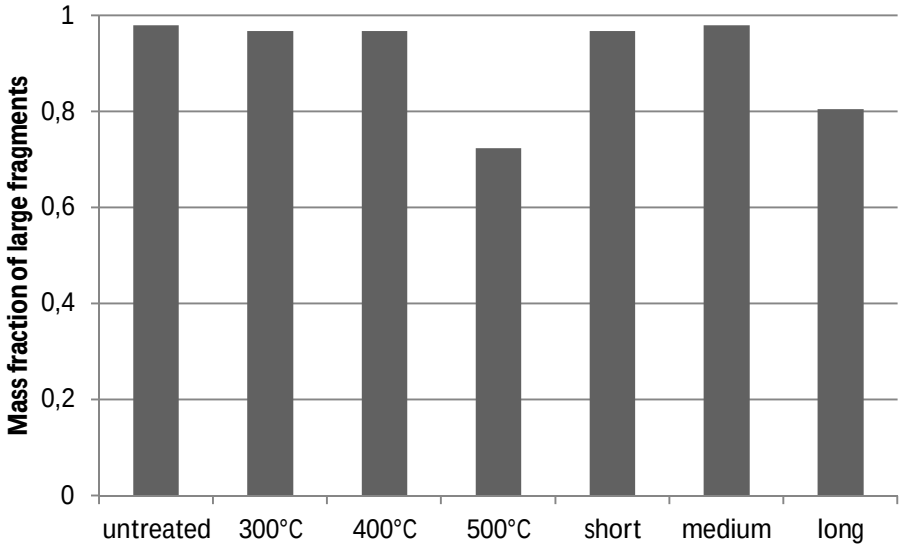

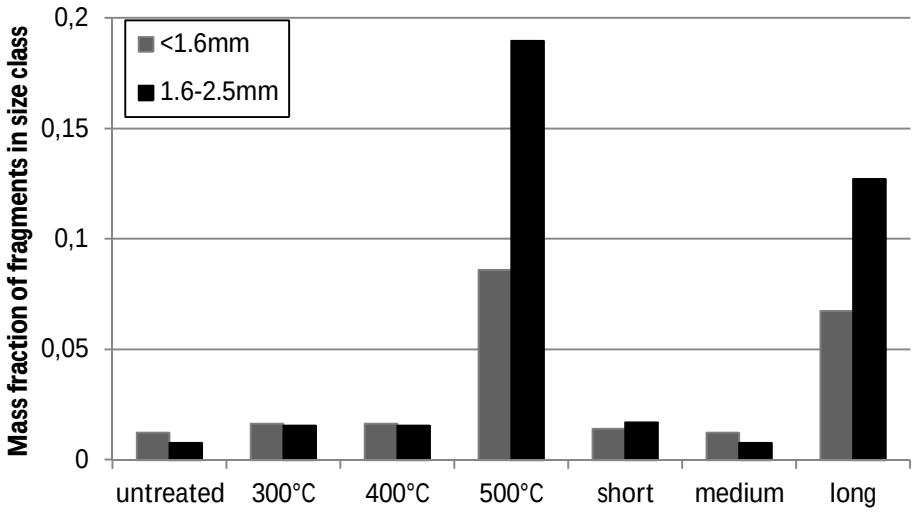

S3 concrete: w/c 0.4 a/c 1.6

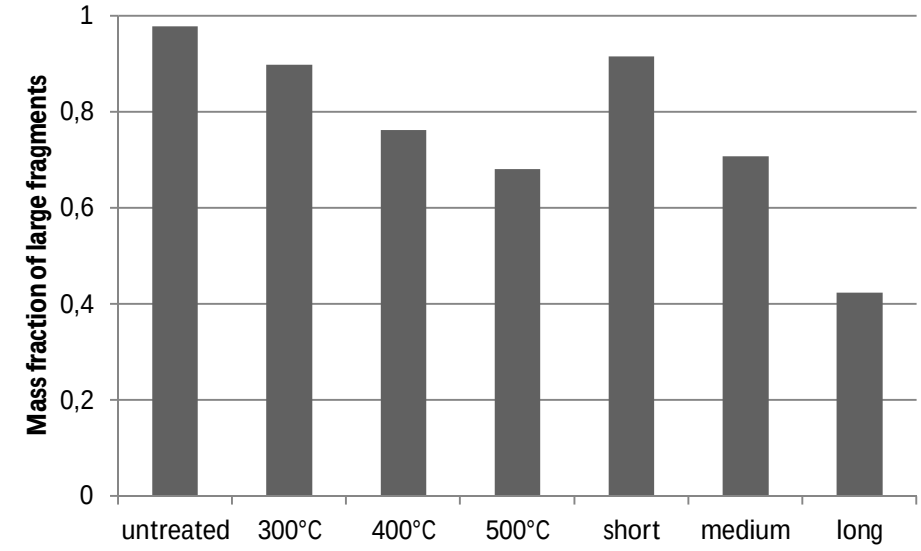

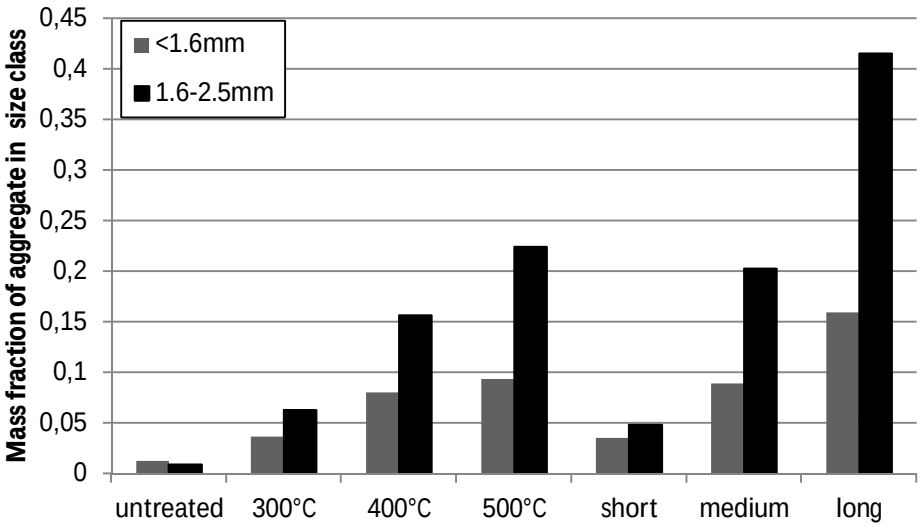

S4 concrete: w/c 0.5 a/c 1.6

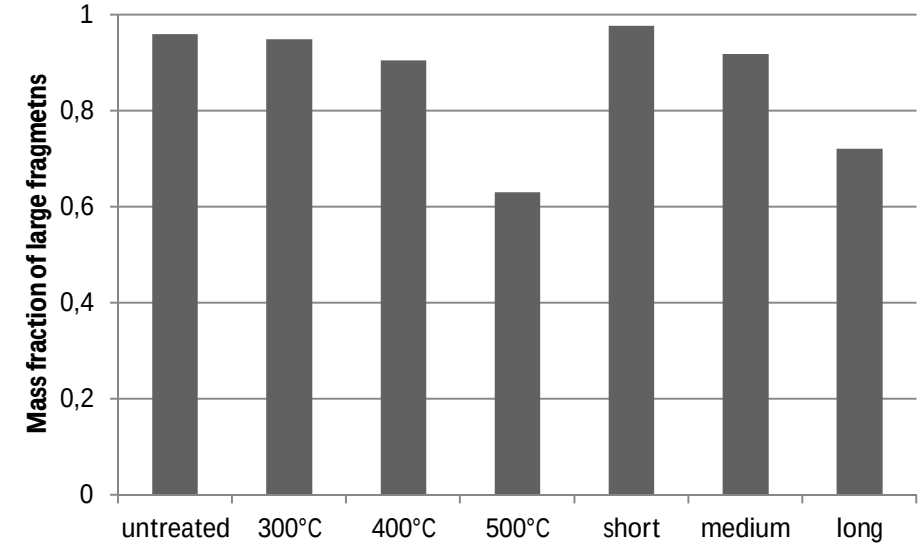

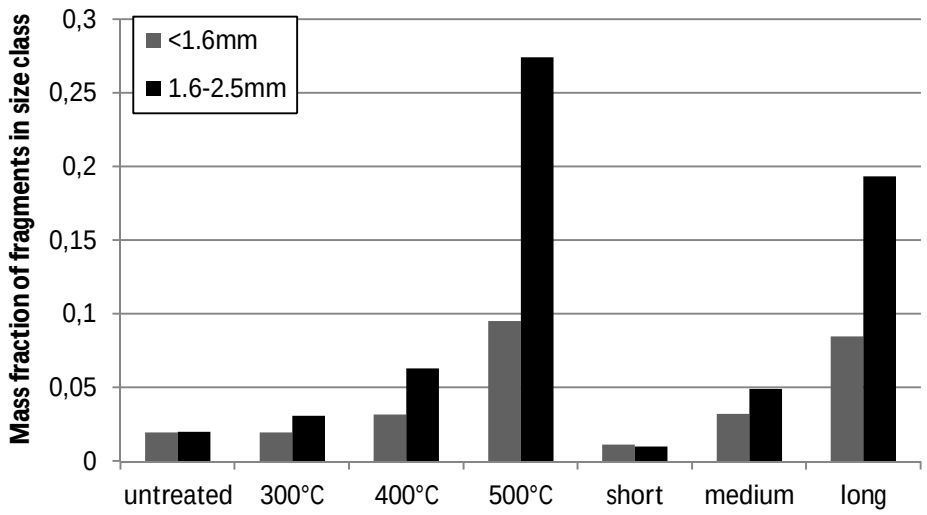

S5 concrete: w/c 0.6 a/c 1.6

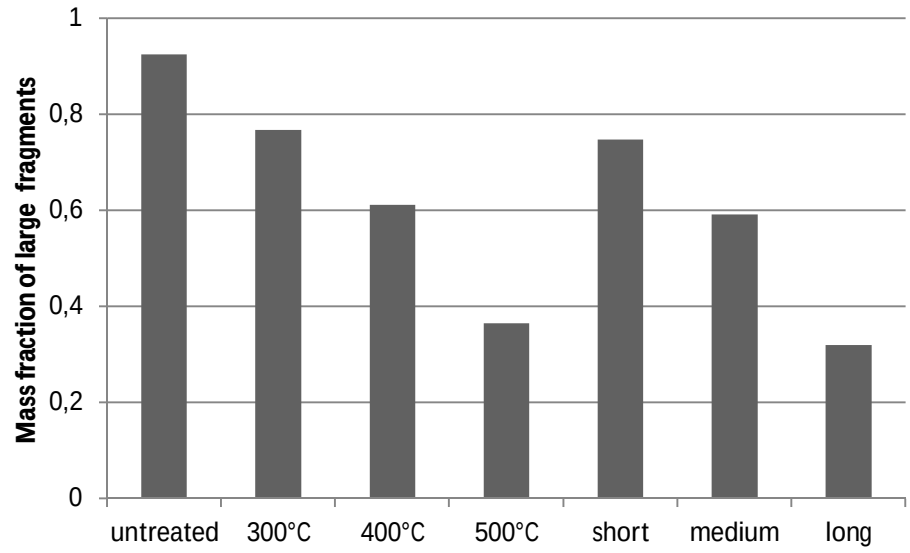

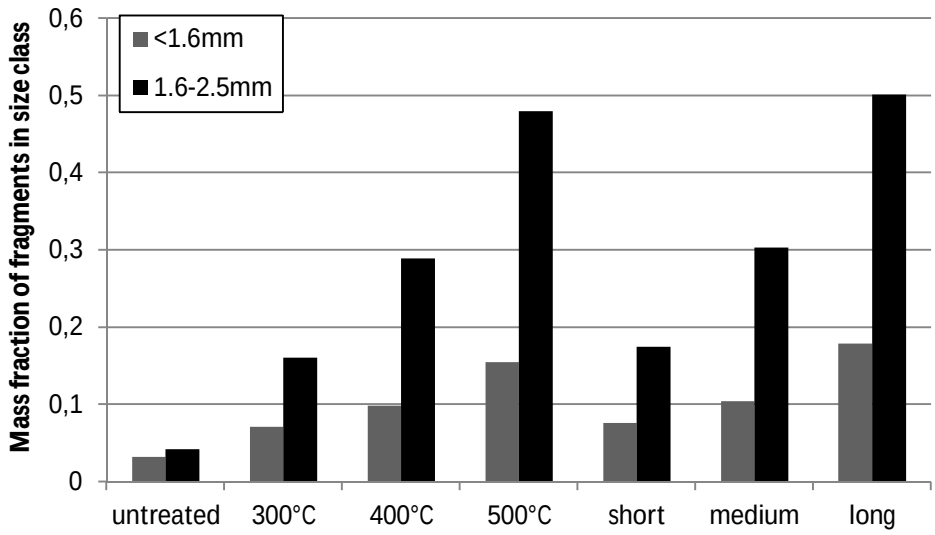

The following tables summarise the size distribution by mass fraction of the fragments of concrete samples after they were broken under single impact fracture.

Size distribution and mass fraction of S1 concrete: w/c 0.4 a/c 0.6

	untreated	**300°C**	**400°C**	**500°C**	**short microwave treatment**	**medium microwave treatment**	**long microwave treatment**
0-0,8	0,0048	0,0034	0,0128	0,0266	0,0059	0,0142	0,0388
0,8-1	0,0020	0,0014	0,0056	0,0121	0,0027	0,0070	0,0166
1-1,4	0,0025	0,0014	0,0086	0,0193	0,0036	0,0089	0,0269
1,4-1,6	0,0011	0,0011	0,0062	0,0125	0,0017	0,0045	0,0161
1,6-1,8	0,0007	0,0008	0,0049	0,0069	0,0007	0,0034	0,0087
1,8-2	0,0023	0,0015	0,0243	0,0559	0,0029	0,0199	0,0738
2-2,24	0,0027	0,0017	0,0200	0,0577	0,0046	0,0270	0,0721
2,24-2,5	0,0000	0,0005	0,0066	0,0126	0,0009	0,0044	0,0146
2,5-2,8	0,0012	0,0001	0,0064	0,0115	0,0018	0,0083	0,0108
2,8-5	0,0150	0,0085	0,0600	0,1497	0,0228	0,0911	0,1537
5-7,1	0,0221	0,0173	0,0459	0,1297	0,0326	0,0852	0,1120
7,1-11,2	0,0618	0,1001	0,0591	0,2097	0,1125	0,2723	0,0863
>11,2	0,8838	0,8621	0,7395	0,2958	0,8074	0,4538	0,3696

Size distribution and mass fraction of S2 concrete: w/c 0.4 a/c 0.85

	untreated	**300°C**	**400°C**	**500°C**	**short microwave treatment**	**medium microwave treatment**	**long microwave treatment**
0-0,8	0,0062	0,0067	0,0067	0,0297	0,0058	0,0062	0,0246
0,8-1	0,0024	0,0030	0,0030	0,0148	0,0025	0,0024	0,0121
1-1,4	0,0025	0,0044	0,0044	0,0225	0,0041	0,0025	0,0187
1,4-1,6	0,0014	0,0024	0,0024	0,0190	0,0018	0,0014	0,0121
1,6-1,8	0,0006	0,0013	0,0013	0,0099	0,0013	0,0006	0,0079
1,8-2	0,0034	0,0053	0,0053	0,0686	0,0065	0,0034	0,0483
2-2,24	0,0030	0,0073	0,0073	0,0969	0,0078	0,0030	0,0608
2,24-2,5	0,0008	0,0017	0,0017	0,0143	0,0015	0,0008	0,0101
2,5-2,8	0,0006	0,0014	0,0014	0,0068	0,0005	0,0006	0,0037
2,8-5	0,0124	0,0308	0,0308	0,1841	0,0212	0,0124	0,1210
5-7,1	0,0281	0,0325	0,0325	0,0900	0,0326	0,0281	0,6807
7,1-11,2	0,1548	0,0765	0,0765	0,1980	0,1228	0,1548	
>11,2	0,7838	0,8268	0,8268	0,2455	0,7917	0,7838	

Size distribution and mass fraction of S3 concrete: w/c 0.4 a/c 1.6

	untreated	300°C	400°C	500°C	short microwave treatment	medium microwave treatment	long microwave treatment
0-0,8	0,0063	0,0145	0,0283	0,0351	0,0150	0,0310	0,0606
0,8-1	0,0020	0,0071	0,0152	0,0184	0,0067	0,0175	0,0279
1-1,4	0,0027	0,0098	0,0225	0,0258	0,0094	0,0257	0,0452
1,4-1,6	0,0015	0,0057	0,0144	0,0147	0,0045	0,0152	0,0261
1,6-1,8	0,0008	0,0038	0,0085	0,0092	0,0032	0,0091	0,0166
1,8-2	0,0028	0,0242	0,0553	0,0837	0,0178	0,0675	0,1832
2-2,24	0,0039	0,0256	0,0772	0,1121	0,0214	0,1035	0,1829
2,24-2,5	0,0016	0,0097	0,0156	0,0198	0,0060	0,0230	0,0333
2,5-2,8	0,0016	0,0027	0,0167	0,0141	0,0047	0,0180	0,0275
2,8-5	0,0177	0,1419	0,1435	0,1310	0,0427	0,1198	0,1516
5-7,1	0,0141	0,1454	0,0627	0,1038	0,0291	0,1077	0,0701
7,1-11,2	0,0604	0,1183	0,2180	0,2615	0,2573	0,1576	0,1244
>11,2	0,8845	0,4912	0,3221	0,1709	0,5823	0,3043	0,0507

Size distribution and mass fraction of S4 concrete: w/c 0.5 a/c 1.6

	untreated	300°C	400°C	500°C	short microwave treatment	medium microwave treatment	long microwave treatment
0-0,8	0,0091	0,0078	0,0129	0,0376	0,0052	0,0135	0,0344
0,8-1	0,0035	0,0038	0,0059	0,0163	0,0022	0,0060	0,0142
1-1,4	0,0038	0,0053	0,0079	0,0246	0,0024	0,0077	0,0223
1,4-1,6	0,0032	0,0030	0,0051	0,0166	0,0018	0,0049	0,0139
1,6-1,8	0,0019	0,0012	0,0026	0,0083	0,0009	0,0026	0,0065
1,8-2	0,0059	0,0110	0,0197	0,0910	0,0034	0,0177	0,0721
2-2,24	0,0091	0,0126	0,0330	0,1532	0,0050	0,0199	0,0981
2,24-2,5	0,0032	0,0061	0,0079	0,0219	0,0009	0,0089	0,0167
2,5-2,8	0,0040	0,0024	0,0064	0,0068	0,0012	0,0055	0,0112
2,8-5	0,0275	0,0520	0,0787	0,1957	0,0258	0,0601	0,1439
5-7,1	0,0438	0,0271	0,0688	0,0860	0,0174	0,0719	0,1075
7,1-11,2	0,1545	0,0260	0,1083	0,1193	0,0698	0,0592	0,1529
>11,2	0,7305	0,8418	0,6431	0,2227	0,8641	0,7221	0,3064

Size distribution and mass fraction of S5 concrete: w/c 0.6 a/c 1.6

	untreated	300°C	400°C	500°C	short microwave treatment	medium microwave treatment	long microwave treatment
0-0,8	0,0161	0,0276	0,0399	0,0644	0,0310	0,0421	0,0790
0,8-1	0,0061	0,0132	0,0179	0,0265	0,0138	0,0174	0,0285
1-1,4	0,0067	0,0183	0,0262	0,0392	0,0196	0,0273	0,0449
1,4-1,6	0,0034	0,0122	0,0143	0,0248	0,0118	0,0178	0,0263
1,6-1,8	0,0031	0,0058	0,0094	0,0148	0,0062	0,0104	0,0167
1,8-2	0,0112	0,0559	0,0929	0,1575	0,0583	0,1019	0,2069
2-2,24	0,0233	0,0824	0,1538	0,2705	0,0892	0,1555	0,2504
2,24-2,5	0,0044	0,0163	0,0334	0,0374	0,0212	0,0355	0,0278
2,5-2,8	0,0051	0,0100	0,0161	0,0208	0,0121	0,0210	0,0168
2,8-5	0,0525	0,1479	0,2500	0,2487	0,1508	0,1876	0,1517
5-7,1	0,0476	0,0947	0,1153	0,0427	0,1188	0,0981	0,0639
7,1-11,2	0,1816	0,2912	0,1090	0,0527	0,2241	0,0978	0,0552
>11,2	0,6391	0,2246	0,1218	0,0000	0,2430	0,1875	0,0319

The following table is the summary table for all physical liberation values for all concretes and all heat treatments. The value is the fraction of all aggregate mass that was found to be in the same fragment size fraction before and after dissolution divided by the total aggregate mass after dissolution, excluding the <0.8mm size fraction.

Physical liberation

	S1	S2	S3	S4	S5
untreated	0,004	0,004	0,004	0,010	0,023
300°C	0,002	0,012	0,064	0,019	0,117
400°C	0,037	0,008	0,131	0,041	0,172
500°C	0,181	0,199	0,199	0,238	0,353
short treatment	0,009	0,084	0,030	0,006	0,109
medium treatment	0,062	0,052	0,193	0,033	0,174
long treatment	0,204	0,101	0,394	0,158	0,456

Example of aggregate size distribution: short treated S1 concrete: w/c 0.4 a/c 0.6

The following is an example of how physical liberation was measured; using the example of S1 concrete that has undergone short microwave treatment. Once the ten impact tests had been completed, the fragments of the 10 samples were collected and the size distribution of samples was measured. This produces the following table.

Fragment size distribution of S1 short microwave treated concrete fragments

Fragment size category (mm)	**<0.8**	**0.8-1**	**1-1.4**	**1.4-1.6**	**1.6-1.8**	**1.8-2.0**	**2.0-2.24**	**2.24-2.5**	**2.5-2.8**	**2.8-5**	**5-7,1**	**7,1-11,2**	**>11,2**
Mass (g)	43,53	6,065	1,756	1,227	0,0989	0,0466	0,250	0,155	0,036	0,094	0,193	0,145	0,318

These fragment size classes were dissolved individually in acid and the product was then re-weighed to give the mass of aggregate in each fragment size class. This gives the following table.

Aggregate mass in each fragment size

Fragment size category (mm)	**<0.8**	**0.8-1**	**1-1.4**	**1.4-1.6**	**1.6-1.8**	**1.8-2.0**	**2.0-2.24**	**2.24-2.5**	**2.5-2.8**	**2.8-5**	**5-7,1**	**7,1-11,2**	**>11,2**
Total mass (g)	1,403	1,396	1,379	1,269	1,424	1,439	1,382	1,317	1,546	1,561	1,637	3,434	16,09
Filter mass (g)	1,283	1,344	1,304	1,316	1,408	1,365	1,277	1,307	1,277	1,297	1,184	1,318	1,189
Mass (g)	0,12	0,052	0,075	0,047	0,016	0,074	0,105	0,01	0,269	0,264	0,453	2,116	14,90

The total mass of aggregate is therefore 18.5 grams.

Once only the aggregate particles remained the resulting product was once again sieved to give a size class distribution. The total mass of material that had the same fragment size class (first column) and aggregate particle size class (first row) was defined as liberated aggregate. The sum of all these values divided by the total mass of aggregate was the liberation fraction. Particles smaller than 0.8mm in size were classed as not liberated because as this was the smallest size class so useful aggregate could not be differentiated from whatever other material that was present, such as silica powder. This mass was included in the denominator when calculating liberated mass fraction.

Short treated S1 concrete: w/c 0.4 a/c 0.6 after acid dissolution

Size (mm)s	**<0.8**	**0.8-1**	**1-1.4**	**1.4-1.6**	**1.6-1.8**	**1.8-2.0**	**2.0-2.24**	**2.24-2.5**	**2.5-2.8**	**2.8-5**	**5-7,1**
<0.8	0,064										
0.8-1	0,01	0,007									
1-1.4	0,003	0,008	0,047								
1.4-1.6	0,003	0	0,004	0,014							
1.6-1.8	0,003	0,004	0	0	0						
1.8-2.0	0,001	0	0,008	0,003	0	0,051					
2.0-2.24	0,008	0,004	0,003	0	0,005	0,025	0,048				
2.24-2.5	0	0	0	0	0	0	0	0			
2.5-2.8	0,056	0	0	0	0	0	0	0,213	0		
2.8-5	0,007	0,003	0,01	0,007	0,019	0,078	0,061	0	0	0	
5-7,1	0,012	0,001	0,022	0,043	0,037	0,2	0,08	0	0	0	0
7,1-11,2	0,089	0,005	0,028	0,063	0,1	0,816	0,588	0	0	0	0
11,2 - 20	2,2	0,102	0,261	0,334	0,558	6,371	4,229	0	0	0	0

The sum of liberated aggregate in this case is 0.167 grams out of 18.5 grams of aggregate particles making the physical liberation 0.9%. If the total aggregate mass is calculated from the above table the result is 16.92 grams making physical liberation 1%. The difference between these two total aggregate mass values was common between tests at approximately 10%. The source of this error is unknown but could be due to the effects of filter paper's high specific surface area. In any case the difference in the value calculated for physical liberation is insignificant.

B. TEXTURE AND POROSITY ANALYSIS

The following tables are a summary of the data from textural analysis with electron microscopy and mercury porosimetry. The first two tables present total values from each magnification and the second two tables show values for the primary and secondary network. All images were 640 × 480 pixels in size.

Concrete			SEM (×200 = 1.8µm/pixel)					SEM (×40 = 9µm/pixel)				MIP
w/c	a/c	Treatment	Total crack area fraction	Total crack length (m^{-1})	Average crack width (µm)	Average width of interface fracture (µm)	Aggregate fracture area fraction	Total Crack Length (m^{-1})	Total crack area fraction	Textural liberation	Aggregate fracture	Total intrusion porosity (ml g^{-1})
0,4	0,6	untreated	0,009	0,004	3,0	2,5	0,00187	0,011	0,015	0,447	0,00043	0,080
0,4	0,6	300°C	0,007	0,003	2,7	2,4	0,00060	0,013	0,018	0,593	0,00081	0,097
0,4	0,6	400°C	0,074	0,037	3,4	6,0	0,01032					0,140
0,4	0,6	500°C	0,087	0,032	4,5	15,5	0,00711	0,029	0,105	0,936	0,00955	0,177
0,4	0,6	short	0,040	0,021	3,3	2,7	0,00029	0,019	0,029	0,761	0,00139	0,098
0,4	0,6	medium	0,073	0,023	5,5	12,2	0,00318	0,024	0,035	0,768	0,00057	0,120
0,4	0,6	long	0,108	0,035	5,2	9,5	0,00614	0,039	0,073	0,814	0,00160	
0,4	0,85	untreated	0,010	0,005	2,6	2,4	0,00075	0,007	0,009	0,384	0,00368	0,075
0,4	0,85	300°C	0,052	0,015	5,5	11,3	0,00059	0,029	0,050	0,781	0,00143	0,095
0,4	0,85	400°C	0,052	0,019	4,2	8,5	0,00054	0,032	0,064	0,866	0,00246	0,108
0,4	0,85	500°C	0,112	0,031	5,6	12,5	0,01311	0,042	0,122	0,905	0,00971	0,151
0,4	0,85	short	0,031	0,014	3,4	4,6	0,00026	0,024	0,034	0,717	0,00034	0,099
0,4	0,85	medium	0,047	0,018	3,9	4,9	0,00125	0,026	0,051	0,827	0,00080	0,107
0,4	0,85	long	0,132	0,022	9,6	17,2	0,00212	0,032	0,098	0,874	0,00229	0,140

Concrete			SEM (×200 = 1.8µm/pixel)					SEM (×40 = 9µm/pixel)				MIP
w/c	**a/c**	**Treatment**	**Total crack area fraction**	**Total crack length (m^{-1})**	**Average crack width (µm)**	**Average width of interface fracture (µm)**	**Aggregate fracture area fraction**	**Total Crack Length (m^{-1})**	**Total crack area fraction**	**Textural liberation**	**Crack in aggregate**	**Total intrusion porosity (ml g^{-1})**
0,4	1,6	untreated	0,014	0,005	2,4	2,4	0,00082	0,018	0,023	0,479	0,00011	0,080
0,4	1,6	300°C	0,009	0,003	2,4	2,3	0,00207	0,037	0,051	0,738	0,00012	0,087
0,4	1,6	400°C	0,046	0,017	3,7	4,9	0,00234	0,032	0,047	0,627	0,00069	0,105
0,4	1,6	500°C	0,101	0,044	4,9	9,7	0,01752	0,035	0,063	0,736	0,00195	0,124
0,4	1,6	short	0,028	0,007	4,3	3,9	0,00089	0,026	0,037	0,676	0,00014	0,121
0,4	1,6	medium	0,060	0,023	3,5	4,9	0,00136	0,039	0,066	0,758	0,00092	0,088
0,4	1,6	long	0,081	0,017	6,8	19,0	0,00450	0,049	0,155	0,918	0,00190	0,170
0,5	1,6	untreated	0,011	0,004	1,3	1,3	0,00032	0,017	0,022	0,417	0,00058	0,085
0,5	1,6	300°C	0,043	0,020	2,0	2,9	0,00048	0,036	0,052	0,612	0,00042	0,111
0,5	1,6	400°C	0,079	0,023	3,0	5,6	0,00067	0,042	0,082	0,662	0,00061	0,131
0,5	1,6	500°C	0,151	0,022	6,1	16,0	0,00176	0,052	0,182	0,905	0,00721	0,156
0,5	1,6	short	0,042	0,016	2,0	3,1	0,00118	0,031	0,045	0,689	0,00013	0,105
0,5	1,6	medium	0,064	0,017	2,7	3,9	0,00538	0,040	0,077	0,801	0,00043	0,109
0,5	1,6	long	0,076	0,023	2,7	5,7	0,00399	0,046	0,089	0,823	0,00170	0,117
0,6	1,6	untreated	0,013	0,005	1,4	1,4	0,00159	0,026	0,034	0,549	0,00038	0,118
0,6	1,6	300°C	0,016	0,008	1,4	1,4	0,00299	0,038	0,054	0,769	0,00027	0,114
0,6	1,6	400°C	0,076	0,028	2,4	5,0	0,00306	0,028	0,045	0,781	0,00014	0,145
0,6	1,6	500°C	0,098	0,034	2,6	5,0	0,01802	0,021	0,056	0,819	0,00098	0,158
0,6	1,6	short	0,043	0,020	1,7	2,2	0,00152	0,035	0,049	0,674	0,00208	0,132
0,6	1,6	medium	0,056	0,026	1,9	3,1	0,00504	0,044	0,060	0,693	0,00126	0,130
0,6	1,6	long	0,109	0,034	2,9	8,2	0,00145	0,036	0,053	0,737	0,00141	0,163

Concrete			SEM (200×, 1.8µm/pixel)					SEM (40×, 9µm/pixel)				
w/c	a/c	Treatment	Secondary length (m^{-1})	Nodes per branch	branch per object	branch per area	Euler number	Primary length (m^{-1})	Secondary length (m^{-1})	Nodes per object	Liberation	Primary area fraction
0,4	0,6	untreated	0,0038	0,7655	2,0659	0,0002	1,915	0,0081	0,0018	1,24	0,3795	0,0106
0,4	0,6	300°C	0,0024	0,8051	2,1455	0,0001	1,139	0,0090	0,0024	1,41	0,5246	0,0119
0,4	0,6	400°C	0,0337	1,1594	4,6239	0,0028	29,70					
0,4	0,6	500°C	0,0296	0,9860	2,9462	0,0023	24,80	0,0213	0,0075	45,17	0,9331	0,0907
0,4	0,6	short	0,0188	1,2389	5,6572	0,0011	11,84	0,0125	0,0053	3,45	0,7165	0,0178
0,4	0,6	medium	0,0214	1,1962	4,9321	0,0012	12,65	0,0124	0,0100	4,56	0,7155	0,0189
0,4	0,6	long	0,0261	0,9105	2,5810	0,0019	22,20	0,0189	0,0191	7,88	0,7916	0,0433
0,4	0,85	untreated	0,0045	0,3792	1,3366	0,0003	3,779	0,0088	0,0008	0,136	0,3839	0,0116
0,4	0,85	300°C	0,0134	0,5492	1,5845	0,0010	10,51	0,0203	0,0080	3,11	0,7561	0,0371
0,4	0,85	400°C	0,0160	0,6353	1,7367	0,0013	14,42	0,0240	0,0072	4,91	0,8501	0,0510
0,4	0,85	500°C	0,0244	0,9162	2,5881	0,0019	22,19	0,0292	0,0128	11,3	0,8961	0,0987
0,4	0,85	short	0,0115	0,7550	2,0236	0,0006	6,535	0,0184	0,0049	1,35	0,6899	0,0261
0,4	0,85	medium	0,0142	0,9130	2,5679	0,0009	9,337	0,0178	0,0089	2,82	0,8099	0,0393
0,4	0,85	long	0,0176	1,1722	4,8202	0,0024	11,92	0,0243	0,0076	4,31	0,8661	0,0833
0,4	1,6	untreated	0,0042	0,6291	1,7371	0,0003	3,010	0,0124	0,0024	0,116	0,4204	0,0161
0,4	1,6	300°C	0,0063	0,7347	1,9652	0,0006	1,609	0,0303	0,0047	1,298	0,7183	0,0402
0,4	1,6	400°C	0,0128	0,6748	1,8315	0,0009	10,37	0,0242	0,0059	1,678	0,5913	0,0355
0,4	1,6	500°C	0,0318	1,0317	3,2611	0,0022	23,39	0,0287	0,0039	1,396	0,7198	0,0525
0,4	1,6	short	0,0047	0,5620	1,5924	0,0003	3,617	0,0231	0,0041	0,958	0,6518	0,0326
0,4	1,6	medium	0,0158	0,9567	2,8135	0,0013	18,15	0,0307	0,0074	1,705	0,7440	0,0518
0,4	1,6	long	0,0122	0,6987	1,8741	0,0009	9,993	0,0357	0,0129	10,6	0,9138	0,1277

Concrete			SEM (200×, 1.8µm/pixel)					SEM (40×, 9µm/pixel)				
w/c	**a/c**	**Treatment**	**Secondary length (m^{-1})**	**Nodes per branch**	**branch per object**	**branch per area**	**Euler number**	**Primary length (m^{-1})**	**Secondary length (m^{-1})**	**Nodes per object**	**Liberation**	**Primary area**
0,5	1,6	untreated	0,0035	0,7060	1,8598	0,0002	2,585	0,0091	0,0038	0,202	0,3108	0,0122
0,5	1,6	300°C	0,0182	0,9657	2,8402	0,0011	11,736	0,0215	0,0137	1,097	0,5957	0,0321
0,5	1,6	400°C	0,0175	0,9217	2,6365	0,0014	15,87	0,0282	0,0120	2,091	0,6320	0,0598
0,5	1,6	500°C	0,0177	0,8514	2,3585	0,0013	14,73	0,0295	0,0233	11,70	0,8991	0,1458
0,5	1,6	short	0,0137	0,7449	1,9924	0,0009	9,985	0,0249	0,0032	1,054	0,6580	0,0364
0,5	1,6	medium	0,0139	0,7840	2,1031	0,0009	10,66	0,0299	0,0074	2,61	0,7785	0,0619
0,5	1,6	long	0,0189	0,8210	2,2245	0,0013	14,40	0,0317	0,0126	3,311	0,8019	0,0670
0,6	1,6	untreated	0,0035	0,7116	1,9127	0,0003	3,196	0,0169	0,0045	0,278	0,4660	0,0218
0,6	1,6	300°C	0,0069	0,8316	2,2741	0,0005	5,438	0,0297	0,0052	0,984	0,7394	0,0408
0,6	1,6	400°C	0,0250	0,8100	2,2006	0,0021	22,84	0,0206	0,0059	1,534	0,7599	0,0334
0,6	1,6	500°C	0,0306	1,0137	3,1658	0,0025	26,83	0,0146	0,0051	3,261	0,7826	0,0450
0,6	1,6	short	0,0165	1,0108	3,1557	0,0013	14,70	0,0250	0,0079	1,773	0,6280	0,0342
0,6	1,6	medium	0,0196	1,1124	4,0224	0,0019	22,64	0,0310	0,0095	1,524	0,6532	0,0412
0,6	1,6	long	0,0287	0,0803	0,6800	0,0297	27,16	0,0268	0,0066	3,180	0,6972	0,0382

C. MECHANICAL TESTING

The following table summarises the results of mechanical testing with the vertical Hopkinson bar impact load cell.

Concrete			Strength				Toughness				Stiffness				Pertubation period			
w/c	a/c	Treatment	mean (N)	median (N)	max	min	mean (mJ g-1)	median (mJ g-1)	max	min	mean (GPa)	median (GPa)	max	min	mean (µs)	median (µs)	max	min
0,4	0,6	untreated	3345	3367	5864	1044	45,7	42,24	72	13	10,81	8,72	20,2	2,2	46,5	45	61	35
0,4	0,6	300°C	1984	2205	2692	1080	30,3	24,25	48	21	5,19	4,45	9,3	1,9	45,0	44,5	53	35
0,4	0,6	400°C	2169	2408	3065	798	52,5	47,12	88	28	3,33	2,61	7,5	1	77,8	67,5	114	62
0,4	0,6	500°C	610	601	1014	20	21,5	19,38	40	7,6	6,51	0,54	1,15	0,22	94,7	114	120	62
0,4	0,6	short	1995	2195	2479	1230	24,3	22,00	40	13	8,06	10,18	11,22	5,2	46,8	48	52	42
0,4	0,6	medium	1560	1573	2427	711	50,3	45,51	71	18	1,84	0,98	6,2	0,84	113,6	100	213	62
0,4	0,6	long	1039	1092	1445	431	25,9	24,22	45	9,3	1,38	1,29	2,8	0,5	162,3	171	224	83
0,4	0,85	untreated	4549	3936	7204	3471	55,6	47,22	80	35	18,01	15,69	37	6,2	44,2	47	53	35
0,4	0,85	300°C	2768	2979	3590	1072	46,0	46,14	55	35	6,55	7,27	9,6	4,1	55,3	59	65	24
0,4	0,85	400°C	2262	2015	4494	675	42,6	30,64	52	25	5,75	3,64	7,8	2,2	75,5	81	96	50
0,4	0,85	500°C	1542	1091	2912	781	41,6	25,34	65	16	1,74	1,62	2,7	1,1	125,0	120	170	105
0,4	0,85	short	3088	3181	4133	2015	53,7	47,84	88	18,3	7,21	6,11	11,5	5,1	59,6	57	77	50
0,4	0,85	medium	2792	3084	3913	1517	60,4	66,18	98	17,7	4,84	3,99	8,3	3,1	57,7	58	77	29
0,4	0,85	long	2234	2057	4533	862	52,3	58,71	63,9	14,8	2,22	1,97	3,5	1,7	78,5	83,5	93	54
0,4	1,6	untreated	1749	1782	3098	697	42,5	36,90	95	12,4	2,95	2,07	7,4	1,04	90,9	83	169	47
0,4	1,6	300°C	1255	1143	2355	1000	25,9	33,76	55,3	3,5	7,48	1,55	22,9	0,6	92,5	97	114	59
0,4	1,6	400°C	1201	1269	1591	615	20,3	18,12	38	3,6	6,40	2,43	23,3	0,97	82,4	77	115	68
0,4	1,6	500°C	734	586	1438	475	17,8	19,08	32	3,3	1,42	1,30	4,1	0,3	163,5	136	265	98
0,4	1,6	short	1810	1701	3457	849	36,6	35,56	64,5	23,5	3,21	2,62	6,3	0,85	76,9	80	85	64
0,4	1,6	medium	1170	1179	1929	316	26,3	28,72	59	6,1	2,31	1,66	5,7	0,24	112,6	109	170	66
0,4	1,6	long	607	672	902	154	20,3	19,18	40	2,9	0,53	0,52	0,99	0,07	172,8	163,5	282	72

Concrete			Strength				Toughness				Stiffness				Pertubation period			
w/c	**a/c**	**Treatment**	**mean (N)**	**median (N)**	**max**	**min**	**mean (mJ g-1)**	**median (mJ g-1)**	**max**	**min**	**mean (GPa)**	**median (GPa)**	**max**	**min**	**mean (µs)**	**median (µs)**	**max**	**min**
0,5	1,6	untreated	2681	2630	3817	873	44,9	51,36	93	4,5	7,96	9,72	13	2,8	64,5	64	107	38
0,5	1,6	300°C	1374	1418	2017	430	30,9	37,65	35	5,6	3,61	2,55	8,55	0,85	65,4	60	164	42
0,5	1,6	400°C	879	920	1585	326	21,8	26,26	32	8,2	1,23	1,19	2,97	0,18	70,6	69	105	54
0,5	1,6	500°C	477	395	763	232	14,3	15,53	30	5,9	0,54	0,41	1,18	0,14	167,9	120	414	80
0,5	1,6	short	4269	4551	5862	2508	70,0	73,70	99,8	38	10,01	10,47	15,9	4,8	57,9	56	87	38
0,5	1,6	medium	2289	2167	4090	712	42,0	39,15	80	24	4,67	4,42	10,3	2,4	60,1	57,5	77	49
0,5	1,6	long	1496	1405	2024	1005	45,0	39,47	75	24	1,51	1,23	2,88	0,6	157,5	149,5	258	68
0,6	1,6	untreated	2368	2289	2737	2035	42,3	38,72	70,6	30,2	4,80	5,42	7,7	1,8	75,4	70,5	133	40
0,6	1,6	300°C	1689	1751	2620	928	27,0	28,31	57	5,8	5,98	3,65	12	1,4	73,0	74	102	40
0,6	1,6	400°C	1115	1100	1940	574	17,8	14,70	35	6,1	4,72	2,56	15	0,5	76,8	76	102	53
0,6	1,6	500°C	974	1033	1248	532	14,7	18,95	27	3,7	4,32	2,74	12,2	1,2	105,7	108	110	96
0,6	1,6	short	1660	1774	2629	710	25,7	32,88	43,6	3,3	7,08	7,13	8,8	1	69,1	69,5	86	47
0,6	1,6	medium	1215	1154	2350	487	17,4	9,90	47	3,3	6,27	3,83	9,3	1,7	85,3	87	136	38
0,6	1,6	long	552	524	1045	196	19,8	13,64	51,3	6,9	0,60	0,27	2,5	0,06	147,8	138	213	91

The following figures compare examples of impact signals from concretes that have experienced different heat treatments. The fracture points are highlighted with red circles.

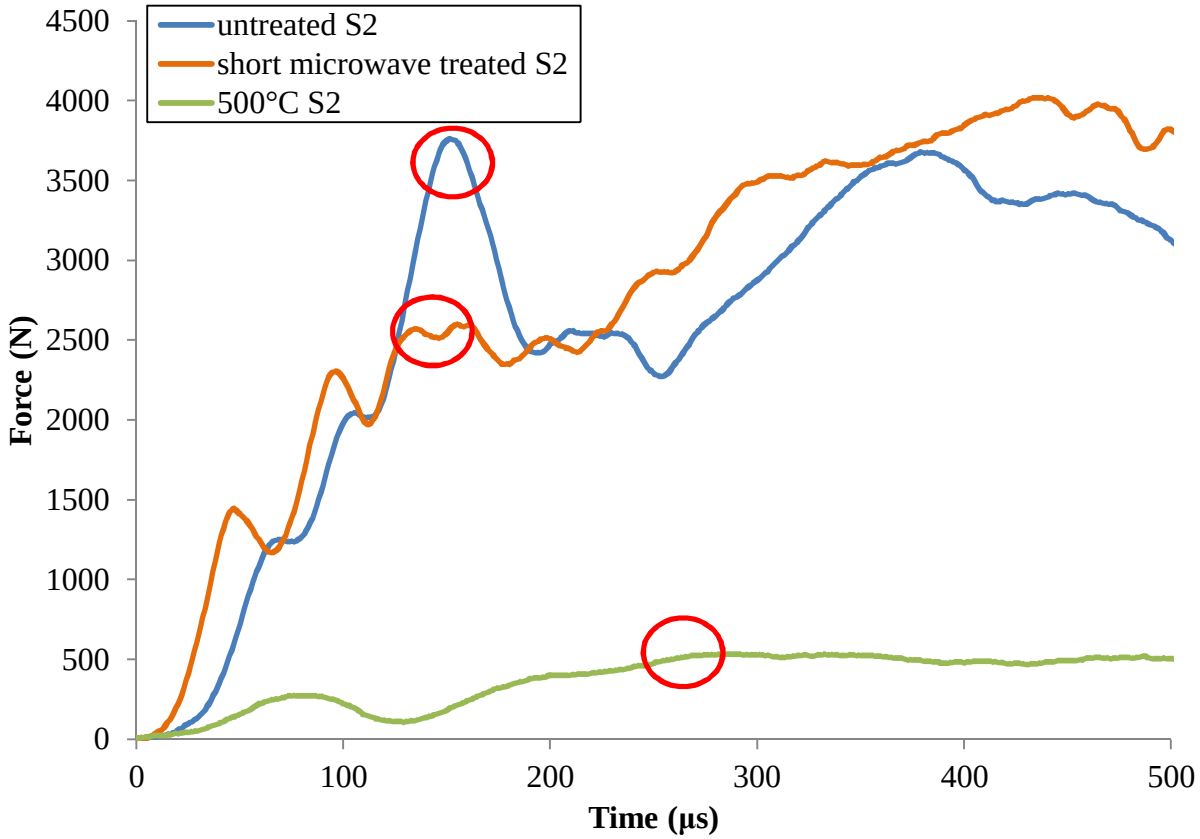

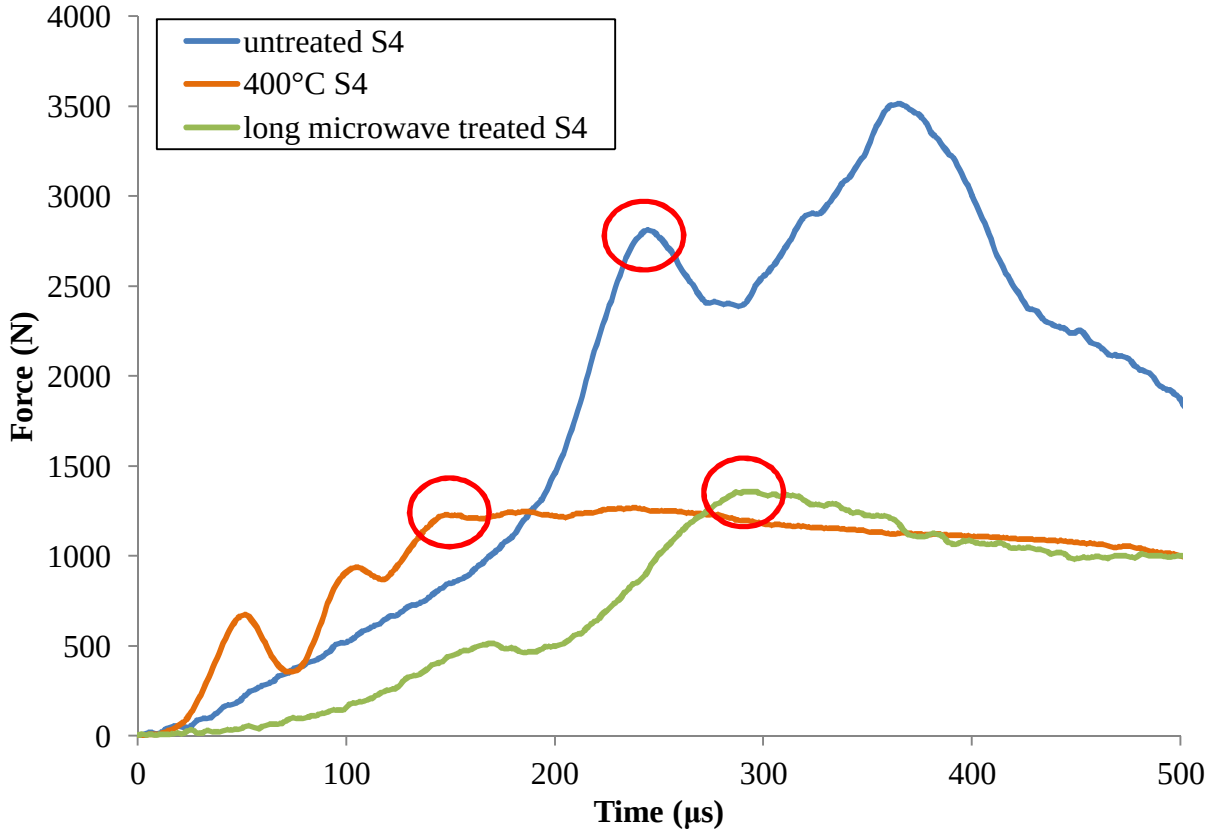

D. THERMOGRAVIMETRIC ANALYSIS

The following two examples show the TGA mass loss curves of two different concretes with a variety of heat treatments.

S5 concrete mass loss under TGA analysis

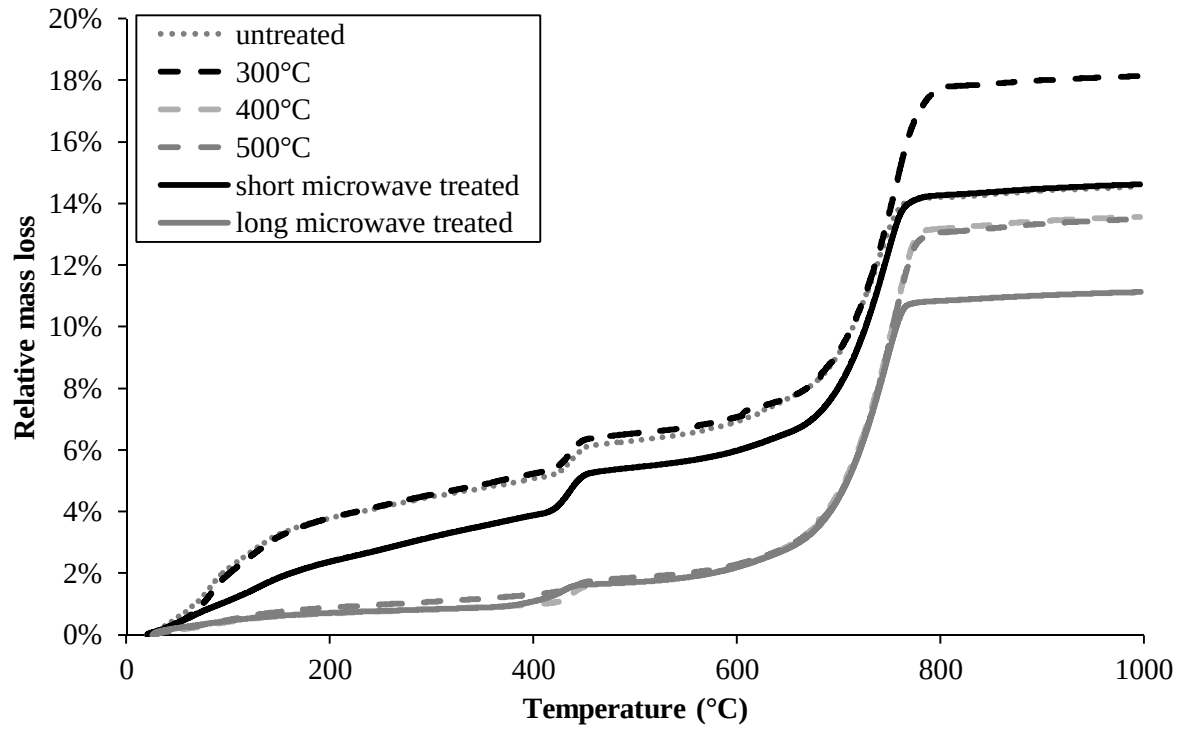

S3 concrete mass loss under TGA analysis

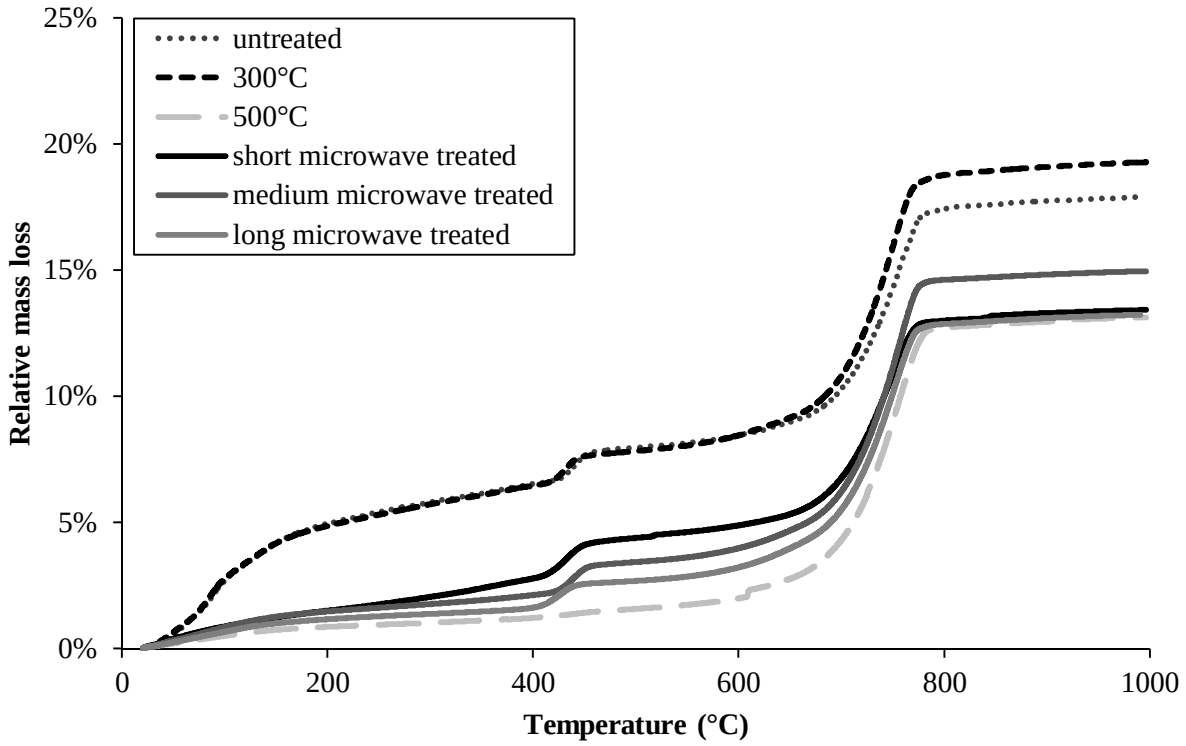

E. MERCURY INTRUSION POROSIMETRY

The following two figures show examples of mercury intrusion porosimetry results for a two different concretes that have experienced different heat treatments.

S1 concrete mercury intrusion porosimetry

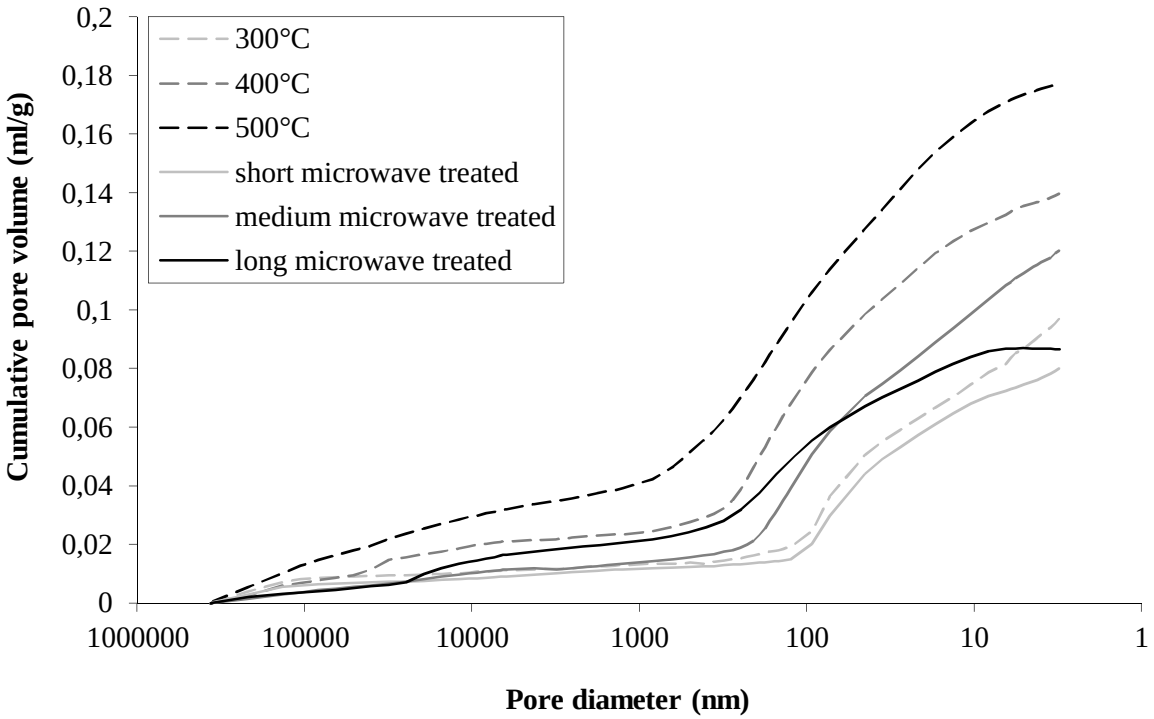

S2 concrete mercury intrusion porosimetry

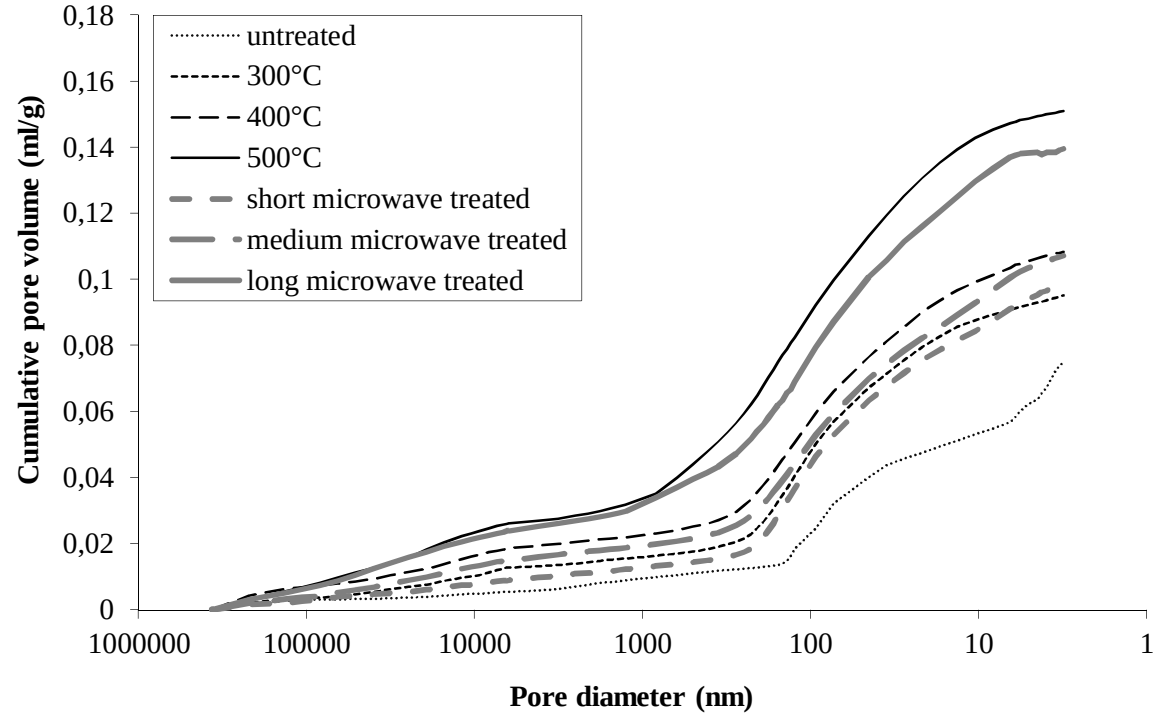

F. MICROWAVE HEATING DATA

The following summarises the results from microwave treatment. Max temperature is the value used to describe typical treatment conditions as described in the experimental methods (Chapter 3).

Microwave heating summary

				energy absorbed (kJ)			max Temperature (°C)			Temperature (°C)		mean mass (g)	
w/c	**a/c**	**exposure time (s)**	**"+/-"**	**mean**	**max**	**min**	**mean**	**max**	**min**	**mean**	**min**	**initial**	**final**
0,4	0,6	15	0	9,0	9,3	8,1	257	306	227	217	144	10,7	10,2
0,4	0,85	15	0	10,6	11,6	9,6	289	312	214	251	167	12,0	11,4
0,4	1,6	15	0	9,0	9,2	8,8	297	331	262	243	192	11,2	
0,5	1,6	15	0	9,4	10,3	8,5	252	280	226	216	136	11,6	11,3
0,6	1,6	15	0	6,5	6,9	6,1	168	177	159	150	120	11,1	10,8
0,4	0,6	30	0	16,8	17,1	16,4	356	438	267	314	148	11,1	10,2
0,4	0,85	30	0	18,5	20,5	16,0	395	417	370	357	232	11,7	11,1
0,4	1,6	40	0	16,3	20,0	10,9	389	467	333	330	256	10,7	10,2
0,5	1,6	30	0	18,0	18,4	14,4	359	428	292	324	145	11,7	11,2
0,6	1,6	30	0	12,1	12,6	11,7	254	271	229	241	215	11,3	10,9
0,4	0,6	48,2	18	25,5	32,3	16,5	431	545	362	400	300	11,3	10,3
0,4	0,85	41,8	15	27,0	32,4	18,3	477	564	523	439	318	12,0	11,1
0,4	1,6	44	10	22,5	30,1	14,9	499	572	405	456	348	10,9	10,2
0,5	1,6	47,6	18	30,5	37,0	23,9	476	536	366	424	299	11,8	11,2
0,6	1,6	55	0	36,4	44,9	27,0	431	599	324	370	248	11,2	10,7

The following figure summarises the mass loss of oven treated samples including the range and standard deviation of the mass of untreated samples.

Oven heating summary

		mean mass (g)					
w/c	**a/c**	**50°C**	**+/-**	**σ**	**300°C**	**400°C**	**500°C**
0,4	0,6	11,4	0,8	0,3	11,4	10,7	10,1
0,4	0,85	11,8	1,1	0,5	10,96	10,96	11,1
0,4	1,6	12,1	1,2	0,6	11,8	11,8	11,8
0,5	1,6	11,4	1,4	0,4	10,76	10,8	10,6
0,6	1,6	11,3	0,4	0,29	11,03	10,3	11,1

G. IMAGE ANALYSIS CODE

The following code was used in MATLAB to do all image analysis steps. This included

- Fracture area
- Cement area
- Aggregate area
- Fracture length
- Identification of nodes, branches and branch terminals

Alternative code was used for the analysis of primary and secondary networks but this only required changing the colour identified as fracture for that analysis.

```
function illlu(foldername)

% example : 'Z:\nicholasb\data\conrete\SEM\0406y1cd5\O_400°C\highlighted'

list_dir=dir([foldername,'\*.bmp']);
for l=1:size(list_dir,1)
z=imread([foldername,'\',list_dir(l).name]);

        bb=z(:,:,3);
        rr=z(:,:,1);
        gg=z(:,:,2);
        bwr=im2bw(rr,254/255);
        bwg=im2bw(gg,254/255);
        bwb=im2bw(bb,254/255);
        gray1=0.5*bwr+0.5*bwg-bwb;
        y=im2bw(gray1,0.6); %Pure yellow
        gray2=bwr-y-bwb;
        r =im2bw(gray2,0.4); %Pure Red
        gray3=bwg-y-bwb;
        g =im2bw(gray3,0.4); %Pure green
        gray4=bwb-bwr-bwg;
        b=im2bw(gray4,0.4); %Pure blue
        gray5=0.5*bwr+0.5*bwb-bwg;
        p=im2bw(gray5,0.6); %Pure purple
        gray6=0.5*bwb+0.5*bwg-bwr;
        az=im2bw(gray6,0.6); %Pure azure

        aggoutline= y+r+p;
        aggregate=imfill(aggoutline,'holes');
        ignore=imfill(az,'holes');
        cement=~aggregate-ignore;
        Cement=cement+y+r;
        CementA=sum(sum(Cement));
        cementA=sum(sum(cement));
        aggregateA=sum(sum(aggregate));

        %Skeletonise to calculate length
        yl = bwmorph(y,'skel',Inf);
        rl = bwmorph(r,'skel',Inf);
        gl = bwmorph(g,'skel',Inf);
        bl = bwmorph(b,'skel',Inf);

 BW=g;
```

```
BW3 = bwmorph(BW,'skel',Inf);
%BW4 = bwmorph(BW3,'spur',10);  % 10=delete noise branchs Inf=Extract Main
branch
BW4=BW3;
BW5 = bwmorph(BW3,'spur',Inf); % 10=delete noise branchs Inf=Extract Main
branch
%[row,col]=size(BW);

[d_map,e_xy,j_xy] = anaskel(BW4);

% junction count
len = length (j_xy(1,:));

% Junction Removing
%       j
%  [ ][ ][ ]
% i[ ][0][ ]
%  [ ][ ][ ]

for i=1:len % 'len' is count of junction
   BW4(j_xy(2,i),j_xy(1,i))=0; % [i,j] = 0

   BW4(j_xy(2,i)-1,j_xy(1,i))=0;
   BW4(j_xy(2,i)+1,j_xy(1,i))=0;
   BW4(j_xy(2,i),j_xy(1,i)-1)=0;
   BW4(j_xy(2,i),j_xy(1,i)+1)=0;

   BW4(j_xy(2,i)-1,j_xy(1,i)-1)=0;
   BW4(j_xy(2,i)+1,j_xy(1,i)+1)=0;
   BW4(j_xy(2,i)-1,j_xy(1,i)+1)=0;
   BW4(j_xy(2,i)+1,j_xy(1,i)-1)=0;
end

% (main tree) - (main branch) = branches
branchs = BW4 - BW5;
sm = bwmorph(BW5,'dilate',3);

%Label object
O=bwlabel(BW3);
nb_element=max(max(O));
%j=bwmorph(BW3,'branchpoints');
%e=bwmorph(BW3,'endpoints');

compt_E_total=0;
compt_J_total=0;

for i=1:1:nb_element
    [row, col] = find(O==i);
    compt_e=1;
    compt_j=1;
    for(j=1:1:length(row))
        ind_e=find((e_xy(1,:)==col(j))&(e_xy(2,:)==row(j)));
        if(~isempty(ind_e))
            E(i,compt_e,:)=e_xy(:,ind_e);
            compt_e=compt_e+1;
            compt_E_total=compt_E_total+compt_e;
        end
        ind_j=find((j_xy(1,:)==col(j))&(j_xy(2,:)==row(j)));
        if(~isempty(ind_j))
            J(i,compt_j,:)=j_xy(:,ind_j);
            compt_j=compt_j+1;
```

```
            compt_J_total=compt_J_total+compt_j;
        else
            J(i,compt_j,1:2)=[0;0];
        end
    end
    clear row;
    clear col;
end



        %% Calculate results
        aggcirc=rl+yl;
        S9=sum(rl);
        S10=sum(S9);
        S11=sum(aggcirc);
        S12=sum(S11);
        nom=list_dir(l).name;
        S13=sum(sum(gl));
        S14=sum(sum(g));
        S15=sum(sum(r+g));
        S16=sum(sum(rl+gl));
        S17=sum(sum(aggregate));
        S20=sum(sum(b));
        M(l+1,:)={nom S10 S17 S12 CementA cementA S13 S14 S15 S16
nb_element compt_E_total compt_J_total S20}
        %figure, imshow(cement)

end
M(1,:)={'Filename' 'aggregate crack length' 'Aggregate area' 'aggregate
interface length' 'Total cement area' 'cement area' 'cement crack length'
'cement crack area' 'Total crack area' 'Total crack length' 'elements'
'ends' 'connections' 'ttlaggcrackarea'}
xlswrite(['\\recherche.ad.inp-toulouse.fr\usersA7-R\nlippiat\Mes
documents\MATLAB\data2_l.xls'],M)
```

This also made use of the ds2nfu function by Scott:

```
%% Process inputs
error(nargchk(1, 3, nargin))

% Determine if axes handle is specified
if length(varargin{1})== 1 && ishandle(varargin{1}) &&
strcmp(get(varargin{1},'type'),'axes')
    hAx = varargin{1};
    varargin = varargin(2:end);
else
    hAx = gca;
end;

errmsg = ['Invalid input.  Coordinates must be specified as 1 four-element
\n' ...
    'position vector or 2 equal length (x,y) vectors.'];

% Proceed with remaining inputs
if length(varargin)==1  % Must be 4 elt POS vector
    pos = varargin{1};
    if length(pos) ~=4,
        error(errmsg);
    end;
else
    [x,y] = deal(varargin{:});
```

```
    if length(x) ~= length(y)
        error(errmsg)
    end
end


%% Get limits
axun = get(hAx,'Units');
set(hAx,'Units','normalized');
axpos = get(hAx,'Position');
axlim = axis(hAx);
axwidth = diff(axlim(1:2));
axheight = diff(axlim(3:4));


%% Transform data
if exist('x','var')
    varargout{1} = (x-axlim(1))*axpos(3)/axwidth + axpos(1);
    varargout{2} = (y-axlim(3))*axpos(4)/axheight + axpos(2);
else
    pos(1) = (pos(1)-axlim(1))/axwidth*axpos(3) + axpos(1);
    pos(2) = (pos(2)-axlim(3))/axheight*axpos(4) + axpos(2);
    pos(3) = pos(3)*axpos(3)/axwidth;
    pos(4) = pos(4)*axpos(4)/axheight;
    varargout{1} = pos;
end


%% Restore axes units
set(hAx,'Units',axun)
```

The size distribution was calculated using the following:

```
function secondisbr(foldername)

% example : 'Z:\nicholasb\data\conrete\SEM\0406y1cd5\O_400°C\highlighted'

list_dir=dir([foldername,'\*.bmp']);

%distr=[0 0 0 0 0];

for fich=1:size(list_dir,1)
z=imread([foldername,'\',list_dir(fich).name]);

bb=z(:,:,3);
rr=z(:,:,1);
gg=z(:,:,2);
bwr=im2bw(rr,254/255);
bwg=im2bw(gg,254/255);
bwb=im2bw(bb,254/255);
gray1=0.5*bwr+0.5*bwg-bwb;
y=im2bw(gray1,0.6); %Pure yellow
gray2=bwr-y-bwb;
r =im2bw(gray2,0.4); %Pure Red
gray3=bwg-y-bwb;
g =im2bw(gray3,0.4); %Pure green
gray4=bwb-bwr-bwg;
```

```
b=im2bw(gray4,0.4); %Pure blue
gray5=0.5*bwr+0.5*bwb-bwg;
p=im2bw(gray5,0.6); %Pure purple
gray6=0.5*bwb+0.5*bwg-bwr;
az=im2bw(gray6,0.6); %Pure azure

aggoutline= y+r+p;
aggregate=imfill(aggoutline,'holes');
ignore=imfill(az,'holes');
cement=~aggregate-ignore;
Cement=cement+y+r;
CementA=sum(sum(Cement));
cementA=sum(sum(cement));
aggregateA=sum(sum(aggregate));

%Skeletonise to calculate length
yl = bwmorph(y,'skel',Inf);
rl = bwmorph(r,'skel',Inf);
gl = bwmorph(g,'skel',Inf);
bl = bwmorph(b,'skel',Inf);

BW=b+r;

BW3 = bwmorph(BW,'skel',Inf);
BW4=BW3;
BW5 = bwmorph(BW3,'spur',Inf); % 10=delete noise branchs Inf=Extract Main
branch
BW6 = bwmorph(BW3,'spur',2);
 [row,col]=size(BW);

%e_xy,j_xy : extrema et jonctions en surnombre dans les branches de largeur
%supérieure à 1 pixel
[d_map,e_xy,j_xy] = anaskel(BW4);

[d_mapspur5,e_xyspur2,j_xyspur2] = anaskel(BW6);

BW7=BW3;

% junction count
len = length (j_xy(1,:));
lenspur2 = length (j_xyspur2(1,:));

for i=1:lenspur2 % 'len' is count of junction
   BW7(j_xyspur2(2,i),j_xyspur2(1,i))=0; % [i,j] = 0
   %modif du 22/03/2013
   BW7(j_xyspur2(2,i)-1,j_xyspur2(1,i))=0;
   BW7(j_xyspur2(2,i)+1,j_xyspur2(1,i))=0;
   BW7(j_xyspur2(2,i),j_xyspur2(1,i)-1)=0;
   BW7(j_xyspur2(2,i),j_xyspur2(1,i)+1)=0;

   BW7(j_xyspur2(2,i)-1,j_xyspur2(1,i)-1)=0;
   BW7(j_xyspur2(2,i)+1,j_xyspur2(1,i)+1)=0;
   BW7(j_xyspur2(2,i)-1,j_xyspur2(1,i)+1)=0;
   BW7(j_xyspur2(2,i)+1,j_xyspur2(1,i)-1)=0;
end


for i=1:len % 'len' is count of junction
   BW4(j_xy(2,i),j_xy(1,i))=0; % [i,j] = 0
```

```
end

%image binarisee green
for j=1:lenspur2 % 'len' is count of junction
       bwg(j_xyspur2(2,j),j_xyspur2(1,j))=0; % [i,j] = 0
       bwg(j_xyspur2(2,j)-1,j_xyspur2(1,j))=0;
       bwg(j_xyspur2(2,j)+1,j_xyspur2(1,j))=0;
       bwg(j_xyspur2(2,j),j_xyspur2(1,j)-1)=0;
       bwg(j_xyspur2(2,j),j_xyspur2(1,j)+1)=0;

       bwg(j_xyspur2(2,j)-1,j_xyspur2(1,j)-1)=0;
       bwg(j_xyspur2(2,j)+1,j_xyspur2(1,j)+1)=0;
       bwg(j_xyspur2(2,j)-1,j_xyspur2(1,j)+1)=0;
       bwg(j_xyspur2(2,j)+1,j_xyspur2(1,j)-1)=0;
end

% (main tree) - (main branch) = branches

branchs = BW4 - BW5;

%Label object
O=bwlabel(BW3);
nb_element=max(max(O));

% Label connected components in binary image
%modif du 22/03/2013
L = bwlabel(branchs);
%L1 = bwlabel(BW3);
L1 = bwlabel(BW4);
L2 = bwlabel(BW7);

% adding branchs and main branch.
L = L + (BW5*20);  % 20 is an assumed number (?)

%tri des e_xy à 3 voisins en config 8 connectivity
kernel = [1 1 1; 1 0 1; 1 1 1];
comptfiltr=1;
for i=1:1:length(e_xy(1,:))
    %imageArray=zeros(3,3);
    bwgg = padarray(bwg, [1 1]);
    imageArray=bwgg(e_xy(2,i):e_xy(2,i)+2,e_xy(1,i):e_xy(1,i)+2);%offset de
1 avec padarray

    pixelCounts = conv2(single(imageArray), kernel, 'same');
    % Mask by original image.
    pixelCounts = pixelCounts .* single(imageArray);
    % Find which pixels have exactly 1 neighbor
    %twoNeighborMax = pixelCounts < 3;
    %if(sum(sum(twoNeighborMax))==1)
    if(pixelCounts(2,2)<3)
        e_xyfiltre(:,comptfiltr)=e_xy(:,i);
        comptfiltr=comptfiltr+1;
    end
end

nb_branch=max(max(L2));
for i=1:1:nb_branch
    [ypos, xpos]=find(L2==i);
    xtext=round(mean(xpos));
    %ytext=round(mean(ypos));
    ytext=row-round(mean(ypos));%trick with ds2nfu !!!!
```

```
    str = num2str(i);
    [xa ya] = ds2nfu(xtext,ytext);
    %annotation('textbox', [xa ya .01 .01], 'String', str, 'Color', 'y');
    clear xpos
    clear ypos
end


for i=1:1:nb_branch
    [rb, cb] = find(L2==i);

    rbcentre=rb(round(length(rb)/2));
    cbcentre=cb(round(length(cb)/2));
    compt_eb=0;
    compt_jb=0;
    acc_ind_jb=[];
    cb_je=[];
    rb_je=[];
    for(j=1:1:length(rb))
        ind_eb=find((e_xyfiltre(1,:)==cb(j))&(e_xyfiltre(2,:)==rb(j)));
        if(~isempty(ind_eb))
            %E(i,compt_e,:)=e_xy(:,ind_eb);
            compt_eb=compt_eb+1;
            cb_je=[cb_je e_xyfiltre(1,ind_eb)];
            rb_je=[rb_je e_xyfiltre(2,ind_eb)];
        end

        for(k=-2:1:2)%-2 à +2 ?
            for(l=-2:1:2)%-2 à +2 ?

ind_jb=find((j_xyspur2(1,:)==cb(j)+k)&(j_xyspur2(2,:)==rb(j)+l));
                if(~isempty(ind_jb))
                    acc_ind_jb=[acc_ind_jb ind_jb];
                end
            end
        end
    end
    uniq_ind_jb=unique(acc_ind_jb);
    compt_jb=length(uniq_ind_jb);
    cb_je=[cb_je j_xyspur2(1,uniq_ind_jb)];
    rb_je=[rb_je j_xyspur2(2,uniq_ind_jb)];


    branch(i).num=i;
    branch(i).extrema=compt_eb;
    branch(i).jonction=compt_jb;
    branch(i).c_extremajonction=cb_je;
    branch(i).r_extremajonction=rb_je;

    xmin=min(cb);
    ymin=min(rb);
    xmax=max(cb);
    ymax=max(rb);

    xmin=min([xmin cb_je]);
    ymin=min([ymin rb_je]);
    xmax=max([xmax cb_je]);
    ymax=max([ymax rb_je]);
    w=xmax-xmin;
    h=ymax-ymin;
```

```
    if(w~=0&h~=0)
        BWgbranch = imcrop(bwg,[xmin ymin w h]);
        %changement de repère (cbcentre,rbcentre)
        cbb=cbcentre-xmin+1;
        rbb=rbcentre -ymin+1;
        %sélection de l'élément après crop
        BWgcropbranch = bwselect(BWgbranch,cbb,rbb,8);

        s  = regionprops(BWgcropbranch, 'Perimeter','Area');
        branch(i).L=round(s.Perimeter/2);
        if (s.Perimeter~=0)
            branch(i).l=round(s.Area/(s.Perimeter/2));
        else
            branch(i).l=branch(i).jonction;
       end

    end


end

distr_new=zeros(nb_branch,5);
for i=1:1:nb_branch
    branch(i).num
    branch(i).extrema
    branch(i).jonction
    branch(i).L
    branch(i).l

     distr_new(i,1)=branch(i).num;
     distr_new(i,2)=branch(i).extrema;
     distr_new(i,3)=branch(i).jonction;
     if (isempty(branch(i).L))
        distr_new(i,4)=1;
     else
        distr_new(i,4)=branch(i).L+branch(i).jonction;
     end
     if (isempty(branch(i).l))
        distr_new(i,5)=1;
     else
        distr_new(i,5)=branch(i).l;
     end

end

if exist('distr')
    distr = [distr; distr_new];
else
    distr=distr_new;
end
  %% Calculate results
nom=list_dir(fich).name;
S17=sum(sum(aggregate));
totalarea=sum(sum(g));
totallength=sum(sum(gl));
M(fich+1,:)={nom S17 cementA CementA sum(distr_new(:,3))
sum(distr_new(:,2)) max(distr_new(:,1)) nb_element totallength totalarea};

end
```

```
M(1,:)={'Filename' 'aggregate area' 'cement area' 'Total cement area' '#
nodes' '# ends' '# branches' '# objects' 'total length' 'total area'}
xlswrite(['\\recherche.ad.inp-toulouse.fr\usersA7-R\nlippiat\Mes
documents\MATLAB\data2nd.xls'],M)
xlswrite(['\\recherche.ad.inp-toulouse.fr\usersA7-R\nlippiat\Mes
documents\MATLAB\distribution.xls'],distr)
```

Thanks once again to Emmanuel Cid for his assistance with creating this code.

H. AGGREGATE SIZE AFTER HEATING TESTS

The following shows the size distribution of aggregate particles after being fractured on the Hopkinson bar and undergoing selective acid dissolution. No significant differences are observed between different microwave treatment durations.

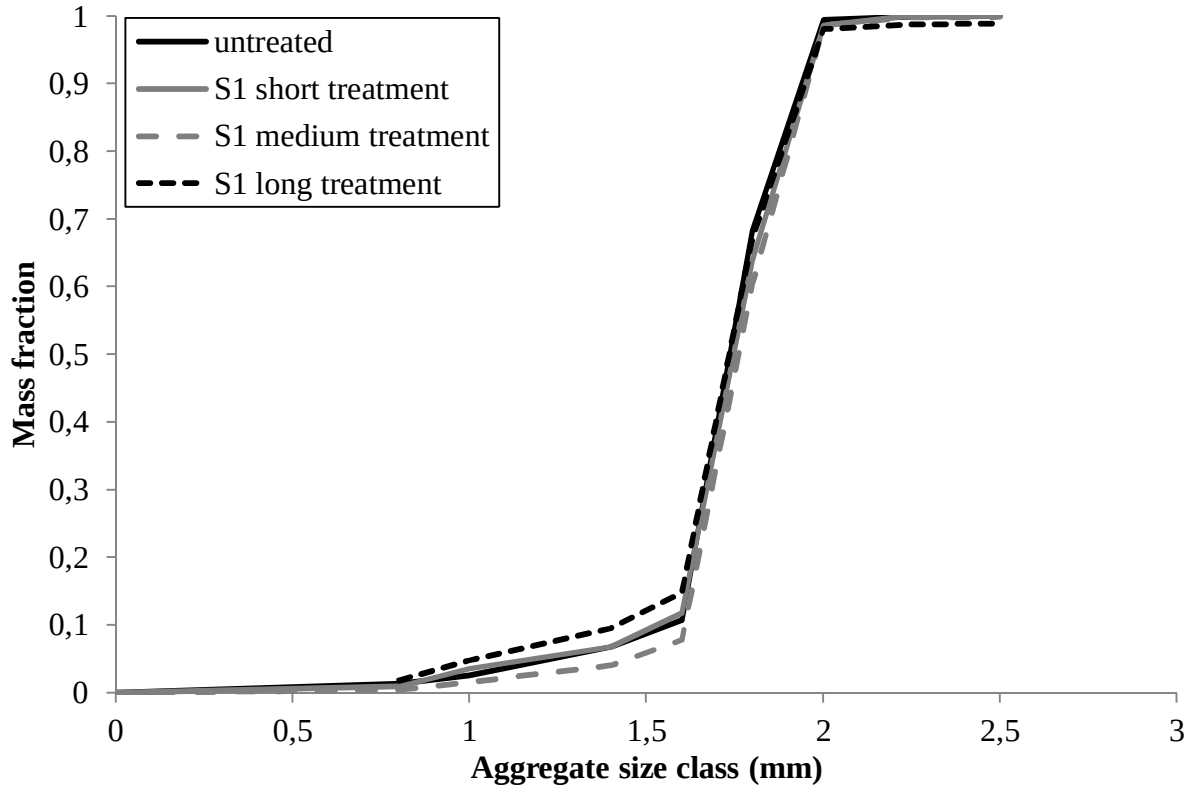

The smallest size fraction is ignored due to the presence of silica powder. The samples that produced the greatest mass of 'aggregate' below 0.8mm were the untreated samples. Medium treated produced the least.